Whole Number 243, ISSN 0429-8284

FUJI ELECTRIC REVIEW

2013
Vol.59 No. 4

Power Semiconductors Contributing in Energy Management

Fuji Electric

Innovating Energy Technology

FUJI ELECTRIC
REVIEW

2013
Vol.59 No. 4

Power Semiconductors Contributing in Energy Management

Toward establishing low carbon societies, expectations are rising significantly for diffusion of renewable energy such as photovoltaic power generation and wind power generation as well as power electronics technology for using such energy efficiently. In order to meet these expectations, Fuji Electric is developing user-friendly power semiconductor products with high energy conversion efficiency and low noise for various sectors such as environment, energy, automobile, industrial machinery, social infrastructure and home appliances.

This special edition introduces the latest technology and products of power semiconductors, which are the key devices of power electronics technology.

Cover Photo:
SiC wafer substrate

FUJI ELECTRIC REVIEW vol.59 no.4 2013
date of issue: December 30, 2013

editor-in-chief and publisher **EGUCHI Naoya**
Corporate R & D Headquarters
Fuji Electric Co., Ltd.
Gate City Ohsaki, East Tower,
11-2, Osaki 1-chome, Shinagawa-ku,
Tokyo 141-0032, Japan
http://www.fujielectric.co.jp

editorial office Fuji Electric Journal Editorial Office
c/o Fuji Office & Life Service Co., Ltd.
1, Fujimachi, Hino-shi, Tokyo 191-8502,
Japan

Contents

Power Semiconductors Contributing in Energy Management

Supplemental Explanation

New Products

1,700 V Withstand Voltage SiC Hybrid Module

KOBAYASHI Kunio* KITAMURA Shoji* ADACHI Kazuya‡

ABSTRACT

In place of Si devices, silicon carbide devices (SiC devices) featuring heat resistance and high breakdown field tolerance are raising expectations for efficiency improvement and miniaturization of equipment. Fuji Electric is moving ahead with the development of a 1,700 V withstand voltage SiC hybrid module for high-efficiency inverters (690 V series). A SiC-SBD chip jointly developed with the National Institute of Advanced Industrial Science and Technology has been applied to a freewheeling diode (FWD), and a Fuji Electric's "V-Series" IGBT chip has been applied to an insulated gate bipolar transistor (IGBT). By improving leakage current and switching characteristics, the module has been verified to be capable of reducing generated loss by approximately 26% in a 300 A product compared to the conventional Si modules.

1. Introduction

Faced with the need to prevent global warming, the urgent task of reducing emissions of greenhouse gases such as CO_2 is greater than ever. One of the means to realize this is to ensure energy saving in power electronics devices. Highly efficient inverters are an important aspect of this, and they require technological innovation for components such as power devices, circuits and controls. In particular, there is a strong demand for lowering power dissipation in power devices that are the main elements of inverters. An insulated gate bipolar transistor (IGBT), a major power device, has used a silicon (Si) IGBT chip and free-wheeling diode (FWD) chip so far. However, Si devices are hitting the theoretical limit in terms of performance based on their physical characteristics. For this reason, there are high expectations now for silicon carbide (SiC) devices because of their properties of heat resistance and high breakdown field tolerance, and it is hoped they will improve equipment efficiency and achieve miniaturization.

This paper describes a 1,700 V withstand voltage SiC hybrid module that deploys SiC devices.

2. Product Features

Fuji Electric has so far completed the development of 600 V withstand voltage SiC- Schottky barrier diode (SBD) for 200 V systems and 1,200 V withstand voltage SiC-SBD for 440 V systems, followed by successful commercialization of an SiC hybrid module that combines these SiC-SBDs and Si-IGBT. SiC-SBD has low resistance and superior switching characteristics in comparison with an Si-PIN diode, a conventional high blocking voltage FWD. With these features, the SiC hybrid module has a capacity to reduce generated loss by approximately 26% compared with conventional Si-IGBT modules.

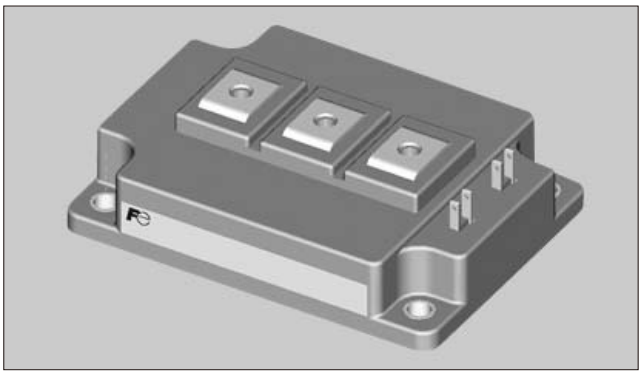

Fig.1 M277 package

The development of a 1,700 V withstand voltage SiC hybrid module is currently underway for 690 V input inverters. The M277 package (see Fig. 1) has been adopted for the SiC hybrid module to allow for easy changeover from conventional Si modules, which use the same package. Fuji Electric developed an SiC-SBD chip jointly with the National Institute of Advanced Industrial Science and Technology, followed by the Company's launch of a mass-production line. This chip has been applied to FWD, while IGBT has been equipped with Fuji Electric's latest product, the sixth-generation "V-Series" IGBT chip.

3. Features

3.1 Forward characteristic of FWDs

Figure 2 illustrates the FWD forward-direction

* Electronic Devices Business Group, Fuji Electric Co., Ltd.
‡ Corporate R&D Headquarters, Fuji Electric Co., Ltd.

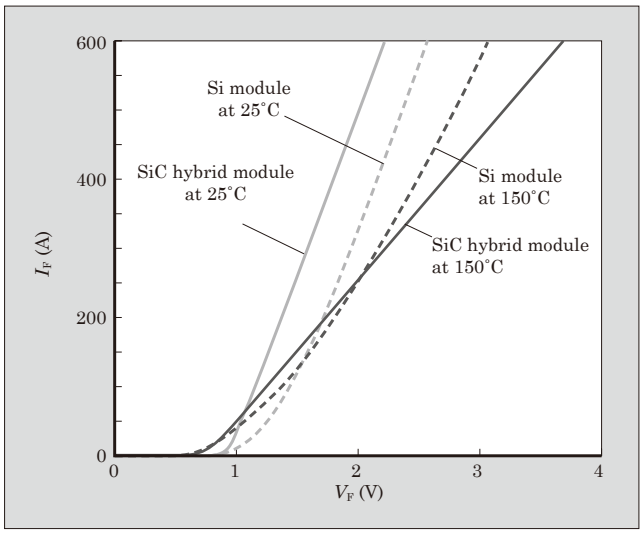

Fig.2 Forward characteristic of FWDs

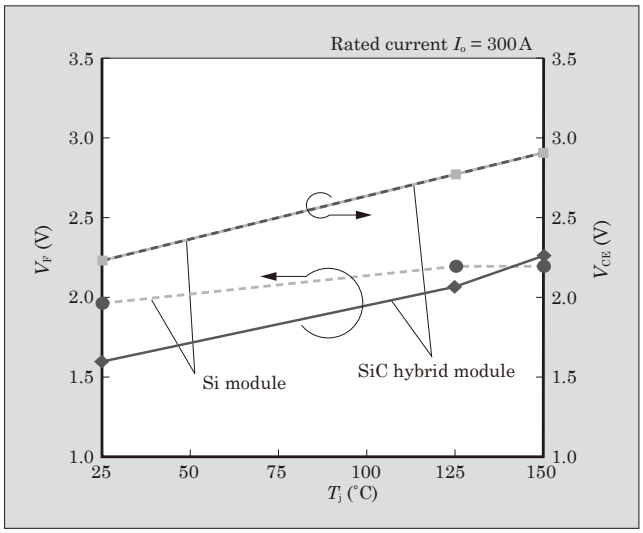

Fig.3 Temperature dependency of FWDs

characteristic of the SiC hybrid module and Si module, and Fig. 3 illustrates the temperature dependency. With a junction temperature at 150 °C and rated current of 300 A, the forward direction voltage V_F is on the same level as the Si module V_F. Owing to its strong positive temperature coefficient, the SiC hybrid module creates smaller current imbalance in multi-parallel connections.

3.2 Leakage current

Figure 4 depicts the leakage current temperature dependency of an SiC hybrid module and Si module. While the leakage current I_{CES} of the SiC hybrid module is nearly ten times greater than that of the Si module at the rated voltage at 125 °C (1,700 V), this difference shrinks to approximately twice at 150 °C. The difference in leakage current value between 125 °C and 150 °C under the rated voltage is smaller in the SiC hybrid module compared to that in the Si module. Therefore, SiC-SBD has a smaller leakage cur-

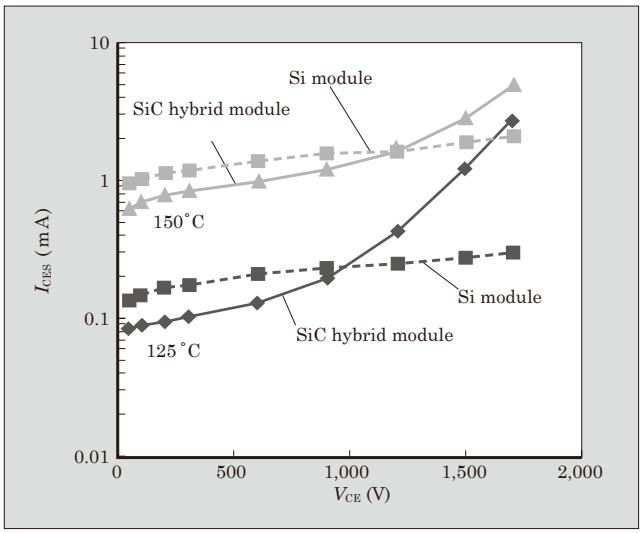

Fig.4 Leakage current temperature dependency

rent temperature dependency compared with Si-FWD. This is because SiC's band gap is approximately three times that of Si, and as SiC-SBD operates at a higher electrical field than Si-FWD, thus the leaked current of SiC-SBD becoming predominantly tunneling current and making it less susceptible to temperature fluctuations. For these reasons, the SiC hybrid module can, like the V-Series, perform in a high temperature environment[1].

3.3 Switching

(1) Reverse recovery loss

Figure 5 illustrates the reverse recovery loss of the SiC hybrid module and Si modules. The SiC hybrid module scarcely has any peak reverse recovery current. This is explained by the fact that SiC-SBD is a unipolar device, and so it causes no minority carrier injection. The reverse recovery loss of 300 A products is lower than that of the Si module by approximately 83%.

(2) Turn-on loss

Figure 6 shows the turn-on losses of the SiC hybrid

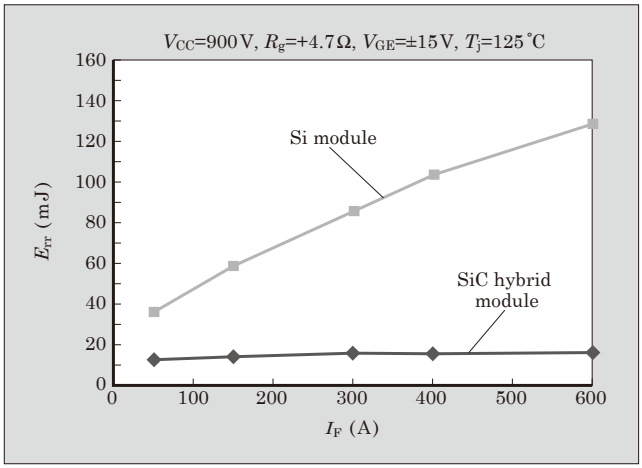

Fig.5 Reverse recovery loss

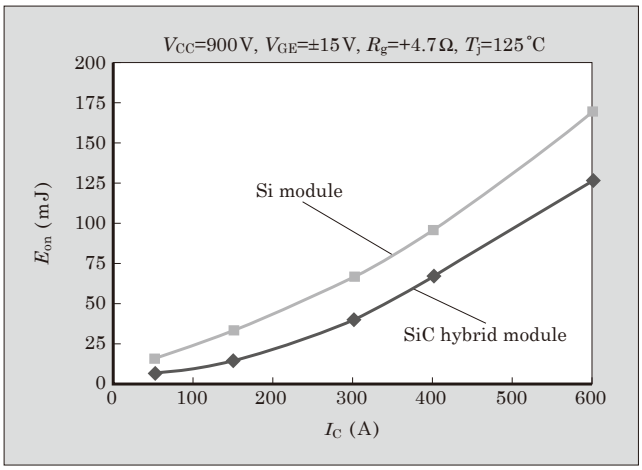

Fig.6 Turn-on loss

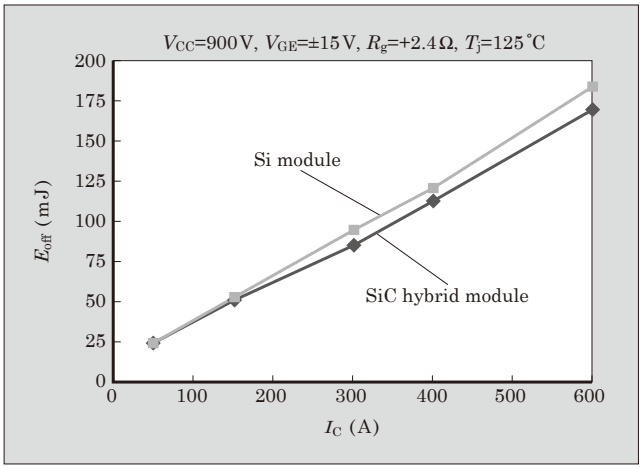

Fig.7 Turn-off loss

module and Si module. The peak reverse recovery current of SiC-SBD affects the IGBT turn-on current in the opposing arm, leading to a lower turn-on loss. The turn-on loss of a 300 A product is lower than that of the Si module by approximately 40%.

(3) Turn-off loss

Figure 7 depicts the turn-off losses of the SiC hybrid module and Si module. The surge peak voltage of the SiC hybrid module at a turn-off can be expressed as shown in Formula (1). Provided that the IGBT element characteristics and inductance of the main circuit are equal, the difference in the transient on-voltage becomes the difference in the surge voltage. The drift layer of SiC-SBD has extremely low resistance compared to Si-FWD, and this lowers the transient on-voltage. Therefore, the surge voltage at turn-off is kept low, and hence there is a low turn-off loss.

$$V_{sp} = V_{cc} + L_s \frac{dI_c}{d_t} + V_{fr} \cdots\cdots (1)$$

V_{sp} : surge peak voltage
V_{cc} : applied voltage
L_s : main circuit inductance
I_c : collector current
V_{fr} : transient on-voltage

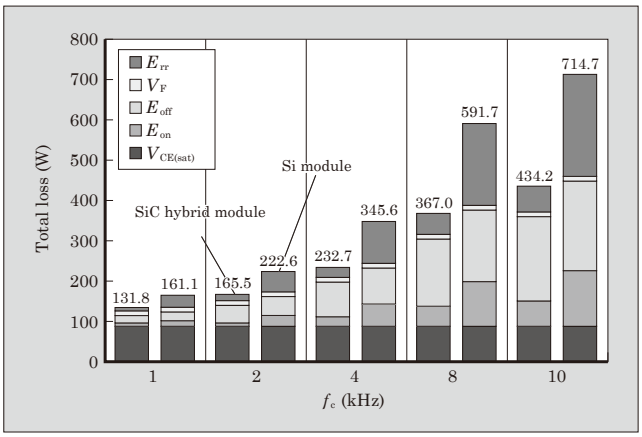

Fig.8 Inverter generated loss

3.4 Inverter generated loss

Figure 8 shows the inverter generated losses of the SiC hybrid module and Si module. The SiC hybrid module's total loss at the carrier frequency f_c of 2 kHz is lower than that of the Si module by approximately 26%. As the loss increase rate of the SiC hybrid module is more suppressed than the Si module at higher carrier frequencies, the SiC hybrid module has an advantage over the Si module in performing at high frequencies.

4. Postscript

The SiC hybrid module is a product deploying SiC-SBD, which was developed jointly with the National Institute of Advanced Industrial Science and Technology, and Fuji Electric's latest product, the sixth-generation "V-Series" Si-IGBT. SiC hybrid module has successfully attained a significant loss-reduction within the device, enabling an efficiency enhancement for inverters to a great extent. We will expand the range of SiC-chip-applied products and develop product families in the future to contribute to energy conservation.

We would like to thank everyone at the Advanced Power Electronics Research Center of the National Institute of Advanced Industrial Science and Technology who contributed to the development of SiC-SBD chip.

References

(1) Nakazawa, M. et al. Hybrid Si-IGBT and SiC-SBD Modules. FUJI ELECTRIC REVIEW. 2012, vol.58, no.2, p.70-74.

Ultra-Compact, High-Reliability All-SiC Module

NAKANO Hayato* HINATA Yuichiro* HORIO Masafumi*

ABSTRACT

SiC devices have excellent characteristics that realize high blocking voltage, low power dissipation, high-frequency and high-temperature operation. Fuji Electric's All-SiC module features direct bonding layout for semiconductors and a plastic molding structure. Compared with the conventional product, the All-SiC module achieves significant improvement of 50% in footprint, 75% lower PN and gate inductances, and approximately 35% lower switching loss. Moreover, for using high power drives, switching is demonstrated in the case of 4 modules being connected in parallel. The All-SiC module is verified to have sufficient reliability in high temperature and humidity, in addition to power cycling, and is better than the conventional products.

1. Introduction

In the power electronics field, a power module serves as central components in a highly efficient power conversion society. There are many applications which need a power module not only in the renewable energy field such as in solar and wind power, but also in in-vehicle field such as in a hybrid electric vehicle (HEV) and electric vehicle (EV).

On the other hand, because of the characteristics of Si devices, the performance of the Si module is approaching its limit. Therefore, new wide band gap semiconductors such as SiC (silicon carbide) and GaN (gallium nitride) have enough potential to be the next-generation device instead of Si[(1)]. Regarding this background, the SiC device is expected to be an excellent device which has a high blocking voltage, low power dissipation, high-frequency and high-temperature operation compared with conventional devices.

This paper describes the All-SiC module that an SiC-metal-oxide-semiconductor field-effect transistor (MOSFET) and SiC-Schottky barrier diode (SBD) are mounted.

2. Comparison of packaging technology

Figure 1 shows a comparison of the structure cross-section of the new and conventional structures. The new structure aims to maximize the SiC device property as mentioned. The existing structure is the conventional Si module. In the new structure, device connections are performed by using a power substrate to the semiconductor element (power chip) with surface bonding. Heat dissipation performance is improved by using a thick copper substrate to the AMB substrate*1.

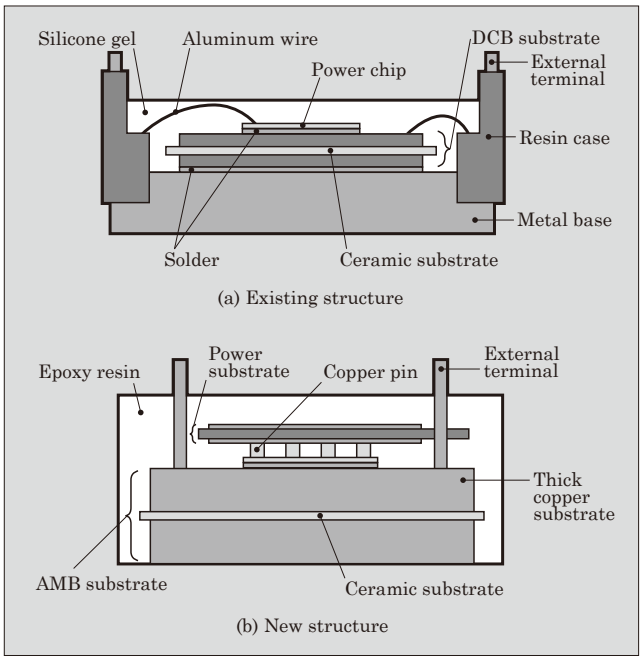

Fig.1 Cross-section of the existing structure and new structure

In order to decrease mechanical stress inside a module, optimization of the linear expansion coefficient of constitution materials and a resin sealing structure are applied. Figure 2 shows the picture of the All-SiC module that is rated 1,200 V/100 A and the Si module of the same rating. Table 1 shows a summary of comparing these two in terms of footprint size and inductance. Regarding this table, the All-SiC module has dramatically reduced the footprint size by 50% and lowered the

* Corporate R&D Headquarters, Fuji Electric Co., Ltd.

*1: AMB substrate: an insulating substrate for radiating heat which is composed of a thick copper substrate and a ceramic substrate joined together via active metal brazing (AMB) method

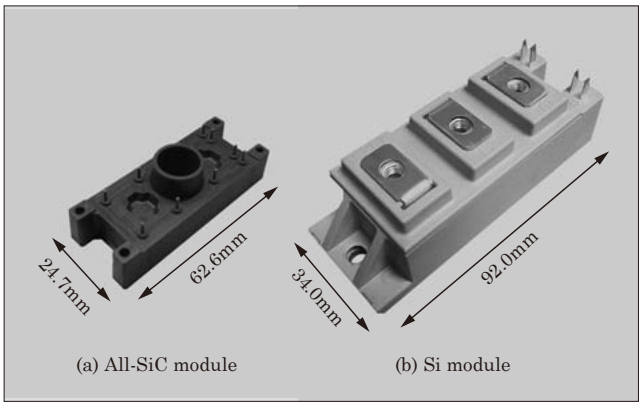

Fig.2 All-SiC module and Si module

Table 1 Comparison between the All-SiC module and the Si module

Package structural characteristic	Reduction rate (comparison between the existing structure and the new structure)
Footprint	50%
Inductance between PN	75%
Gate inductance	75%

PN and gate inductance by 75% compared with the Si module. Therefore, the new structure has compact and lower inductance advantages for high speed and high temperature drive which is able to maximize the SiC device characteristics.

3. The All-SiC Module for Solar PCS

3.1 Effect of mounting All-SiC module for high frequency switching

The All-SiC module, for which development is in progress, is ultra-compact and has high-speed switching capability. In the case of high-frequency switching, it is possible to shrink the size of subsidiary parts such as reactors because of its frequency dependency. Therefore, high-speed switching enables to downsize the entire system volume. This scenario ends up with a power conditioner to downsize the photovoltaic power generation (solar PCS) described in this paper.

At the advantage of high-frequency switching capability, the All-SiC module generates lower loss, which means there is no requirement to increase the number of modules instead of having multipul modules in parallel. Figure 3 shows the switching frequency dependency of loss of the SiC and the Si modules. This is the result of calculating loss for switching frequency in the case of the SiC and the Si device being mounted on the 2-in-1 module. For the module composed of the Si device, switching frequency increases the switching loss. On the other hand, the All-SiC module does not increase switching loss even though the All-SiC module works under high switching frequency. Therefore, the All-SiC module have been reduced the loss, which depends on switching frequency.

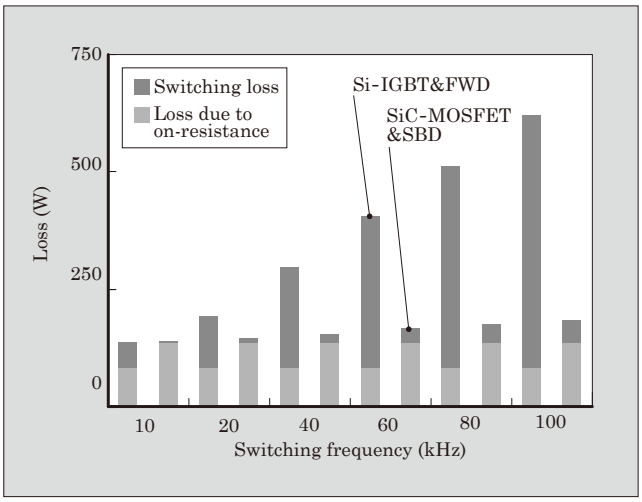

Fig.3 Switching frequency dependency of occurrence loss of the SiC device and the Si device

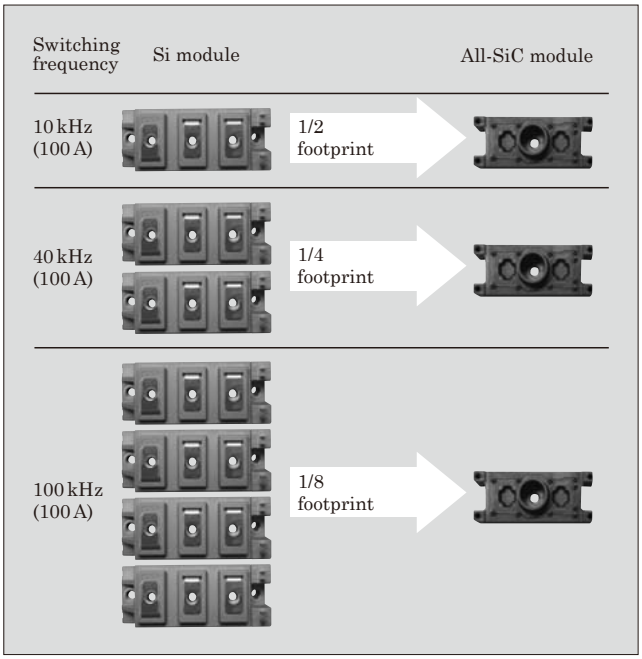

Fig.4 Effect of All-SiC module for high-frequency purpose

Figure 4 shows the impact of the All-SiC module for a high-frequency application. This is a comparison of the number of All-SiC and Si modules when the loss is roughly even. For example, at the switching frequency of 10 kHz, the All-SiC and the Si modules have almost identical losses. In this case, the footprint of the All-SiC module is 1/2 of the Si module. At the switching frequency is 40 kHz, the loss of the Si module should be double compared with the All-SiC. Therefore the loss of the two Si modules and the one All-SiC module become almost even. In the terms of footprint, the All-SiC module has 1/4 that of the Si module. When the switching frequency is 100 kHz, the downsizing effect becomes so significant that the All-SiC footprint is 1/8 of the Si module.

3.2 Switching result

Since it is necessary to clarify the advantage of the All-SiC structure, the SiC devices were put into the new and conventional structures and evaluated their packaging technology. The evaluation conditions of switching characteristics were as follows: V_{ds} is 600 V, I_d was 100 A, V_g was +15/−5 V, R_g was 6.8 Ω and T_j was 200 °C.

Figure 5 shows the temperature dependence of the surge voltage that occurs at turn-off. With the new structure, the surge voltage is decreased by approximately 50 V compared to the existing structure. This advantage is accomplished by low inductance. In addition, the gap of the surge voltage at room temperature and 200 °C is approximately 10 V.

The temperature dependency of switching loss of the existing and the new structures is shown in Fig. 6. Switching loss is the total loss of turn-on, turn-off and reverse recovery. The evaluation condition was the same as in the previous surge voltage test. The SiC devices are mounted on both structures, and therefore the temperature dependency is low. Switching loss of the new structure becomes approximately 35% lower than the existing structure due to the low inductance.

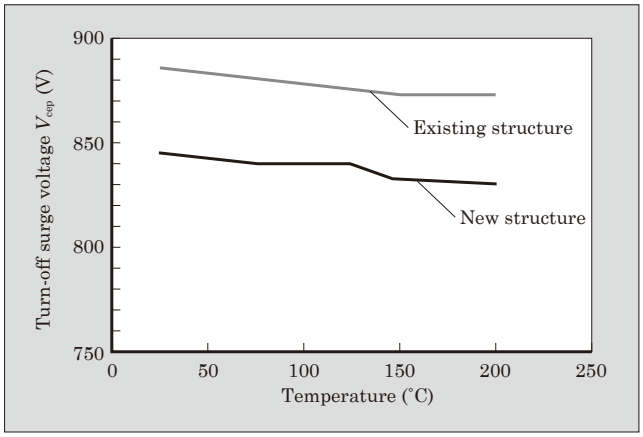

Fig.5 Temperature dependence of surge voltage at turn-off

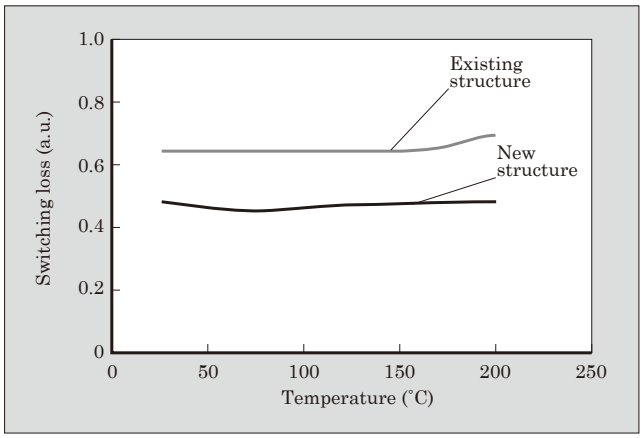

Fig.6 Temperature dependency of switching loss

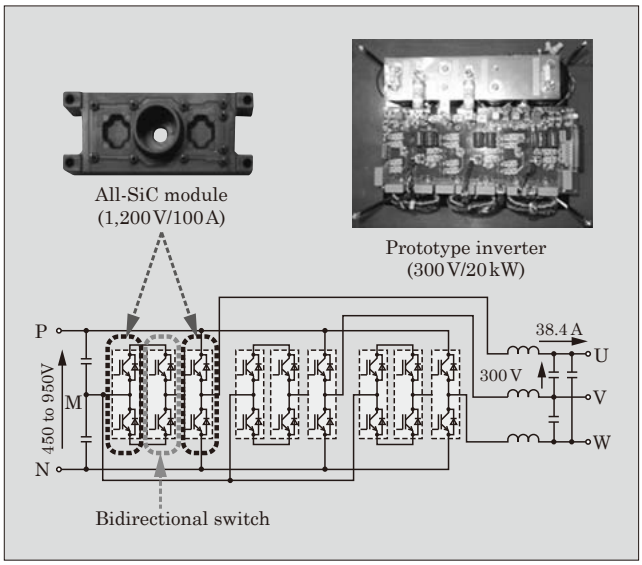

Fig.7 Circuit structure of solar PCS inverter section

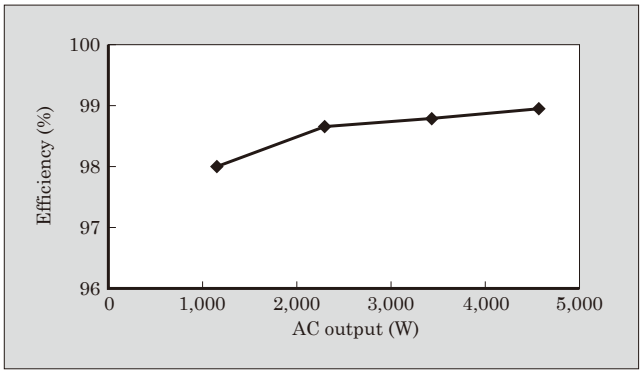

Fig.8 Efficiency of solar PCS

3.3 Continuous operation

The All-SiC module is integrated in the proto-type solar PCS inverter application. Figure 7 shows the circuit structure of the inverter. It uses 3-level control that enables more higher efficiency and downsizing of the system compared with the existing 2-level control including the bidirectional-switching. In this case the switching frequency is 20 kHz. Figure 8 shows the efficiency of solar PCS is about 99% at the maximum. Solar PCS efficiency means the efficiency when converting the electric power generated by a solar panel into the intended voltage. In addition, because the module size becomes smaller, it is possible to downsize the volume of the conventional solar PCS chassis to approximately 75%[2].

4. High Power All-SiC Module Concept

A high power SiC module is expected to be part of a future product strategy. It can be achieved by producing large size of the SiC chip; however, there are issues such as the high defect density of the SiC substrate and in the case where the chip area becomes

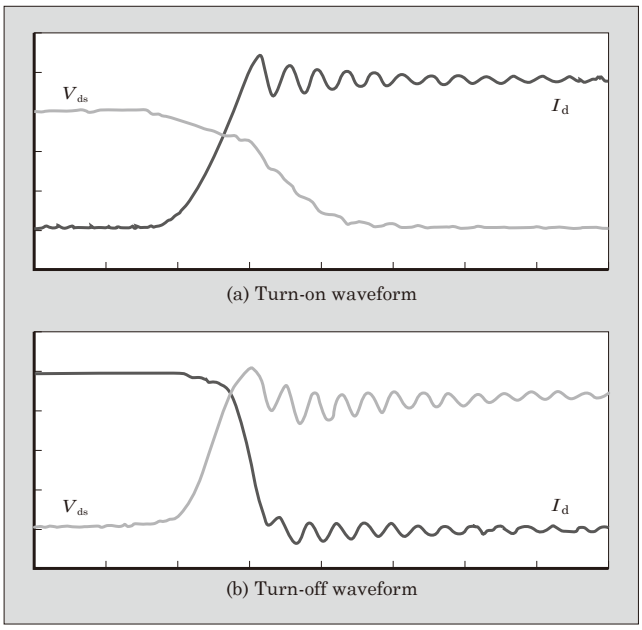

Fig.9 Switching of large-capacity module

larger, reduction in the yield rate becomes low. One of the options to solve this issue is to increase the output capacity of the module by connecting the chip in parallel instead of producing large size of the SiC chip. It is possible to connect the All-SiC module in parallel to have further high-power capability. Here, it is important to design the high-power All-SiC module to have low inductance by having a bus bar connection.

Switching evaluation of the All-SiC module in parallel was performed. The All-SiC module comprised a 1,200 V/400 A module by connecting 4 modules of 1,200 V/100 A module. The evaluation conditions were as follows: V_{ds} was 600 V, I_d was 400 A, V_g was +15/−5 V and R_g was 9.7 Ω. In the high-power module, because the output power is high, a turn-off surge voltage issue emerges. With the high-power module for which development is in progress, this issue is solved by connecting the module in parallel with a low inductance bus bar. This design has to be used in order to prevent losing the low inductance advantage of the All-SiC module. Figure 9 shows the switching waveforms of the high-power module. There is no critical failure as oscillation and the excessive surge voltage. It was demonstrated that switching is feasible even when 4 modules of the All-SiC are connected in parallel.

5. Reliability

It was confirmed that the All-SiC module has better reliability than the existing Si module by performing multiple tests as power cycle, heat cycle, high-temperature and high-humidity reverse bias tests.

In the power cycle test, it was found that the new structure has 10 times the power cycle capability compared with the existing structure when T_{jmax} is 200 °C (ΔT_j=175 °C).

It is important to clarify the humidity capability of the All-SiC module because it has a totally different structure compared with the Si module. Therefore, high-temperature and high-humidity reverse bias tests are important. The new structure is molded by resin, and the resin easily absorbs moisture under a highly humid environment and the moisture is likely to be a cause of mechanical or electric failure.

Figure 10 shows the result of high-temperature and high-humidity reverse bias tests (leak current). This is the electric characteristics trace result during reliability test, which was continued up to a cumulative total of 3,000 hours with the temperature of 85 °C and relative humidity of 85%, and by applying 0 V to the V_g and reverse bias voltage was 960. This 3,000-hour test was conducted to confirm performance up to three times the Fuji Electric standard in the high-temperature and high-humidity environment load test. In an arbitrary time, samples (N=5) were extracted to check leak current I_{DSS} and evaluated at 1,200 V to check reverse bias voltage V_{ds} and abnormality in characteristics. The module was abandoned under a high-temperature and high-humidity environment for as long as 3,000 hours with reverse bias applied simultaneously, no remarkable increase in leak current was found and

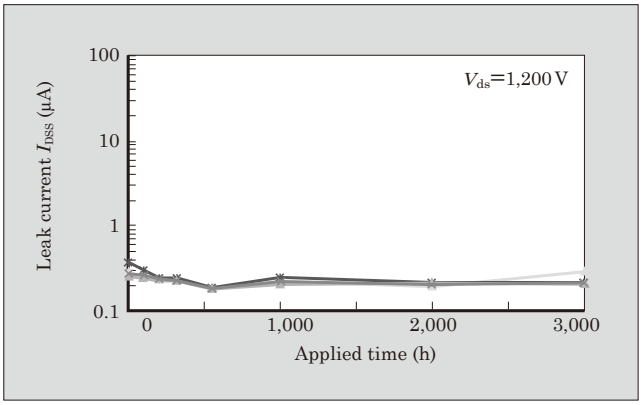

Fig.10 Result of high-temperature and high-humidity reverse bias test (leak current)

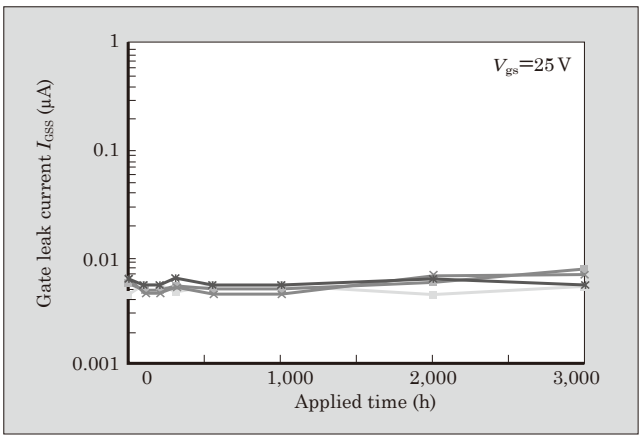

Fig.11 Result of high-temperature and high-humidity reverse bias test (gate leak current)

the value was approximately equal to the initial.

Transition of the gate leak current I_{GSS} in the similar reliability test is shown in Fig. 11. Evaluation condition of I_{GSS} is the gate leak current when V_{gs} +25 V is applied. There is no critical behavior from the evaluation of I_{GSS} and since the leak current is stable, deterioration of a gate structure under an environment with high temperature and high humidity is not observed. As a result, it was confirmed that the new structure that is applied to the All-SiC module is more reliable than the existing products, under a high-humidity environment.

6. Postscript

Fuji Electric is progressing with the development of the All-SiC module in the terms of maximizing the SiC device properties such as high blocking voltage, low power dissipation, high-frequency and high-temperature operation. The All-SiC module has sufficient reliability compared with a conventional Si packaging technology. By applying the All-SiC module, downsizing and high efficiency drive are realized. In particular, the high-frequency operation maximizes the characteristics of the downsizing effect. In the future, Fuji Electric will expand the range of applications via module capacity enlargement, and contribute to the development of power electronic society.

References

(1) Prof. B. Jayant Baliga. "The Role of Power Semiconductor Devices in Creating a Sustainable Society". Plenary Session APEC 2013.

(2) Matsumoto, Y. et al. Power Electronics Equipment Applying SiC Devices. FUJI ELECTRIC REVIEW. 2012, vol.58, no.4, p.212-216.

New Assembly Technologies for T_{jmax}=175°C Continuous Operation Guaranty of IGBT Module

MOMOSE Fumihiko* SAITO Takashi* NISHIMURA Yoshitaka*

ABSTRACT

In order to meet the needs for miniaturization and cost reduction of inverters, IGBT modules are required to offer higher power density than ever. Fuji Electric has developed a new aluminum wire, solder alloy and surface electrode protection layer to improve the continuous operating temperature of an IGBT module from the conventional 150 °C to 175 °C, thereby realizing higher power density. A power cycle lifetime has been more than doubled compared with the conventional products in all temperature ranges, and thus 20% improvement of inverter maximum output can be expected.

1. Introduction

General-purpose inverters are widely used and demand for them is expanding as they contribute to significant energy saving. There is a strong market need for energy efficiency and miniaturization as well as for a comprehensive reduction of costs including system development costs[1].

In order to meet such market demand, Fuji Electric has been working on loss improvement and miniaturization of insulated gate bipolar transistor (IGBT) chips, which are a main component of an IGBT mounted on a general-purpose inverter. The "V-Series" of IGBT modules has improved the guaranteed continuous operation at 150 °C, which is 25 °C higher than the IGBT module operation temperature of the "U-Series." This has been done to support miniaturization and cost reduction of inverter systems as a whole. Figure 1 illustrates the transition of rated IGBT module chip area (1,200 V; 50 A). As there is limited room for further improving the power losses of IGBT chips, we considered miniaturizing and higher power density of IGBT modules by raising the upper limit of the operating temperature. It is estimated that a 20% improvement in the output of a general-purpose inverter is expected when the upper limit of the operating temperature is raised to 175 °C from the conventional 150 °C. This article will describe the assembly technology for IGBT modules that realizes highly reliable and continuous operation at T_{jmax} 175 °C.

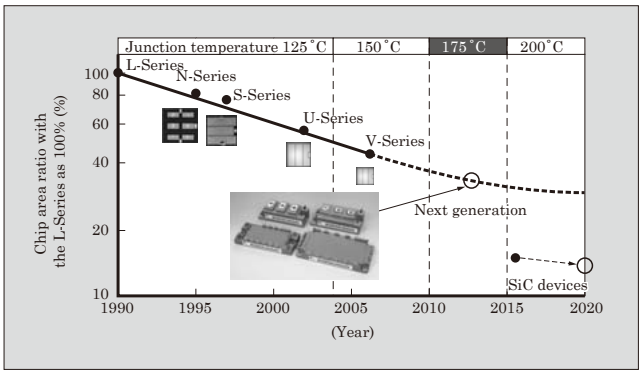

Fig.1 Transition of IGBT chip area (1,200 V/50 A)

2. Technical Challenges to Guarantee Continuous Operation at 175°C

One of the important elements in realizing guaranteed continuous operation at 175 °C is power cycle lifetime. Raising the maximum operational temperature from the conventional 150 °C by 25 °C means there is an increase of thermal stress on component materials. It also increases the temperature fluctuation range between operation and downtime. Thus the materials need guaranteed resistance against more thermal fatigue than the previous product.

Figure 2 shows the power cycle lifetime of previous modules at fixed maximum operational temperature T_{jmax} with a cumulative failure rate of 1%. The lifetime is reduced by 30% to 50% as T_{jmax} increases to 175 °C from 150 °C. It is therefore essential to create a highly reliable assembly that guarantees a power cycle lifetime equal to that of previous 150 °C-range products and yet is operable at a T_{jmax} of 175 °C.

It is generally considered that fractures in an IGBT module incurred in the power cycle test are mainly due to fatigue from repeated stress applied between components differing in coefficient of thermal expansion during temperature fluctuations[2]. In a continuous operation at T_{jmax} 175 °C, the effect from a metallic microstructure change in the components

* Corporate R&D Headquarters, Fuji Electric Co., Ltd.

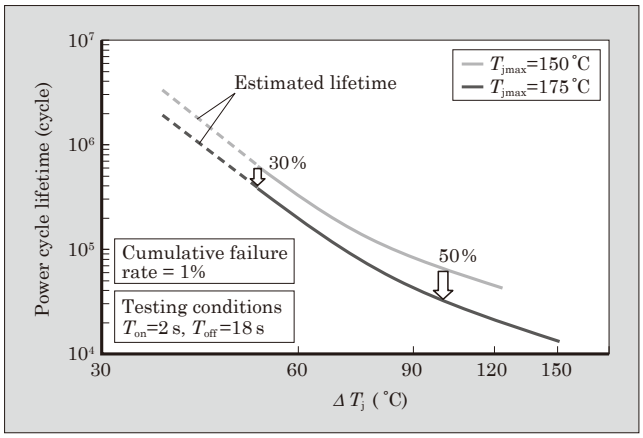

Fig.2 Power cycle lifetime in the conventional structure

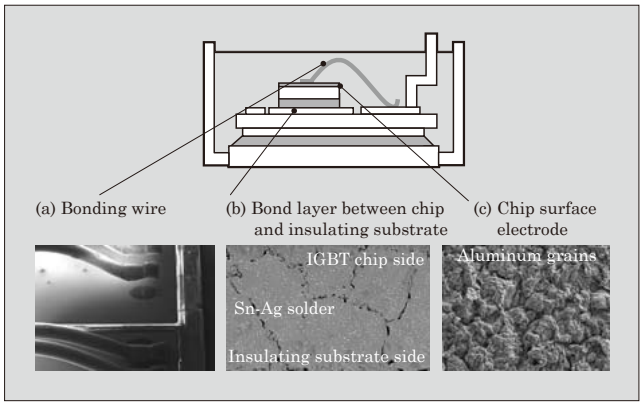

Fig.3 Fractures after power cycle testing (T_{jmax} = 175 °C)

must be taken into account in addition to the repetitive stress. The components in question are solder and aluminum. We therefore observed fractures in a module subject to the power cycle test at the continuous operational temperature of T_{jmax} 175 °C.

Figure 3 illustrates fractures under power cycle testing (T_{jmax}=175 °C). There are mainly three parts susceptible to fracture.

(a) Bonding wire

Sheer stress created by the difference in coefficient of thermal expansion between aluminum wire and silicon (Si) chip causes cracks in the base material, and eventually the wire detaches.

(b) Bonding between chip and insulating substrate

The solder used between the chip and insulating substrate undergoes microstructural changes and thermal fatigue, which exacerbate the development of cracks in the solder bonding portion.

(c) Chip surface electrode

Cracks are caused in the chip surface electrode due to coarsening of aluminum grains and the fact that aluminum has a coefficient of thermal expansion that is different from that of silicon. In order to secure continuous operation at T_{jmax} 175°C, lifetime of material in these three fracture areas need to be improved.

3. New Bonding Technology to Achieve High Reliability

3.1 New aluminum wire

Figure 4 shows a cross-section of aluminum wire after a power cycle test (T_{jmax}=175 °C; ΔT_j=75 °C). The bond was broken as the cracks developed within the aluminum wire material. This suggests that the lifetime primarily depends on the material strength of the aluminum wire.

Power cycle test at T_{jmax} 175 °C suggests that aluminum particles in the wire coarsen as they recrystallize because the temperature is within the recrystallization temperature range of the material.

The following Hall-Petch Equation expresses the relationship between metallic grain diameter and strength[3].

$$\sigma_y = \sigma 0 + k d^{-1/2} \quad \cdots\cdots (1)$$

σ_y : Yield stress
d : Average grain diameter of the metal
σ_0, k : Material dependent constants

The Hall-Petch Equation indicates that growth in metal grain size weakens the material. Therefore, Fuji Electric has developed new aluminum wire that has a recrystallization temperature higher than 175 °C. Figure 5 illustrates a cross-section of aluminum wire

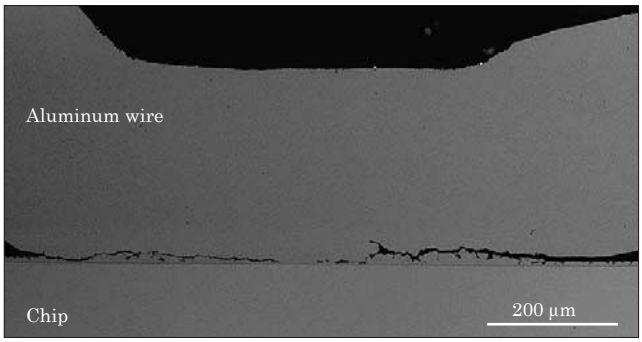

Fig.4 Cross-section of the bonding wire after power cycle testing

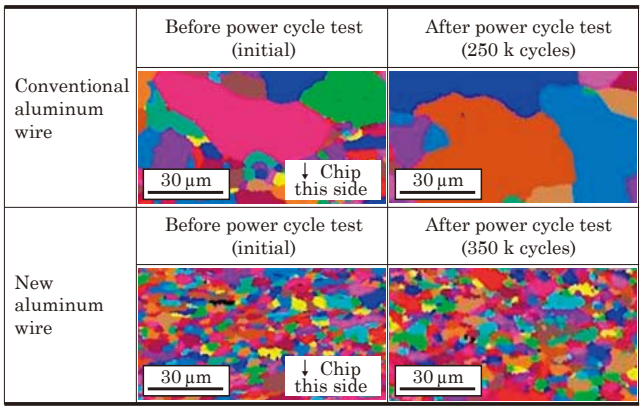

Fig.5 Cross-section of aluminum wire before and after power cycle test (T_{jmax} = 175 °C)

before and after a power cycle test (T_{jmax}=175 °C). This is a cross-section image using electron back scatter diffraction (EBSD). The aluminum grain growth was observed in the conventional wire after the power cycle test, but there was no change in the grain in the new aluminum wire. Therefore, it is supposed that the base material strength of the aluminum wire is not compromised by the power cycle test.

3.2 New solder

There is a concern that the degradation of solder layer between the chip and substrate due to heat and thermal fatigue is accelerated during the continuous operation at T_{jmax} 175 °C. We attempted to reinforce the soldering material against high temperature, based on microstructural considerations.

There are two methods to strengthen metal with additional elements: precipitation strengthening and solid-solution strengthening. Figure 6 shows structural models of solder before and after a thermal aging process*1. The diagrams depict microstructural changes in the metal caused by the strengthening methods. Sn-Ag solder is the representative of precipitation strengthening.

In this case, Ag_3Sn minuscule inter-metallic compounds precipitate between Sn particles, reinforcing the yield point of the grain boundary and preventing the development of cracks. However, Sn grains grow and Ag_3Sn aggregates under high temperature, resulting in cracks. On the other hand, Sn solder with added Sb and In within the solid solubility limit is the model for the solid-solution strengthening. The particles of Sb and In dissolve in the Sn grains to suppress coarsening under high temperature.

Figure 7 is an illustration of the tensile strength variance in solder after thermal aging test. Stored under the conditions of 150 °C and 175 °C for 1,000 hours, Sn-Ag solder significantly weakens from its initial

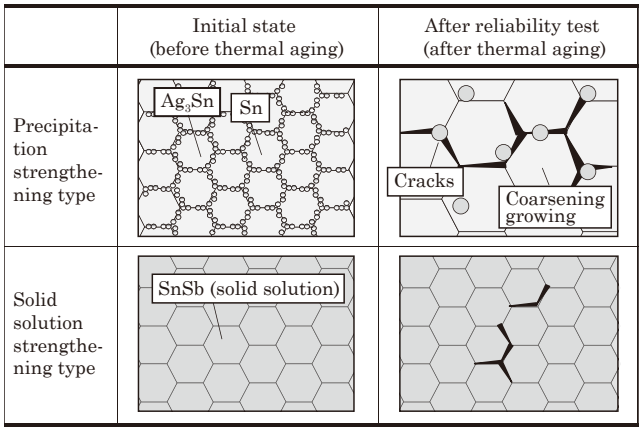

Fig.6 Structural diagram of solder before and after thermal aging

*1: Aging: a phenomenon in which metallic properties (for example hardness) change over time.

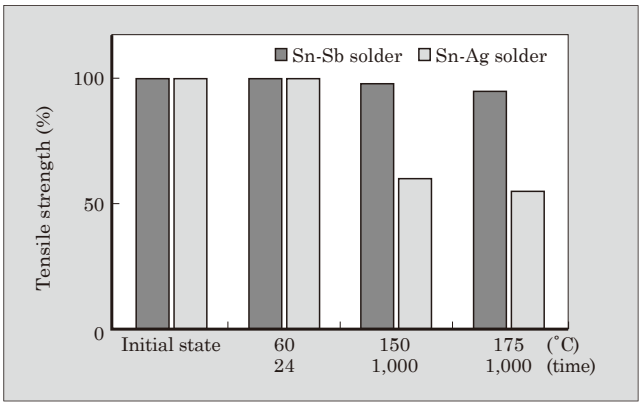

Fig.7 Tensile strength variance in solder after thermal storage test

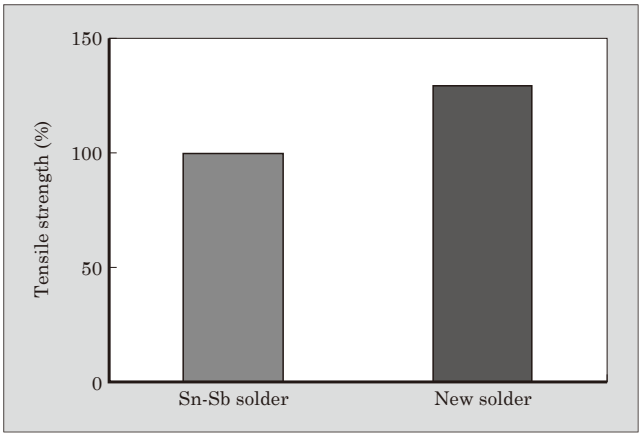

Fig. 8 Tensile strength of Sn-Sb and new solder

state while Sn-Sb maintains its strength. We also conducted a power cycle test (T_{jmax}=175 °C) using samples of both Sn-Ag and Sn-Sb solder to compare the effects on the power cycle lifetime. As a result, we verified that Sn-Sb had superior improvement of power cycle lifetime over Sn-Ag. Furthermore, by adding Sb in excess of the solid solubility limit, residual Sb precipitates as SnSb, creating an effect of the solid-solution strengthening and precipitation strengthening combined[4].

Leveraging this feature, Fuji Electric has developed a Sn-Sb-based new solder with additional new elements having characteristics of both solid solution strengthening and precipitation strengthening. This will be followed by mass production of the next-generation IGBT modules in the near future. Figure 8 shows the tensile strength of Sn-Sb and new solder. The new solder has a higher tensile strength than Sn-Sb solder. We have also verified its enhanced power cycle lifetime over Sn-Sb in a power cycle test (T_{jmax}=175 °C).

3.3 New surface electrode protection layer

Si chip surface electrode is usually made of pure aluminum or with Si or Cu compounds. In power cycle test, the surface electrode sustains stress due to coarsening of aluminum grains from the heat generated in

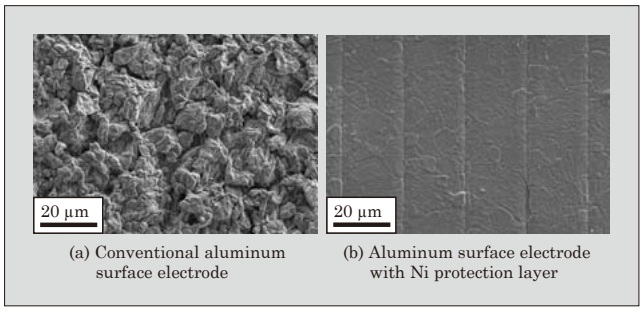

Fig.9 Surface electrode after power cycle test (T_{jmax}=175 °C)

the chip as well as from the difference in coefficient of thermal expansion from the Si chip, resulting in cracks caused in the surface electrode as well as in the aluminum wire bonding[5]. In order to prevent this, we have developed a structure with Ni, which has a coefficient of thermal expansion closer to silicon than to aluminum, forming a layer over the aluminum electrode to reduce the stress exerted upon it. Figure 9 illustrates the observation results from the power cycle test (T_{jmax}=175 °C) for a chip surface electrode without aluminum wire bonding. It is possible to lessen degradation by forming a protection layer over the aluminum electrode using Ni.

4. Effects of New Technology

We prepared a sample to which we applied the three new technologies described in Section 3 and conducted power cycle test.

Figure 10 shows the test results (T_{jmax}=175 °C). The new technology yielded a significant improvement

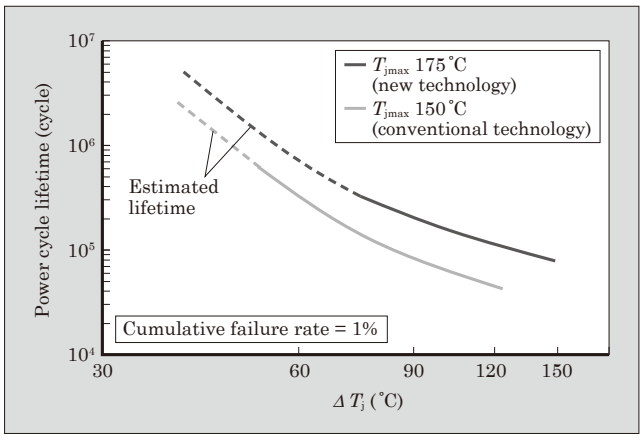

Fig.10 Power cycle test results (T_{jmax} = 175 °C)

at T_{jmax} 175 °C over the target power cycle lifetime of conventional technology at T_{jmax} 150 °C. The lifetime was more than doubled at all temperature regions.

5. Postscript

We have described the IGBT module assembly technology that accomplished reliable continuous operation at T_{jmax} 175 °C. The developed IGBT module has guaranteed continuous operation at T_{jmax} 175 °C while achieving a longer lifetime than conventional modules as a result of combining three new bonding technologies: new aluminum wire with high thermal resistance, new solder with high strength at high temperature and a new surface electrode protection layer providing high strength at high temperature and lower thermal stress between silicon and aluminum.

These technologies can be deployed without changing the current manufacturing processes at Fuji Electric, enabling easy mass production of items with guaranteed continuous operation at T_{jmax} 175 °C. By increasing high power density, improvements are expected to be made to the maximum power output of general-purpose inverters. We will continue our efforts with the development and expansion of offerings of the T_{jmax} 175 °C continuous operation guaranteed IGBT module family, and contribute to the improvement of industrial equipment for higher efficiency and better energy saving.

References

(1) Sakai, T. et al. Latest Technology for General-purpose Inverters and Servo Systems. FUJI ELECTRIC REVIEW. 2009, vol.55, no.4, p.154-161.
(2) Morozumi, A. et al. “Reliability of power cycling for IGBT power semiconductor modules” Proceedings IEEE, 36th Industry Applications Conference vol.3, p.1912-1918, 2001.
(3) N. J. Petch, J. Iron Steel Inst., 174, Part I. 1953, p.25-28.
(4) Morozumi, A. et al. Direct Liquid Cooling Module with High Reliability Solder Joining Technology for Automotive Applications, Proceedings of the 25th ISPSD & ICs, Kanazawa, May 26-30, 2013.
(5) Ikeda, Y. et al. “A study of the bonding wire reliability on the chip surface electrode in IGBT” Proceedings of the 22nd International Symposium on ISPSD, Hiroshima 2010.

High-Power IGBT Modules for 3-Level Power Converters

CHEN Shuangching* OGAWA Syogo* ISO Akira*

ABSTRACT

Recently, renewable energy has been attracting attention and, photovoltaic and wind power generation markets are growing rapidly in particular. In these fields, low- and medium-power IGBT modules are often connected in parallel to realize high power converters; but this will cause high surge voltage due to wiring inductance. Fuji Electric is developing one package for high-power IGBT modules for 3-level power converters. Improvement for power conversion efficiency and miniaturization of equipment can be expected. It has also realized a laminated structure for the main terminal bus bar to reduced internal inductance.

1. Introduction

Renewable energy has come to be valued more than ever in recent years for its role in the prevention of global warming and effective use of energy resources. For this reason, there is a fast-growing market for photovoltaic and wind-power generation systems as they provide power while lowering greenhouse gas (CO_2) emissions. Power electronics technology facilitates efficient use of electrical power, allowing for low CO_2 emissions in power generation, leading to wider use of renewable energy.

Fuji Electric is developing high-power insulated gate bipolar transistor (IGBT) modules for three-level power converters designed for high-power converters for photovoltaic and wind power generators. This paper describes their characteristic and features.

2. 3-Level Power Conversion

Two-level power conversion is common in electrical power conversion, but 3-level power conversion*1 is also available to enhance conversion efficiency. Having a neutral point, this method facilitates switching at half the voltage of 2-level power converters and gives advantages such as suppressing harmonics, reducing generated losses and enabling equipment miniaturization. There are two types of 3-level power conversion: a neutral-point-clamped type (NPC)[1], which has switching elements arranged in series, and an advanced T-type (AT)-NPC[2], which uses intermediate bidirectional switching.

*1: 3-level power conversion: see "Supplemental explanation 1" on p.255.

* Electronic Devices Business Group, Fuji Electric Co., Ltd.

Fuji Electric is focusing on developing 3-level modules to be applied for photovoltaic power generation and uninterruptible power supplies (UPSs). So far Fuji Electric expanded a line-up of low- to mid-power AT-NPC IGBT modules[2]-[4] which are contributing to efficiency improvement of equipment[5].

A multiple number of low/mid-power IGBT modules are commonly used in parallel to develop high-power photovoltaic power generators (mega solar) and UPSs. However, there are issues to overcome in using IGBT modules in parallel such as a high surge voltage, which occurs due to wiring inductance between modules or between the modules and the main circuit. There is also a tendency for the cooling fin to have a larger area when IGBT modules are used in parallel. For these reasons, high-power IGBT modules have been eagerly anticipated by the market.

3. Features and Electrical Characteristics of High-Power IGBT Modules for 3-Level Power Converters

3.1 Features

The high-power IGBT module for a 3-level power converter is a one-package IGBT module with AT-NPC/NPC conversion circuit and a thermistor. Figure 1 shows the external appearance of the IGBT module and Fig. 2 illustrates the equivalent circuit.

The maximum ratings of the module are 1,200 V/900 A for AT-NPC and 1,200 V/600 A for NPC. "V-Series" chips and reverse blocking (RB)-IGBT chips are used for the module. These modules leverage electromagnetic induction to keep the internal inductance within the IGBT module at a low level.

These modules have the following advantages against low/mid-power IGBT modules in parallel:

(a) Reduced internal inductance by one package

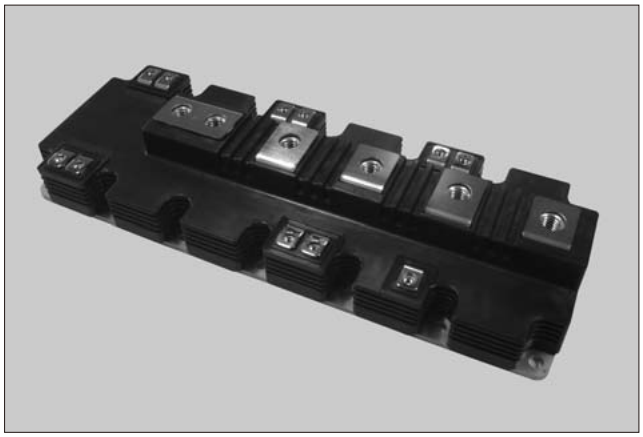

Fig.1 High-power IGBT modules for 3-level power converters

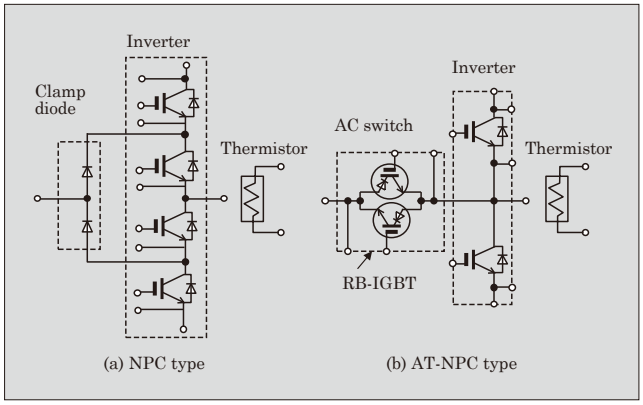

Fig.2 IGBT equivalent circuit

(b) Because of small mounting footprint and a smaller area for a cooling fin, miniaturization of equipment can be achieved

The external appearance of AT-NPC and NPC IGBT modules are the same. AT-NPC IGBT modules can reduce conduction losses because the inverter blocking voltage is identical to 2-level inverter, and the current passes through fewer devices than in the case of the NPC IGBT module. On the other hand, switching devices of NPC IGBT modules are in a serial connection. Therefore, the device blocking voltage is halved from a 2-level power converter, and the module is suited for high-voltage operations. The characteristics of the two IGBT modules are as follows:

(a) Switching voltage is half of that for a 2-level power conversion circuit, so that the switching losses of the converter can be reduced.
(b) Switching waveforms are stepwise, so that it can suppresses harmonics more than a 2-level power conversion. It makes it possible to fit smaller filters and therefore miniaturize the device.

3.2 Electrical characteristics of the IGBT modules

Table 1 shows types and device ratings of high-power IGBT modules for 3-level power converters. We have three different rated current products of AT-NPC IGBT modules for 1,000 V DC-bus application. We are also developing a NPC IGBT module for 1,500 V DC-bus application.

Table 1 Descriptions of IGBT modules

Type	Model	Package dimensions	Rated voltage	Rated current
AT-NPC	4MBI450VB-120R1-50	L250×W89×H38 (mm)	Inverter: 1,200 V AC switch: 900 V	450 A
	4MBI650VB-120R1-50	L250×W89×H38 (mm)	Inverter: 1,200 V AC switch: 900 V	650 A
	4MBI900VB-120R1-50	L250×W89×H38 (mm)	Inverter: 1,200 V AC switch: 900 V	900 A
NPC	4MBI600VC-120-50	L250×W89×H38 (mm)	1,200 V	600 A

The characteristics of the chips used are as follows:

(1) Inverter of AT-NPC IGBT module and NPC IGBT module

The latest "V-Series" IGBT chips and free-wheeling diode (FWD) chips are used.

(a) A field stop structure and trench-gate structure are optimized for the reduction of on-voltage $V_{CE(sat)}$ and switching losses.
(b) The turn-on di/dt controllability by gate resistance R_g was improved.

(2) AC switch of AT-NPC IGBT modules

Fuji Electric's RB-IGBT[6] having a junction isolation region and reverse blocking voltage is deployed to enable bi-directional switching.

(a) According to reverse blocking voltage of RB-IGBT, it is possible to switch in either direction by connecting the RB-IGBTs in antiparallel.
(b) Reverse recovery can be performed as FWD when forward bias voltage above the threshold is applied to the gate.

Figure 3 illustrates cross-sectional structures of IGBT and RB-IGBT chips. The RB-IGBT chip has a thick p+ junction isolation region covering the dicing side, which prevents the depletion layer from reaching the diced surface to secure the reverse blocking voltage.

Figure 4 shows the structure of a bi-directional switch. Bi-directional switches can be configured with the form of RB-IGBT or IGBT+FWD. IGBTs need to connect with diodes in serial because it is impossible to secure blocking voltage when reverse bias is applied to IGBT. This happens due to the facts that the PN junction, which supports the voltage, is in direct contact with the dicing surface, and that a large amount of carrier is generated because of the faults in high-density crystals created in the dicing process. Therefore, there is a problem that the on-voltage will be increased in case of IGBT+FWD. On the other hand, RB-IGBTs have lower on-voltage than the IGBT+FWD combination type owing to the structure with reverse blocking voltage. Lower on-voltage means less conduction losses.

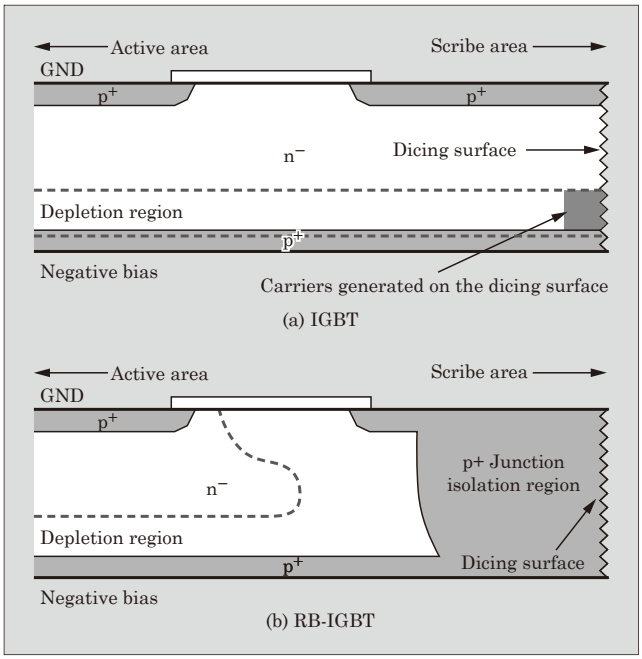

Fig.3 Cross-sectional structures of IGBT and RB-IGBT chips

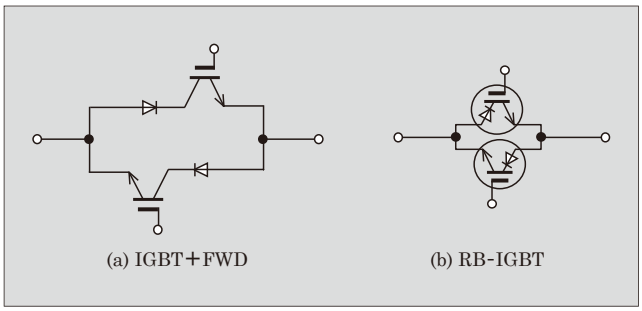

Fig.4 Structure of bi-directional switch

In the photovoltaic power system, 1,000 V DC bus is becoming a mainstream feature. With 3-level inverters at 1,000 V DC-bus application, the bi-directional switch is switched at 500 V. Therefore, intermediate devices in AT-NPC with a blocking voltage of 600 V may not withstand the voltage. On the other hand, raising the blocking voltage of devices to 1,200 V will result in reducing the rated current of the IGBT modules and increasing the conduction losses.

To address this issue, Fuji Electric is developing 900 V RB-IGBT to be adopted in a 1,000 V DC-bus application for the photovoltaic power system market. Figure 5 illustrates output characteristics of 900 V RB-IGBT and 1,200 V IGBT+FWD in the IGBT module with a rated current of 450 A. On-voltage of 900 V RB-IGBT is 30% lower than that of 1,200 V IGBT+FWD.

3.3 Switching waveforms

Fuji Electric AT-NPC IGBT modules provide two switching modes. Mode A runs on the basis of IGBT switching and RB-IGBT reverse recovery, and mode B lets the RB-IGBT do the switching and FWD performs the reverse recovery.

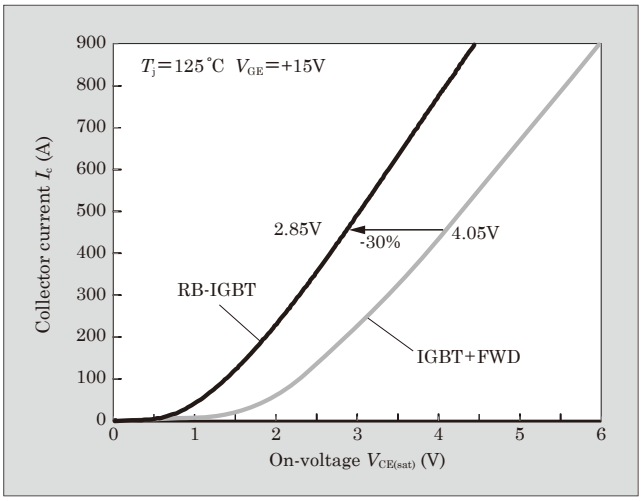

Fig. 5 Output characteristics of 900 V RB-IGBT chip and 1,200 V IGBT+FWD chip

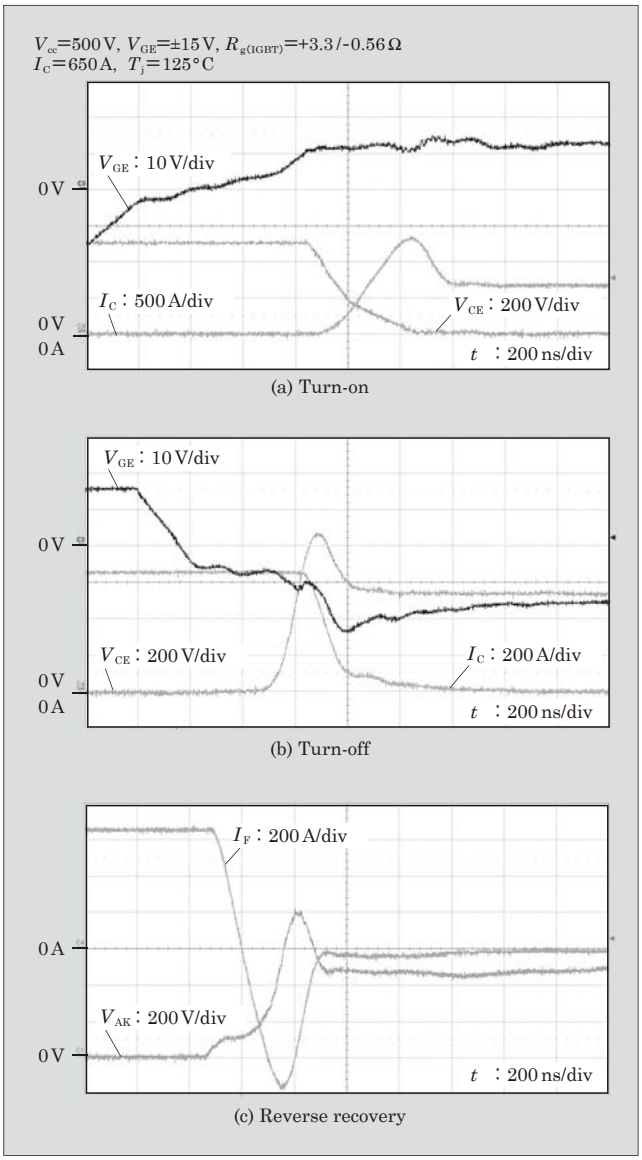

Fig.6 Switching waveforms of prototype IGBT module in switching mode A

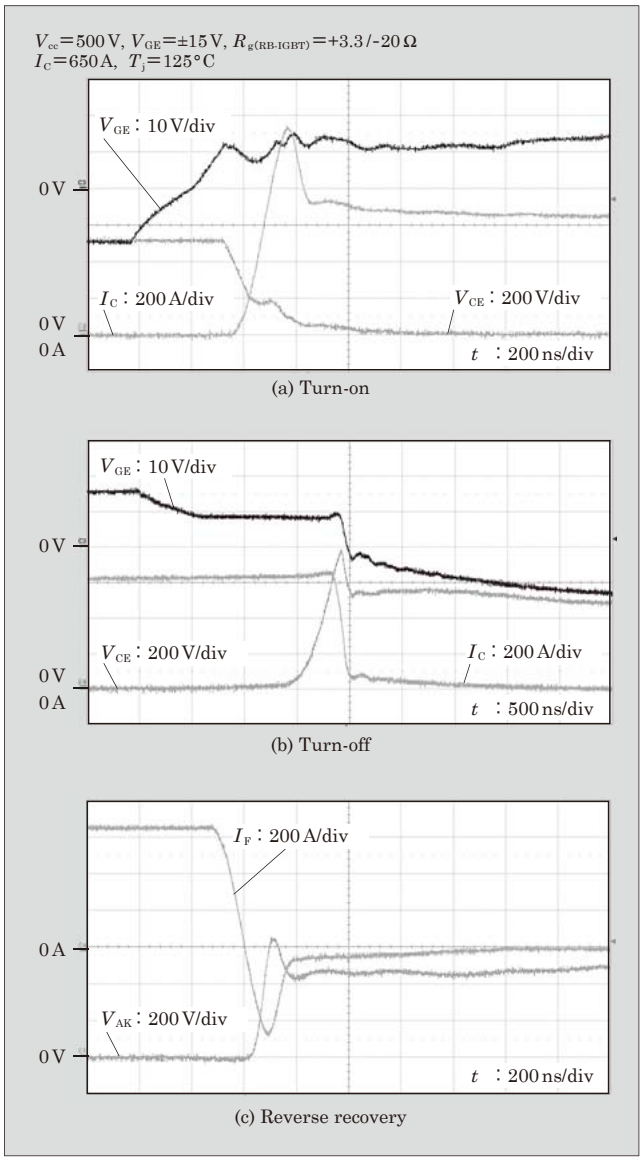

Fig.7 Switching waveforms of prototype IGBT module in switching mode B

Figures 6 and 7 show the switching waveforms of a prototype module (4MBI650VB-120R1-50). Figure 6 shows the waveforms in the mode A (V_{cc} 500 V, I_c 650 A, $R_{g(IGBT)}$ +3.3/−0.56 Ω, T_j 125 °C). The switching losses are 21.7 mJ at turn-on, 85.4 mJ at turn-off, and 76.4 mJ at reverse recovery. All waveforms are in good forms.

Figure 7 shows the waveforms in mode B (V_{cc} 500 V, I_c 650 A, $R_{g(RG+IGBT)}$ +3.3/−20 Ω, T_j 125 °C). The switching losses are 31.6 mJ at turn-on, 136.8 mJ at turn-off, and 35.3 mJ at reverse recovery. All waveforms are in good forms.

3.4 Package structures

The package structures are described below:

(1) Main terminals with P-M-N layout

The terminals are arranged for easy installation of a snubber capacitor to reduce surge voltage (between P and M, and M and N terminals).

(2) Environmental compliance

Lead-free solder is used to comply with the RoHS Directive*2.

(3) High blocking voltage package

The package structure supports 690 V AC input, and an insulation blocking voltage (V_{iso}) of AC 4 kV/min can be guaranteed.

(4) Ultrasonic bonding

Ultrasonic bonding is applied to this IGBT module with directly connecting copper terminals and copper patterns on direct copper bonding (DCB) substrate. High reliability is achieved due to the fact that the bonded surfaces have no difference in their thermal expansion coefficient. Tensile strength of conventional solder bonding will be reduced by approximately 50% after 300 cycles in a thermal cycle test (between −40 and +150 °C). The ultrasonic bonding hardly causes weakening of the tensile strength. Figure 8 shows the external appearance and cross-section of DCB substrate and the ultrasonic bonding.

(5) Low inductance

The parallel arrangement for P-M and M-N terminals realize low inductance by electromagnetic mutual induction. Compared with the M403 package, its volume increases approximately 2.36 times, but internal inductance is a maximum of 30nH and minimum of 18nH. The internal inductance is lower than M403 (33nH).

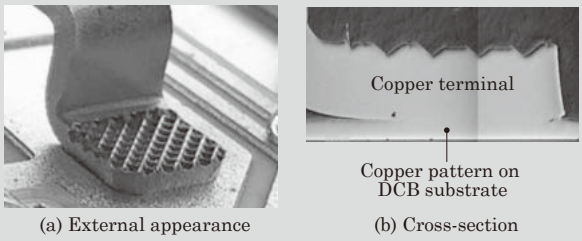

Fig.8 Ultrasonic bonding between DCB substrate and copper terminal

4. Postscript

This paper described the high-power IGBT modules for 3-level power converters, which Fuji Electric is developing. The IGBT modules feature high power, low inductance, high reliability, low power dissipation, and they are anticipated to apply to the renewable energy field.

We will continue enhancing the technologies for semiconductors and assembly to meet the needs, and

*2: RoHS Directive: The Restriction of Hazardous Substances Directive adopted by the European Union, specifying hazardous substances in electrical and electronic equipment and restricting their use.

develop products that contribute to the efficiency improvement of photovoltaic power system and UPSs.

References

(1) Nabae, A. et al. "A New Neutral-Point-Clamped PWM Inverter". IEEE Trans. on industrial applications. 1981, vol.1 A-17, no.5, p.518-523.

(2) Komatsu, K. et al. "New IGBT Modules for Advanced Neutral-Point-Clamped 3-Level Power Converters". IPEC '10 proceedings, 2010, p.523-527.

(3) Komatsu, K. et al. IGBT Module for Advanced NPC Topology. FUJI ELECTRIC REVIEW. 2011, vol.57, no.3, p.72-76.

(4) Komatsu, K. et al. IGBT Module Series for Advanced-NPC Circuits. FUJI ELECTRIC REVIEW. 2012, vol.58, no.2, p.50-54.

(5) Yatsu, M. et al. "A Study of High Efficiency UPS Using Advances Three-level Topology". PCIM '10 Europe, Proceedings. 2010, p.550-555.

(6) Wakimoto, H. et al. "600 V Reverse Blocking IGBTs with Low On-state Voltage". PCIM '11 Europe. Proceedings, 2011, p.317-322.

Packaging Technology of IPMs for Hybrid Vehicles

GOHARA Hiromichi * ARAI Hirohisa ‡ MOROZUMI Akira *

ABSTRACT

Intelligent power modules (IPMs) control the power of hybrid vehicles. IPMs are needed to be downsized and lightweight due to the request for fuel efficiency and comfort. To achieve these requirements, Fuji Electric has developed a high-capacity IPM for hybrid vehicle integrated buck-boost converter and two inverters. This time, we have developed cooling design technology and high-strength solder technology, which realize a direct liquid cooling module with an integrated aluminum heat sink. This product has achieved a product volume reduction of 30% and mass reduction of 60% compared with the conventional indirect cooling structures and high reliability required for vehicles. The mass production of the product has already begun.

1. Introduction

Prevention of global warming and effective use of resources are gaining importance as activities shared by all the countries of the world. In the automobile industry, the development of hybrid electric vehicles (HEVs) and electric vehicles (EVs) are accelerating. In this situation, Fuji Electric started mass production of intelligent power modules (IPMs) for HEVs in December 2012. This product integrates inverter units for controlling two motors and a buck-boost converter unit, and realizes the high output required for HEVs with a compact and lightweight module. We have used low-loss sixth-generation insulated gate bipolar transistors (IGBTs) and free-wheeling diodes (FWDs) for high efficiency. Direct liquid cooling structure was realized to enhance the cooling performance. Lightweight aluminum was applied to a heat sink to reduce the weight.

In addition, it is equipped with a high-precision buck-boost control function and high-precision chip temperature communication function besides the IBGT protection function.

This paper presents an overview of the product and describes two new packaging technologies. One is cooling design technology with the direct liquid cooling structure and the other is high-strength soldering technology that allows solder bonding between aluminum, which has a large coefficient of thermal expansion, and an insulating substrate.

2. Overview of Product

Figure 1 shows the external picture of the developed IPM and Fig. 2 the circuit configuration. With conventional IPMs, it was common that the inverter unit–power drive unit (PDU)–and buck-boost converter unit–voltage control unit (VCU)–are mounted on them with configuring different modules for respective functions. This product is an all-in-one package integrating the two inverter units, buck-boost converter and controller (gate driver) and achieves high output with a small and lightweight module.

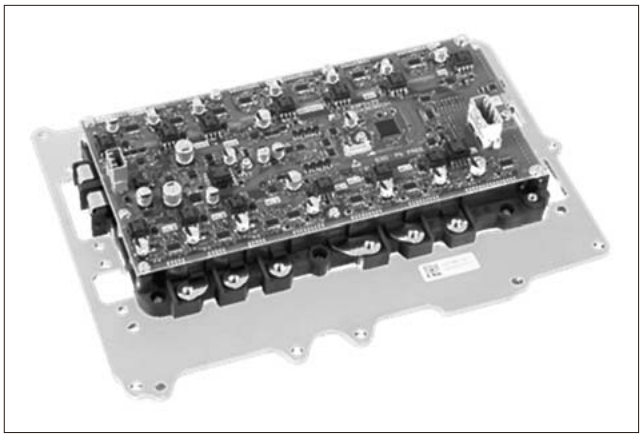

Fig.1 IPM for HEV

2.1 Structural characteristics

The following describes the major structural characteristics.

(a) 1,200 V/500 A, 14 in 1 IPM
(b) Size: L340×W233×H70 (mm) (30% volume reduction from previous product)
(c) Mass: 3.6 kg (60% mass reduction from previous product)
(d) High cooling performance due to aluminum direct liquid cooling structure
(e) Mounted with low-loss sixth-generation IGBTs

* Corporate R&D Headquarters, Fuji Electric Co., Ltd.
‡ Electronic Devices Business Group, Fuji Electric Co., Ltd.

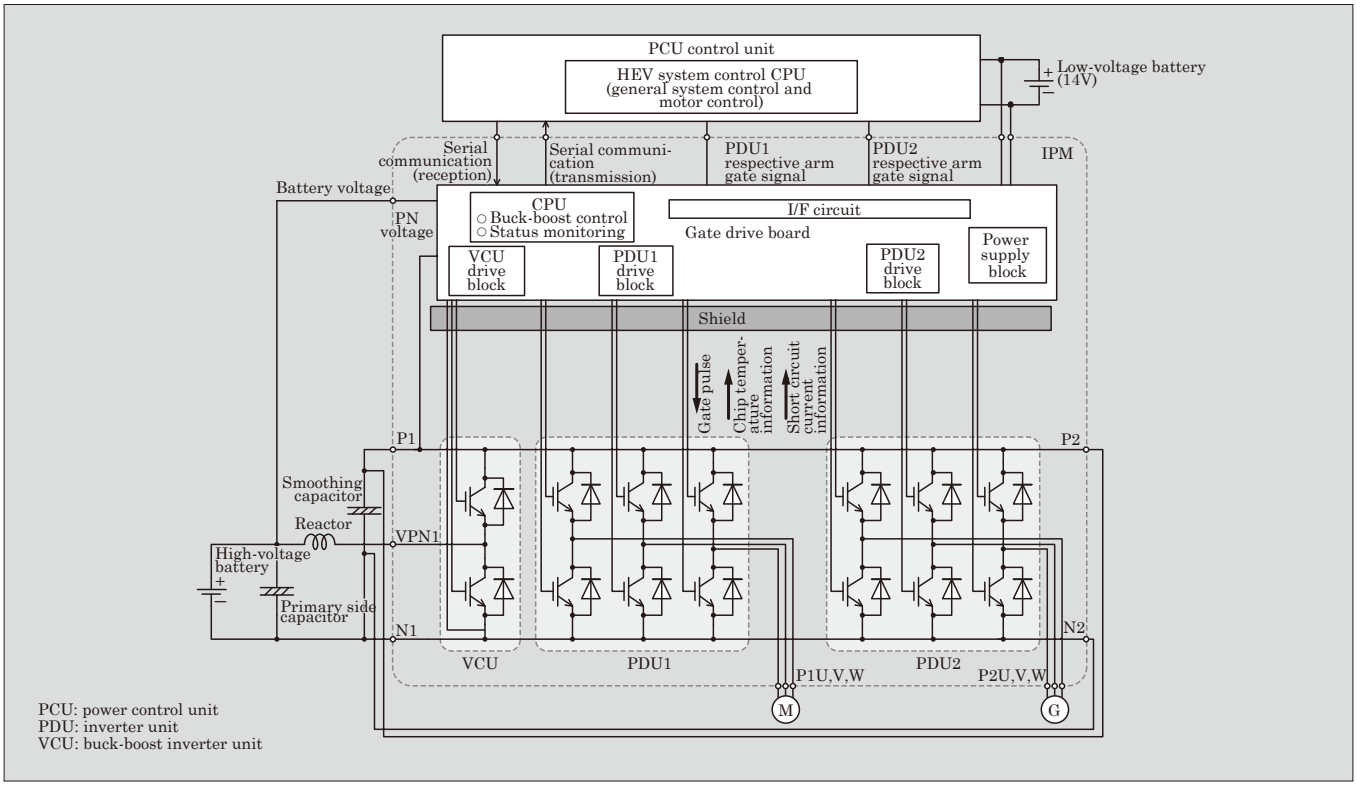

Fig.2 IPM circuit configuration

and FWDs

A gate drive board is placed on the module to realize the high functionality as described in Section 2.2

2.2 Functional characteristics

The following describes the major functional characteristics.

(a) Power supply for respective outputs generation from low-voltage battery

Insulated power supply with 18 outputs including IGBT driver power supply is provided.

(b) Built-in protection function for short-circuiting, overheat and power supply voltage drop

(c) High-precision IGBT chip temperature communication

(d) Gathering of operating status information and serial communication by integrated CPU

IPM operating status information and alarm information from the IGBT drive circuits are used for linking with the upper level to handle abnormal statuses.

(e) Buck-boost control by high-precision voltage measurement of high-voltage battery

The high-voltage battery voltage and PN voltage are monitored by the integrated CPU with instructions from the upper level for constant voltage control. For voltage measurement, high precision is achieved by CPU correction.

This product helps to achieve the industry's best fuel efficiency of high-output HEVs*1.

3. Characteristics of Direct Liquid Cooling Structure

3.1 Direct liquid cooling structure with aluminum heat sink

Figure 3 describes the cross-section structure of the power module unit. Figure 3 (a) shows an indirect liquid cooling structure, which is a common cooling method. With the focus on cooling performance, this structure uses copper for the base plate. However, thermal grease with a low thermal conductivity of 1 W/(m·K) was used for thermal bonding between the base plate and the heat sink, which caused the thermal resistance to increase. For this reason, cooling performance was insufficient in the environment of a vehicle engine compartment with high ambient temperature. In addition, the high specific gravity of copper led to an increase in the mass of the power module unit, and this hindered the improvement of the vehicle's fuel ef-

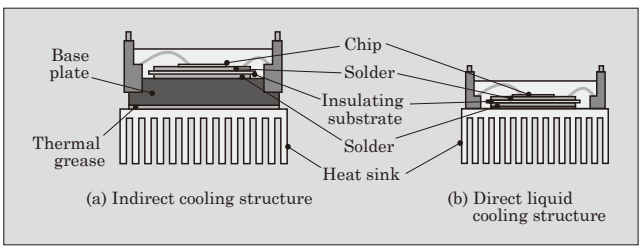

Fig.3 Cross-section structure of power module unit

*1: Highest fuel efficiency in class as of January 2013.

Table 1 Fundamental physical properties of insulating substrate and heat sink materials

	Thermal conductivity [W/(m·K)]	Thermal expansion coefficient (ppm/K)	Density x 10^{-6} (kg/mm^3)
Silicon nitride	90	3.4	3.3
Aluminum nitride	170	4.6	3.3
Copper	393	16.5	9.0
Aluminum	170	23.5	2.7

ficiency.

Figure 3 (b) shows a direct liquid cooling structure that uses an aluminum heat sink. This structure eliminates the need for the base plate and thermal grease by solder bonding the insulating substrate and aluminum heat sink, resulting in successful reduction of thermal resistance by 30%. By using aluminum for the heat sink, the mass has been reduced to 1/3 of the existing structure of a copper heat sink, and corrosion resistance against long life coolant (LLC) has also been achieved.

3.2 Technical issues with adoption of aluminum heat sink

This product is an all-in-one package and, for preventing thermal coupling between IGBTs due to high integration, improvement in cooling performance is required. Table 1 shows the fundamental physical properties of the insulating substrate and heat sink materials. Aluminum has 1.5 times larger thermal expansion coefficient than copper. This causes higher stress to be applied on the solder bonding between the aluminum heat sink and insulating substrate than the conventional product, and hence further strength enhancement was necessary. There are two issues to overcome for realizing a direct liquid cooling structure using a lightweight aluminum heat sink:

(a) Improvement in cooling of aluminum heat sink
(b) Solder life time of thermal cycling test

In order to solve these issues, we have attempted to improve the cooling design technology and developed a high-strength solder.

4. Cooling Design of Aluminum Direct Liquid Cooling Structure

4.1 Relation between IGBT chip temperature and coolant temperature

In a liquid cooling structure, heat generated from IGBTs and FWDs is dissipated from the coolant through the module material and heat sink. Figure 4 shows the relation between the IGBT chip temperature and coolant temperature.

The IGBT chip temperature is highly dependent on the coolant temperature and is less correlated with the flow rate change. That is, lowering the coolant temperature is more effective than increasing the flow rate

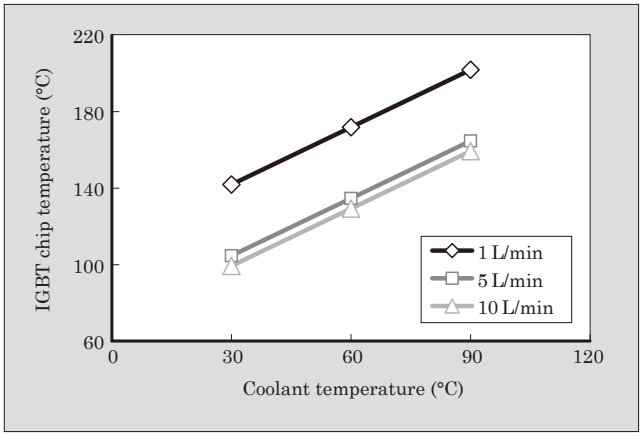

Fig.4 Relation between IGBT chip temperature and coolant temperature

of the coolant that flows through the heat sink to lower the IGBT chip temperature, or reducing the thermal resistance.

4.2 Flow channel design

It has been clear that the temperature of the coolant under the IGBT chips has an influence on the cooling performance and we have used a flow channel design with the coolant temperature taken into account.

Figure 5 shows heat sink and flow channel configuration examples. Type A is a structure in which the coolant flows in the longer direction with reference to the cooling unit. Meanwhile, Type B has a structure with the coolant flowing in the shorter direction and the number of devices that can be arranged for a coolant flow is less than that of Type A. The fewer the number of devices, the smaller the temperature increase of the coolant.

The structure that allows the device temperature to be lowered more is Type B, which coincides with the thermo-fluid analysis result. Making the cooling unit wider as in Type B allows the pressure loss of the heat sink to be reduced. The rate of flow in the cooling unit is inclined to be uneven, and we prevented this by optimizing the cooling structure.

4.3 Optimization of flow rate distribution

For improving the cooling performance, it is important to improve the heat exchange performance of the cooling fins not only by keeping the coolant at low temperature but also by increasing the flow rate. This

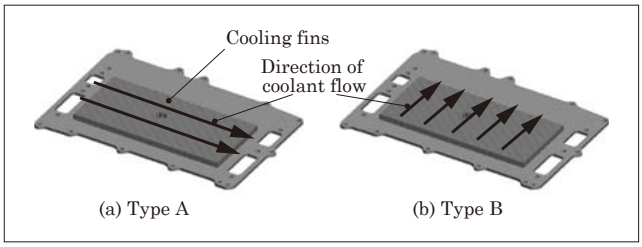

Fig.5 Example of heat sink and flow channel configuration

product is a module integrating three functions and the respective function has different maximum heat generation condition. Accordingly, we attempted to improve the cooling performance by providing optimized distribution of the coolant according to the heat generation distribution of each IGBT.

Figure 6 shows an image of the flow rate distribution of the coolant flowing in the heat sink. The rates of flows between fins are indicated by arrows. Before improvement, as shown in Fig. 6 (a), the flow resistance decreases and the flow rate increases as the distance from the inlet becomes longer. With this product, the heat generation density of PDU1 is higher than those of PDU2 and VCU. It is necessary to increase the flow rate of the coolant in a portion with a higher heat generation density. In order to adjust the flow rate distribution of the cooling unit, we have provided resistors in the channel as appropriate, as shown in Fig. 6 (b). This has allowed the flow rate distribution to be controlled according to the heat generation density[1].

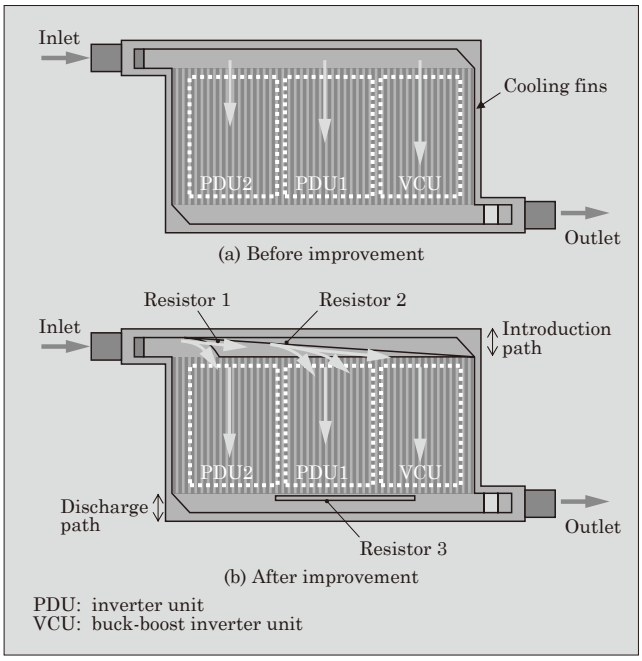

Fig.6 Image of coolant flow rate distribution

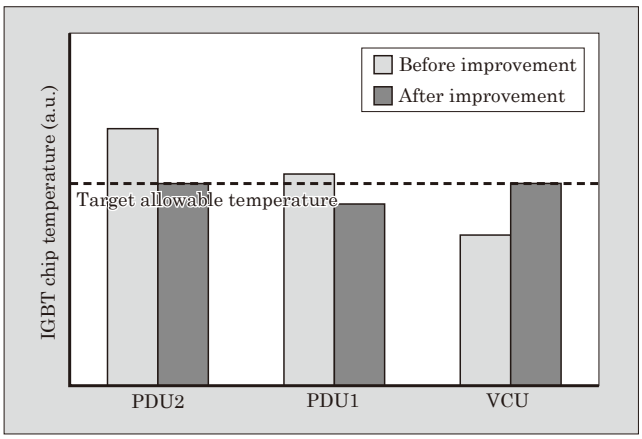

Fig.7 IGBT chip temperature before and after optimization

Figure 7 shows a comparison of IGBT chip temperature before and after the optimization. The temperature of each device has been averaged to equal to or lower than the target allowable temperature of the device by optimizing the flow rate distribution[2].

5. High-Strength and High-Reliability Solder

The thermal expansion coefficient of aluminum, which constitutes the heat sink material, is 23.5 ppm/K, or approximately 1.4 times that of copper, and the stress on the solder layer increases. To address this issue, we have developed a high-strength solder that ensures the service life required for in-vehicle products.

5.1 Development concept

Figure 8 shows a schematic diagram of the solder structure after a reliability test. It illustrates changes of the microstructure of solid solution strengthening and precipitation strengthening under high temperature, as metal strengthening mechanisms. Conventionally, solders using a single strengthening mechanism have been used. For even higher reliability, we worked on developing a high-strength solder that combines two strengthening mechanisms.

For the development, commonly used Sn (tin) has been selected as the base material and, Sb (antimony), which has been proven as material effective for improving mechanical characteristics and heat resistance, has been selected as the second element. With the additive amount of Sb with reference to Sn equal to or smaller than the solid solubility limit, solid solution strengthening is expected to become effective[3]. In addition, when the additive amount of Sb is increased to higher than the solid solubility limit, an SnSb compound that cannot dissolve will separate. Simultaneous appearance of two mechanisms of strengthening, namely solid solution strengthening and precipitation strengthening, gives rise to expectations for suppressing grain boundary cracking[4, 5].

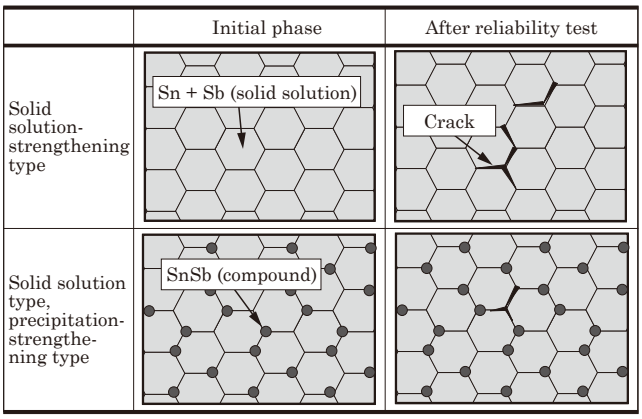

Fig.8 Schematic diagram of solder structure after reliability test

Based on this idea, we have verified the influence of the additive amount of Sb on the solder material characteristics.

5.2 Influence of Sb additive amount on solder strength

In order to demonstrate the development concept described in Section 5.1, we have conducted strengthening evaluation on two types of Sn-Sb solders with different additive amounts of Sb: Type 1 and Type 2. With Type 1, the additive amount of Sb was adjusted to equal to or smaller than the solid solubility limit with reference to Sn. With Type 2, the additive amount of Sb was adjusted to larger than the solid solubility limit.

Figure 9 shows the results of tensile tests using solders Type 1 and Type 2. The tests were conducted under room temperature conditions with JIS-compliant specimens molded by casting them into the respective compositions. Based on the results, we have confirmed that Type 2, which added more Sb than the solid solubility limit, presented strength at least 1.5 times that of Type 1, and we confirmed that strength enhancement can be realized by precipitation strengthening.

Then, in order to evaluate the heat resistance of solder Type 2, we examined the strength change after high-temperature aging*2 by simulating the actual operating environment. Figure 10 shows the tensile strength after high-temperature storage as compared with the initial strength. In this examination, Sn-Ag solder, which is a representative precipitation-strengthening solder, is used for comparison.

Type 2 solder maintains the initial strength after 1,000 hours at both 150 °C and 175 °C. Meanwhile, the Sn-Ag solder had its strength in a high-temperature environment reduced by approximately 40% as compared with the Sn-Sb solder (Type 2).

As a result of this, we have confirmed that combining solid solution strengthening and precipitation strengthening provides excellent strength in high-temperature conditions and satisfactory heat resistance.

Then, we carried out reliability evaluation on Type 2.

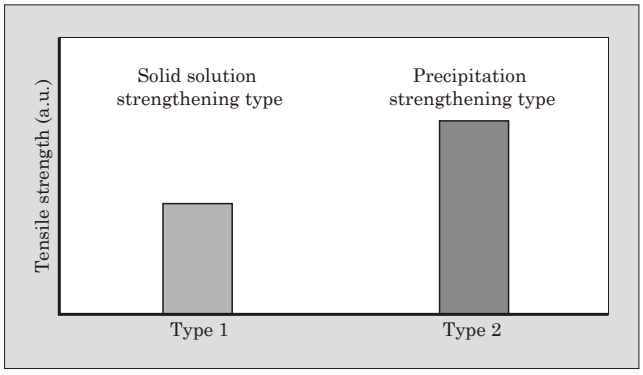

Fig.9 Comparison of tensile strength of Sn-Sb solder

*2: Aging: a phenomenon in which metallic properties (for example hardness) change over time.

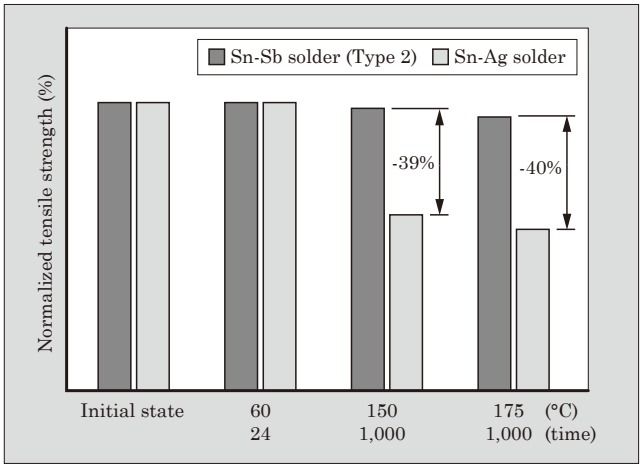

Fig.10 Tensile strength after high-temperature storage test

5.3 Reliability evaluation of Sn-Sb solder

We made specimens with the insulating substrate solder-bonded to an aluminum plate and carried out temperature cycle lifetime evaluation. The test was conducted under the conditions of −40 to +105 °C for temperature cycle evaluation and the crack length was imaged by a scanning acoustic tomograph (SAT) for measurement.

As result of comparing Sn-Sb and Sn-Ag solders, Fig. 11 shows SAT images of solder bonding after 2,000 cycles in the temperature cycle test, and Fig. 12 shows

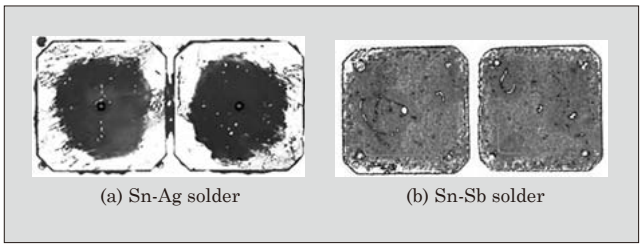

Fig.11 SAT images of solder bonding after temperature cycle test

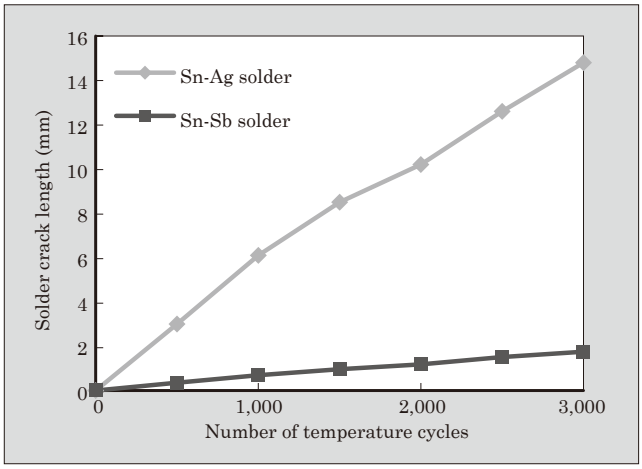

Fig.12 Crack length increase in temperature cycle test

the crack length increase of the respective solders in the temperature cycle test.

The SAT images show areas with cracks progressing in white. Specimens that use the Sn-Sb solder show only minor progress of cracks. On the other hand, a noticeable progress of cracks is observed in specimens that use the Sn-Ag solder. Accordingly, the Sn-Sb solder has been confirmed to have higher durability than the Sn-Ag solder.

We have, therefore, made it clear that the developed Sn-Sb solder ensures high reliability in bonding between the insulating substrate and aluminum heat sink, which have significantly different thermal expansion coefficient.

6. Postscript

This paper has outlined the intelligent power module (IPM) for hybrid vehicles and described two packaging technologies.

Packaging technologies support customers with inverter development and design. We intend to use these technologies as the basis for working on further technological innovation to offer products that contribute to high efficiency and energy conservation.

References

(1) Gohara, H. et al. Cooling device for semiconductor module and semiconductor module. Patent Application. PCT/JP2012/072554.

(2) Saito, K.; Otuka, H. "Development of PCU for a new HEV drive". Proceedings of Japan Society of Automotive Engineers Annual Congress (Spring). Kanagawa, Japan, 2013.

(3) Nishiura, A, Morozumi, A. "Improved life of IGBT module suitable for electric propulsion system". Proceedings of the 24th EVS, Stavanger, 2009.

(4) Morozumi, A. et al. "Direct Liquid Cooling Module with High Reliability Solder Joining Technology for Automotive Applications". Proceedings of the 25th ISPSD & ICs, Kanazawa, 2013.

(5) Saito, T. et al. "New assembly technologies for Tjmax=175°C continuous operation guaranty of IGBT module". Proceedings of PCIM Europe 2013, Nuremberg, p.455-461.

IGBT Modules with Pre-Applied TIM

ISO Akira* YOSHIWATARI Shinichi*

ABSTRACT

When an IGBT module is mounted, thermal grease is applied between the cooling fin and the IGBT module to promptly transfer the heat generated from the IGBT module. An increasing number of customers are requiring IGBT suppliers to perform this thermal grease application. To meet this requirement, Fuji Electric has developed a family of IGBT modules with pre-applied thermal interface material (TIM) of phase change type. The adopted TIM features a high heat dissipation performance that is three times or better than that of the conventional products, and is liquefied at around 45 °C and solidified below that temperature, thus offering ease of transportation. This has realized IGBT modules with improved heat dissipation properties and reliability (thermal management).

1. Introduction

Insulated gate bipolar transistor (IGBT) modules are a vital component in various fields such as renewable energy (photovoltaic and wind power generation), automobiles, industrial equipment and social infrastructure. It is particularly important to improve aspects such as generated loss, heat dissipation properties and reliability for the improvement of the IGBT module features.

This paper describes an IGBT module with pre-applied thermal interface material (TIM) that improved heat dissipation properties and reliability (thermal management).

2. Background

Energy losses in power conversion in IGBT modules occur in the form of heat dissipation. Heat dissipation properties significantly affect the product lifetime and performance in power conversion. It is a common practice to apply thermal grease for conducting heat between the IGBT module and air/water cooling fin[(1)]. The thermal grease that is referred to as 1 W has a thermal conductivity of around 1 W/(m·K), and it is often used for this purpose. Application patterns and applied quantity are very important[(2)]. In recent years, an increasing number of customers have been requesting IGBT suppliers to perform thermal grease application in order to avoid incurring costs for application tools and grease printers, which would be necessary for assuring accurate application processing. In order to meet such demand, Fuji Electric has developed an IGBT module with pre-applied TIM. For this module, a 3 W-class TIM has been adopted, which has a heat dissipation performance that is three times or more effective than the conventional type. It is a phase-change type, with the property of liquefying around 45 °C but solidifying under this temperature for ease of transportation.

Although it is difficult to control the wet-spread of phase-change type TIMs, Fuji Electric has realized it by using the stencil mask designed by ourselves.

3. Characteristics of Phase-Change Type TIM

The most significant feature of the newly developed IGBT module with pre-applied TIM is the use of the phase-change type TIM. This TIM has the following characteristics:

(a) It comes initially in a grease form.
(b) It transforms into rubber-like form by heat-treating to remove volatile solvent.
(c) It reverts to greasy consistency once further heated up beyond certain temperature.

The TIM usage procedures are as follows:

(a) Apply the grease-form TIM onto the IGBT module. A stencil mask should be used to even out the applied grease in patterns.
(b) Heat up the grease to remove volatile solvent and change it into a rubber-like form. As the TIM is solidified, the module can be packed for transportation.
(c) Mount the modules onto a heat sink at normal temperature.
(d) Activate the device: the heat generated by the IGBT module transforms the TIM into grease and it spreads over a cooling fin evenly.

The procedure is illustrated in Fig. 1.

Table 1 shows a comparison between conventional and phase-change type thermal grease. The thermal conductivity is 0.9 W/(m·K) for the conventional

* Electronic Devices Business Group, Fuji Electric Co., Ltd.

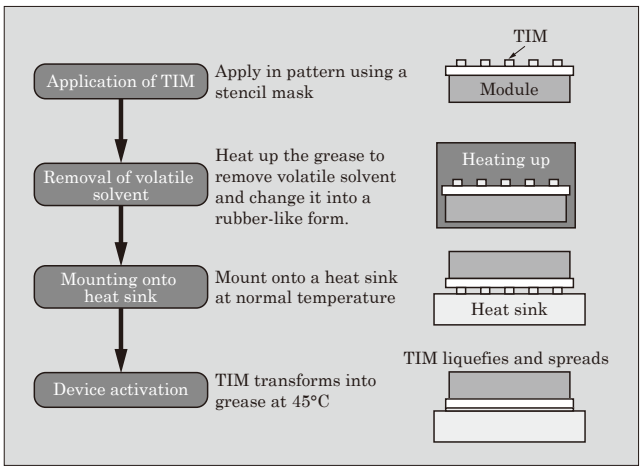

Fig.1 Phase-change TIM application procedure

Table 1 Basic specifications of TIMs

Product name	Newly developed product (phase-change TIM)	Conventional product A (thermal grease)	Conventional product B (thermal grease)
Appearance	Gray	White	White
Base oil	Non-silicon	Silicon	Non-silicon
Consistency (Pa・S)	135	39	195
Thermal conductivity [W/(m・K)]	3.4	0.9	0.9

grease, and it is 3.8 times higher for the phase-change TIM at 3.4 W/(m・K).

4. Performance of IGBT Module with Pre-Applied TIM

We conducted a performance test on the IGBT module with pre-applied TIM. The module and TIM subjected to the test are as follows:

○ Tested module: 1,200 V/600 A IGBT (2MBI600VJ-120)

○ Applied TIM: phase-change TIM

4.1 Wet-spreading property

The TIM was applied using the stencil mask designed by Fuji Electric[3], and dried for 20 minutes at 60 °C (manufacturer's recommendation) before the module was mounted on a glass block at a rated torque (see Fig. 2). The module activation was simulated by storing the modules in an oven at 60 °C, and test pieces were removed from the oven after the durations of 10, 30 and 60 minutes to verify the wet-spreading of TIM (wet-spreading property). The module temperature in the oven is shown in Fig. 3. We verified that the phase change from rubber-like form to grease-like form took place after 10 minutes of heating, and the grease-form TIM wet-spread satisfactorily in 50 minutes (see Fig. 4).

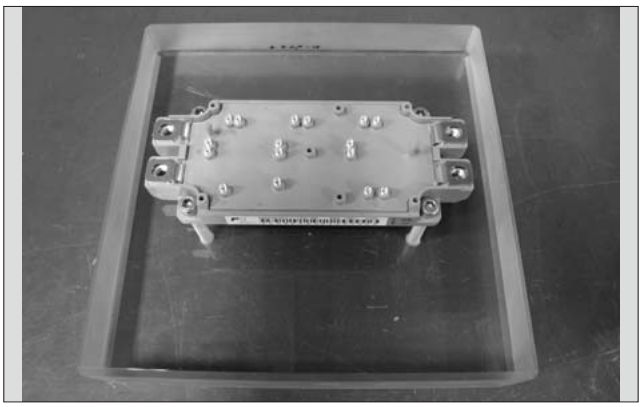

Fig.2 Glass block mounted condition

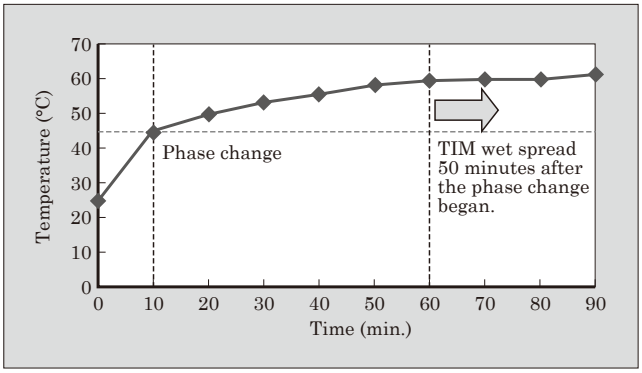

Fig.3 Module temperature when heated in oven

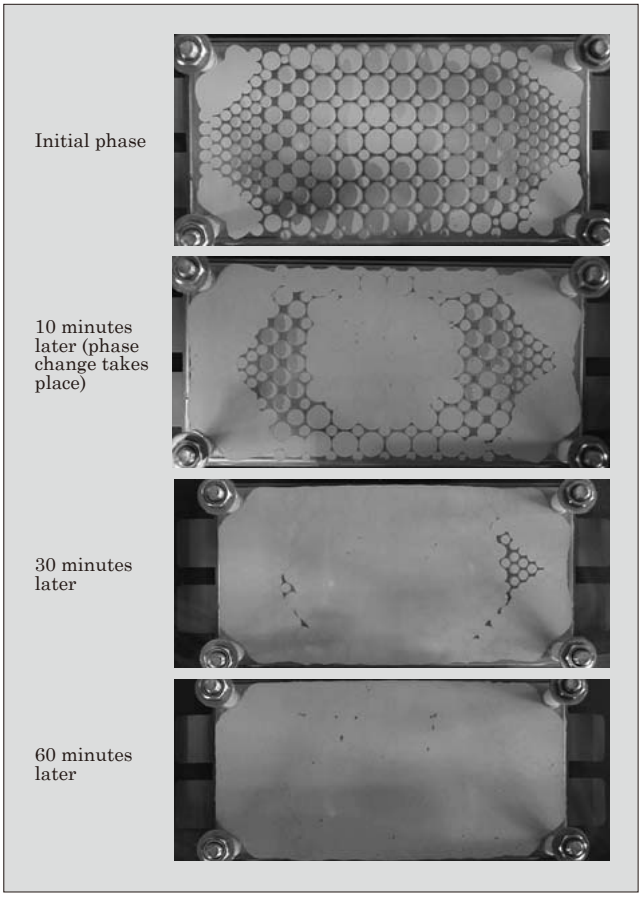

Fig.4 Wet-spreading property of TIM

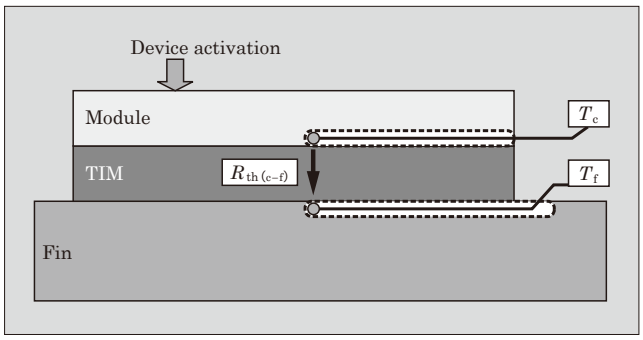

Fig.5 Thermal resistance measurement method

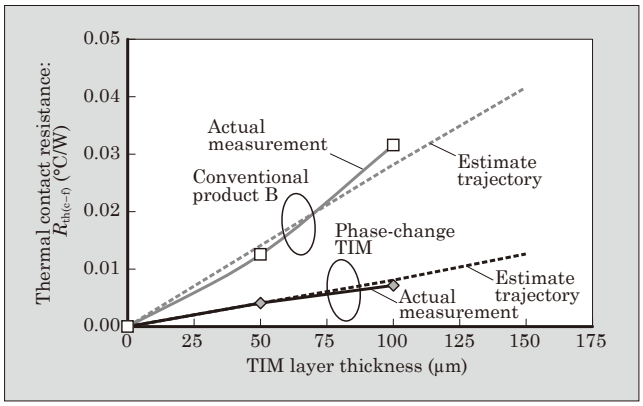

Fig.6 Comparison of thermal contact resistance

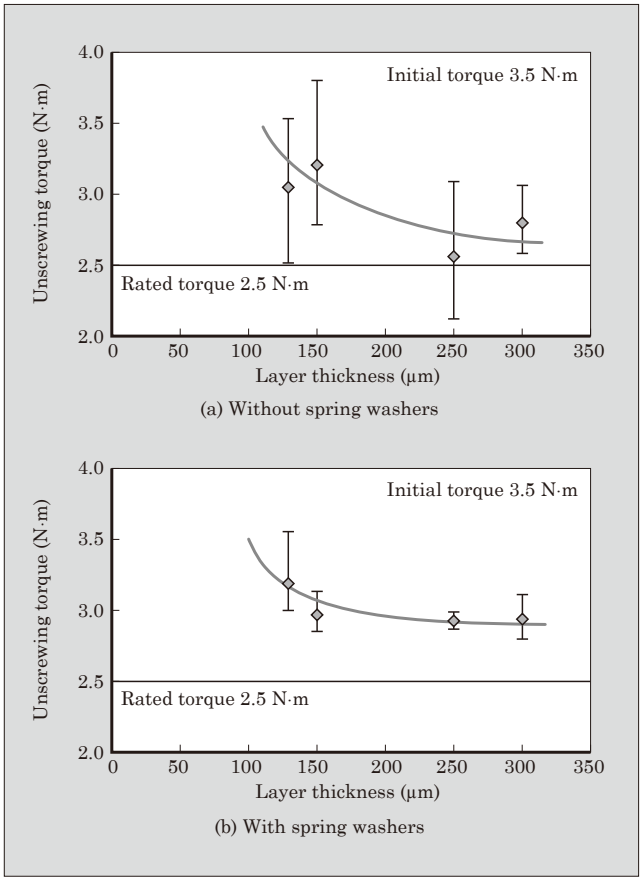

Fig.7 Torque loss assessment

4.2 Thermal contact resistance

We verified the effects in reducing thermal contact resistance obtainable by replacing 1 W thermal grease with 3 W phase-change TIM. Figure 5 illustrates the measuring procedure of thermal contact resistance. Thermocouples are attached to both the module and fin, and the thermal contact resistance was calculated using Equation (1).

$$R_{th(c-f)} = (T_c - T_f)/P \quad \cdots\cdots (1)$$

$R_{th(c-f)}$: thermal contact resistance
T_c : temperature of the module casing
T_f : temperature of the fin
P : power applied to the device

Figure 6 shows the measurement results. The measured thermal contact resistance was approximately identical with the calculated value, and it was able to be decreased to a third of the conventional one.

4.3 Torque loss

In terms of heat dissipation properties, there is another point for consideration apart from the performance of TIM: torque loss during heat-sink mounting. It is a phenomenon of decrease in the torque of the screws securing the module on the heat sink (screws loosen). It occurs when the TIM liquefies and spreads, and thereby the layer becomes thinner. This tends to occur more easily when the initial TIM layer is thicker. In addressing this issue, we recommend the use of spring washers for the fixing screws of heat sinks. We verified that using spring washers allowed the heat sink to be mounted without a torque loss issue (see Fig. 7). Regarding torque loss assessment, return torque is defined as the maximum torque at loosening a screw after tightening with initial torque of 3.5 N・m. When a return torque is larger than a rated torque, we judge it normal. Although a degree of torque loss occurred against the tightened torque of 3.5 N・m, the tightened torque did not decrease less than the rated torque of 2.5 N・m even if a layer thickness is increased. It gives the equivalent result as that of using the conventional thermal paste.

5. Future Development

Currently, M254 and M629 are the two available package types of IGBT modules with pre-applied TIM. We have already commenced the development of M271 and M272 package offerings and will extend the range for other types of packages in the future.

IGBT modules with pre-applied TIM are expected to be marketed to an increasing number of customers who demand grease application of IGBT suppliers because they are improved in heat dissipation and can be transported with TIM being applied (see Fig. 8).

Fig.8 Shipping arrangement

6. Postscript

In this paper, we described the IGBT module with pre-applied TIM that improved heat dissipation properties and reliability.

We will continue expanding the product range to meet customer needs and further improve the thermal management technologies for IGBT modules by developing TIM and other high heat dissipating materials for the development of new products.

References

(1) Momose, F. Thermal management of IGBT module systems, PCIM Asia'.

(2) FUJI IGBT MODULES APPLICATION MANUAL. "Chapter 6 Cooling Design".

(3) Nishimura, Y. et al. Thermal Management Technology for IGBT Modules. FUJI ELECTRIC REVIEW. 2010, vol.56, no.2, p.79-83.

2nd Generation LLC Current Resonant Control IC, "FA6A00N Series"

CHEN Jian* YAMADAYA Masayuki* SHIROYAMA Hironobu‡

ABSTRACT

LLC current resonant power supply, which is characterized by soft switching, resonance control with a duty ratio of 50% and leakage transformer structure, is suitable for efficiency improvement, noise reduction and profile lowering in switching power supply. Fuji Electric has developed the 2nd generation "FA6A00N Series," which inherits the characteristics of the 1st generation LLC current resonant control IC, "FA5760N," and is enhanced with lower standby power and improved protective functions. It integrates the world's first high-precision secondary side over-load protection function while further reducing the standby power by approximately 20%. For the over-current protection function, the delay time can be externally adjusted.

1. Introduction

Switching power supply products, which are used in various types of electronic equipment, are rapidly being improved in terms of efficiency, noise reduction and low profile to meet the demands for energy efficiency and space saving. An LLC current resonant power supply is characterized by its use of high-efficiency, low-noise soft switching technology and low-profile leakage transformer structure. These characteristics facilitate efficiency improvement, noise reduction and profile lowering and make it suitable for use as a power supply of 100 to 500 W, which is a medium capacity range for a switching power supply. The LLC current resonant power supply, however, is prone to a switching shoot-through phenomenon*1 during a start-up, heavy load conditions or low input voltage conditions. The power supply has problems including a breakdown of a power metal-oxide-semiconductor field-effect transistor (MOSFET) due to this phenomenon and efficiency degradation with a light load due to an excitation current, and these factors limited its scope of application.

In order to solve these problems, Fuji Electric commercialized "FA5760N," an LLC current resonant control IC that uses its unique new control system. FA5760N is an LLC resonant converter that eliminates the need for a PFC converter and dedicated standby converter and allows a power management system configuration that offers high efficiency, low standby power and compactness. This has expanded the scope of its application such that it is adopted to a power supply of about 50 W without a PFC converter.

Fuji Electric has recently developed the "FA6A00N Series," the 2nd-generation LLC current resonant control IC. With the characteristics of the 1st-generation LLC current resonant control IC "FA5760N" inherited, it is enhanced with a lower standby power, improved protective functions, higher quality and lower system cost and offers a higher degree of design freedom.

2. Overview of Product

Figure 1 shows the external appearance of the FA6A00N Series and Fig 2 the block diagram. Table 1 lists the major ratings, Table 2 the major functions and Table 3 shows the product lineup. The following outlines the LLC current resonant control IC of the FA6A00N Series.

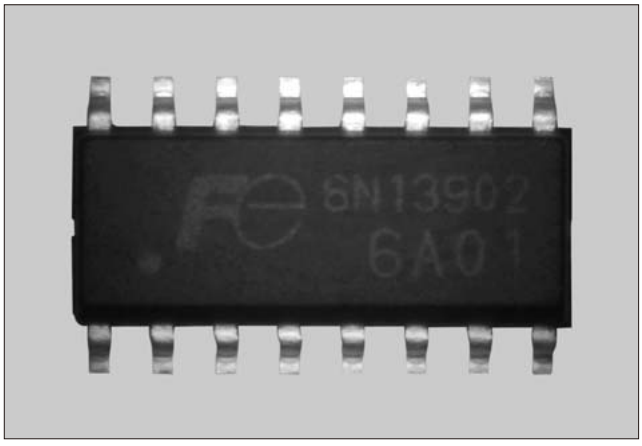

Fig.1 "FA6A00N Series"

*1: Switching shoot-through phenomenon: a phenomenon in which, when a current flows through the body diode of one power MOSFET in a bridge switching circuit, the opposing power MOSFET turns on to instantaneously generate a large current.

* Electronic Devices Business Group, Fuji Electric Co., Ltd.
‡ Sales Group, Fuji Electric Co., Ltd.

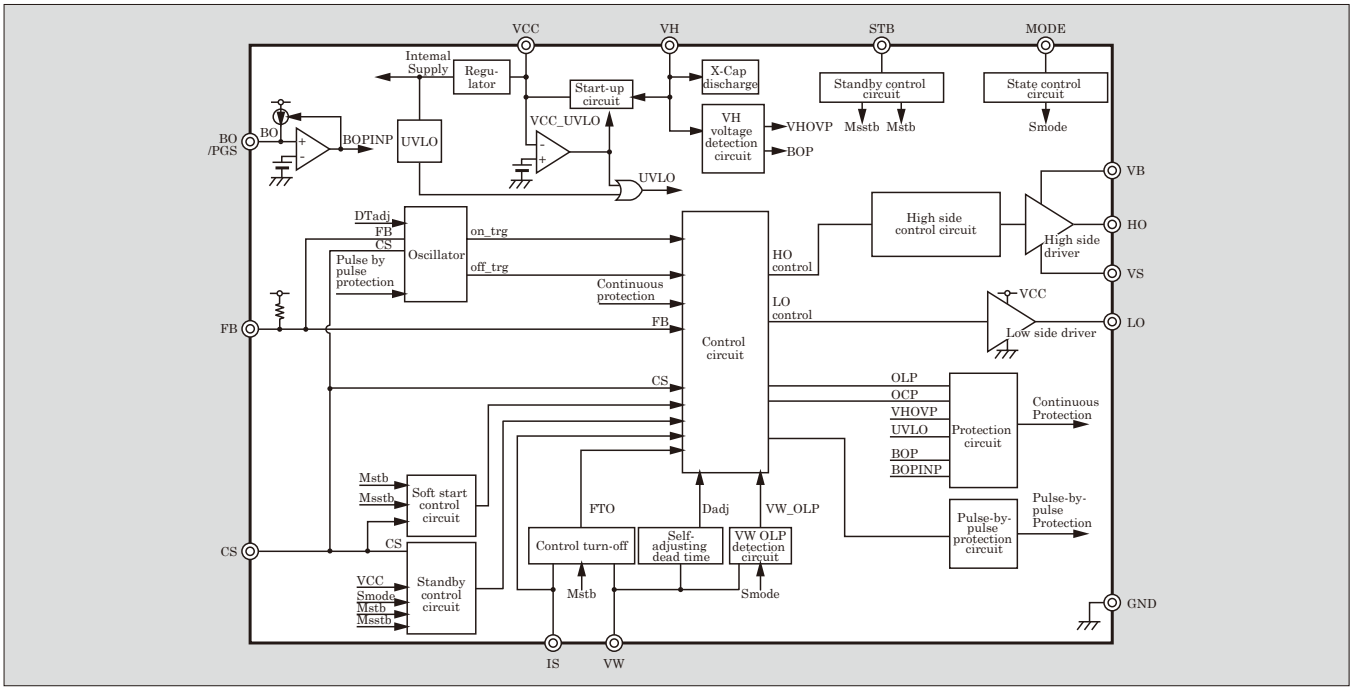

Fig.2 “FA6A00N Series” block diagram

Table 1 Major ratings

Item	Rated value
High side power supply voltage to ground	−0.3 to +630 V
High side power supply voltage (V_{BS})	−0.3 to +30 V
Low side power supply voltage (V_{CC})	−0.3 to +30 V
VH terminal input voltage	−0.3 to +600 V
Maximum allowable offset power supply voltage dv/dt	±50 kV/μs (max.)
Total loss	0.83 W
Operating junction temperature	−40 to +150 °C

Table 2 Major functions and terminals

Function	Terminal (No.)
Start-up circuit	VH (1), VCC (10)
Low voltage malfunction prevention circuit	VCC (10), VB (16)
State setting function	MODE (7)
X-Cap discharge function	VH (1)
Fixed brown-in/brown-out	VH (1)
Variable brown-in/brown-out	BO (3)
Overvoltage protection	VH (1), VCC (10)
Over-current protection with variable delay time	IS (8), MODE (7)
Overload protection	VW (9), FB (4)
Overheat protection	Integrated
External latch signal input	MODE (7)
Forced turn-off function	VW (9), IS (8)
Automatic dead time adjustment function	VW (9)
High-precision overload protection function	VW (9)
Soft start function	CS (5)
Low standby power operation mode	VCC (10), CS (5), VH (1)
Power Good signal	PGS (3)

Table 3 Product lineup

Product name	Terminal 3	Overload protection	Over-current protection
FA6A00N	PGS terminal	Auto-restart	Latch stop
FA6A01N	PGS terminal	Auto-restart	Auto-restart
FA6A10N	BO terminal	Auto-restart	Auto-restart
FA6A11N	BO terminal	Latch stop	Latch stop

(a) Control circuit with 3.3 V, 5 V and 30 V breakdown voltage for controlling the LLC current resonant circuit
(b) Driver circuit with 630 V breakdown voltage capable of directly driving the high side and low side switching devices in the half bridge circuit
(c) Built-in 600 V breakdown voltage start-up device realizing IC start-up with low power consumption
(d) JEDEC-compliant 16-pin small outline package

The high side and low side outputs alternately operate with a high-precision duty cycle of 50% and the operating frequency range is 38 to 350 kHz.

3. Features

3.1 Low power dissipation burst control

FA5760N, the 1st-generation product, used the VCC and CS terminals for hysteresis burst control and achieved a world-class low standby power without the standby converter. The FA6A00N Series, which is the 2nd generation, is additionally provided with burst control optimization to further reduce the standby power by approximately 20% from FA5760N.

The LLC current resonant control has a high side

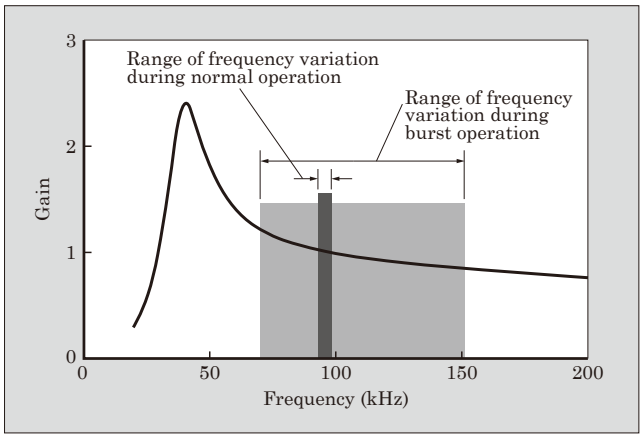

Fig.3 Current resonant gain diagram

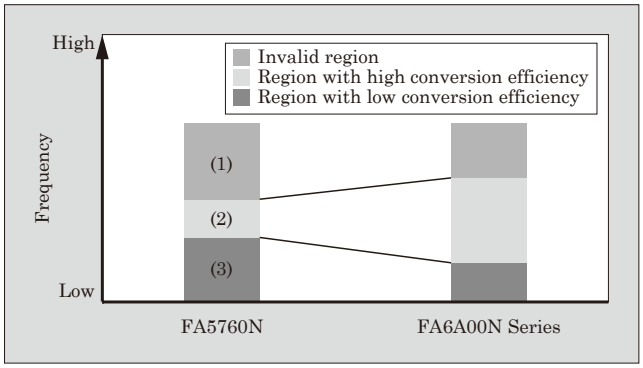

Fig.4 Frequency during burst operation

and low side duty cycle of 50% and controls the gain by the switching frequency. Figure 3 shows the current resonant gain diagram. The frequency variation range is narrow in principle during normal operation and widened during burst operation.

Figure 4 shows the frequency during burst operation. The high frequency region (1) is an invalid region in which the gain is low and switching cannot transfer energy. In the low frequency region (3), the gain is high and excitation current is large, which makes energy transfer inefficient; hence there is a low conversion efficiency. With the FA6A00N Series, the invalid region and the region with low conversion efficiency have been reduced to widen the region with high conversion efficiency (2), resulting in successful reduction of standby power. Audible noise has also been suppressed.

3.2 High-precision overload protection function

The 1st-generation product FA5760N used the primary side auxiliary winding P2 (see Fig. 5) to supply power to the VCC terminal and realized hard switching protection and shoot-through current prevention. The FA6A00N Series, which is the 2nd generation, uses this auxiliary winding to integrate the high-precision overload protection function for the first time in the world while inheriting the functions of FA5760N.

The overload protection, which is intended for

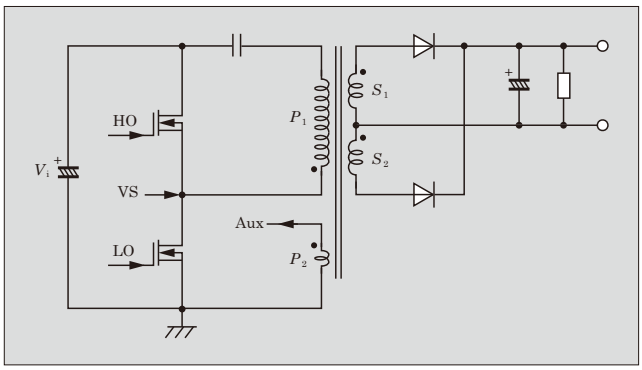

Fig.5 Schematic circuit diagram of current resonance

protecting the power management system, is a function that stops switching when a certain delay time has elapsed after a load increases to approximately 1.5 times the rated load. Degradation of the precision of this function causes insufficient output power or failure to limit the output power, thus the overload protection cannot perform adequately. In addition, the overload protection level must be maintained within a certain range (about ±20%) even if an input voltage varies in a wide range.

Figure 6 shows the circuit configuration of the high-precision overload protection function of the FA6A00N Series. The auxiliary winding voltage is detected by the resistor-divided voltage, V_W voltage. The recommended precision of this voltage-dividing resistor is ±1%. The V_W voltage exceeding the threshold voltage V_{olpvw} is recognized as an overload state, and when the overload state continues for 76.8 ms, switching is stopped. In order to improve the detection precision, variation of V_{olpvw} has been specified to be within ±3%, which is highly precise. The commercialized versions are the auto-restart version, which restarts when the switching stop time has reached 550 ms, and the latch stop version that does not restart.

Figure 7 shows a waveform during overload protection operation. In overload protection operation, switching is suspended and the output voltage drops along with an energy transfer stop.

Figure 8 shows how the overload protection operating power depends on the input voltage. FA5760N provides overload protection with general resonant current detection. With this method, the overload

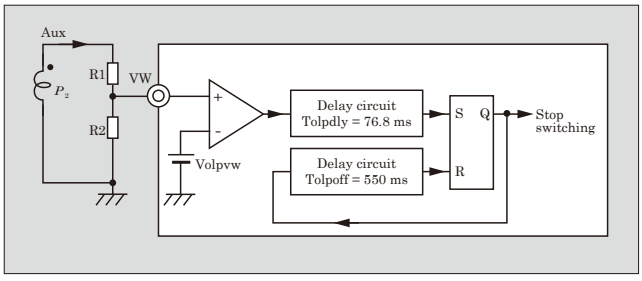

Fig.6 Circuit configuration of high-precision overload protection function

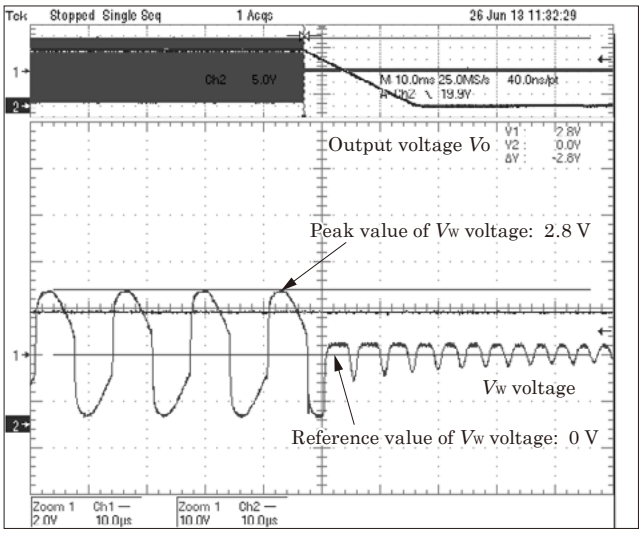

Fig.7 Operation waveform during overload protection

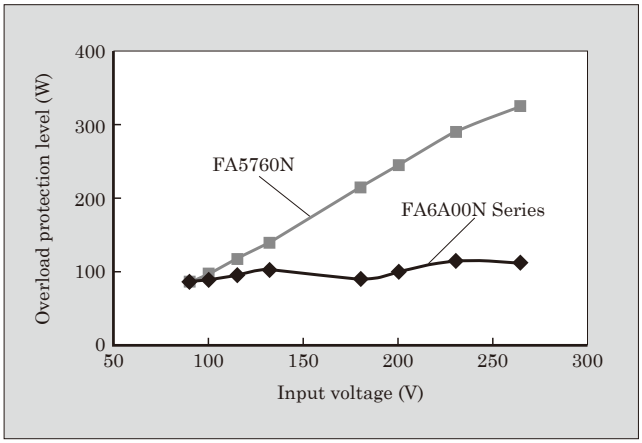

Fig.8 Input voltage and overload protection operating power

protection level is highly dependent on the input voltage when the input voltage range is wide, and this has necessitated the addition of a dedicated overload protection circuit. With the FA6A00N Series, variation of the overload protection level is small even if the input voltage varies, allowing for a high-accuracy overload protection function without a dedicated overload protection circuit. As a result, the number of power supply system components can be reduced, allowing for a cost reduction of a power supply system.

3.3 Over-current protection function with variable delay time

When a load short circuit occurs and an over-current state has continued for the specified time T_{ocp}, switching stops. This is called the over-current protection function. The power device has a possibility of being damaged if the Tocp setting is too long. If the T_{ocp} setting is too short, it causes an over-current state at start-up, and this may be detected as a load short circuit state and might hinder the start-up. The optimum T_{ocp} depends on a power supply and capability to adjust Tocp with an external component offers a higher degree of flexibility in power supply design.

Fig.9 Waveform during over-current protection operation

With the FA6A00N Series, adjustment of T_{ocp} is shared by the MODE terminal for state setting, which has led to the realization of the over-current protection function with a variable delay time without increasing the number of terminals. Figure 9 shows a measured waveform. When a resonant current rapidly increases, an over-current state is detected on the IS terminal. The MODE terminal voltage is clamped to 0.5 V after state setting and, when an overload state is detected, oscillates between 0.6 and 0.8 V. When the number of oscillations reaches 36, switching stops and provides over-current protection. The duration of one oscillation can be adjusted by the capacitor connected to the MODE terminal.

4. Effect on Application to Power Circuit

4.1 Standby power reduction effect

Figure 10 shows a sample application circuit and Tables 4 and 5 the specification of the sample application circuit and major semiconductor components in the circuit. Figure 11 shows the measured standby power with a 35 mW load. The FA6A00N Series can reduce the standby power by approximately 20% from FA5760N, which allows elimination of the standby converter even if requirements for standby power are severe.

4.2 Number of circuit components reduction effect

Figure 12 shows the configuration of a general LLC current resonant power supply. A general LLC current resonant power supply is composed of a filter for EMI (electromagnetic interference) noise elimination, PFC converter for power factor correction, standby converter and LLC converter. Use of the FA6A00N Series allows significant reduction in the number of components, making it possible to build a low-cost LLC current resonant power supply (see Table 6).

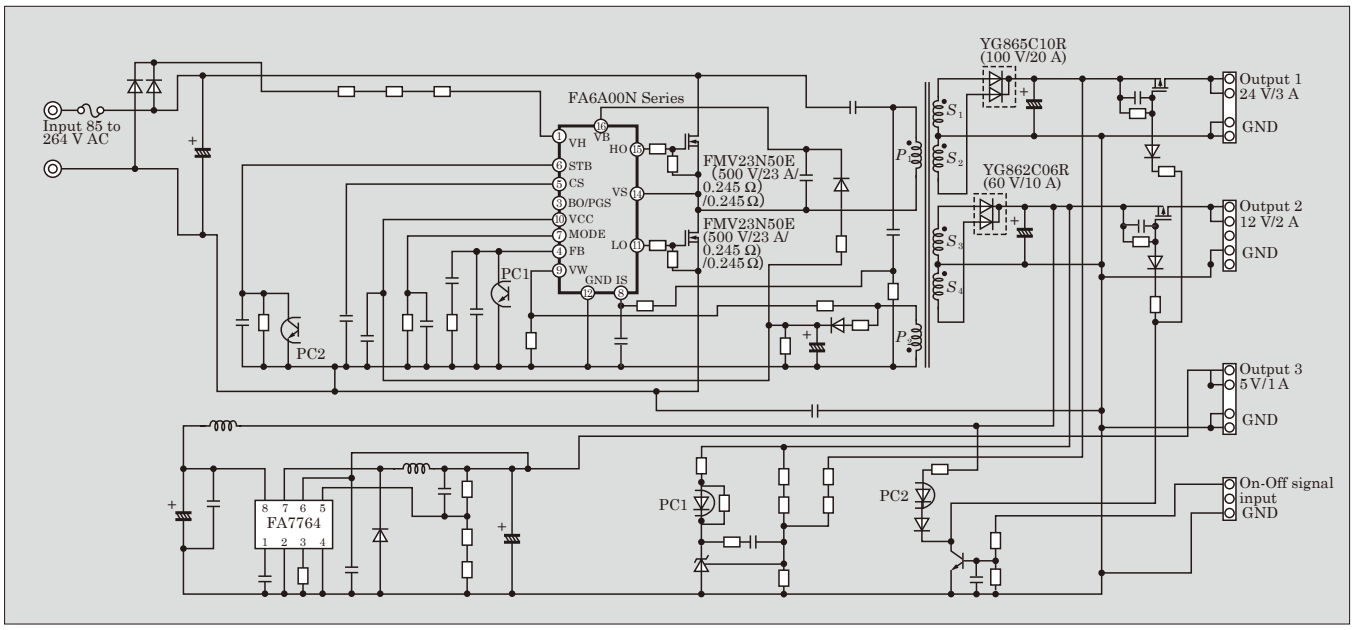

Fig.10 Sample application circuit

Table 4 Specifications of sample application circuit

Item	Characteristic, etc.
Input voltage	85 to 264 V AC
Output voltage/current	24 V/3 A, 12 V/2 A, 5 V/1 A
Output power	100 W (max.)

Table 5 Major semiconductor components in sample application circuit

Component	Model
Control IC	FA6A00N Series
Bridge MOSFET	FMV23N50E (500 V/23 A/0.245 Ω)
Diode (24 V)	YG865C10R (100 V/20 A)
Diode (12 V)	YG862C06R (60 V/10 A)
5 V AC/DC converter	FA7764AN

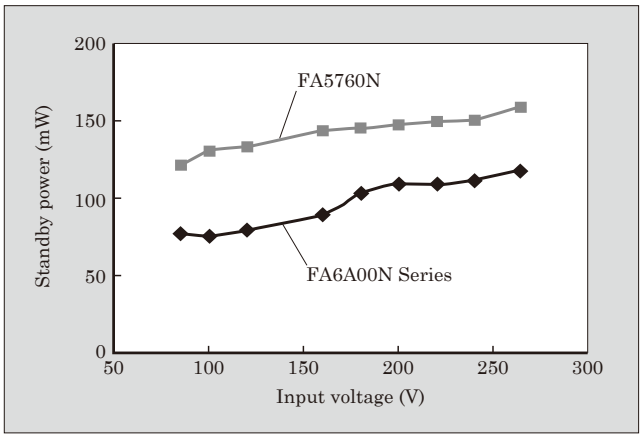

Fig.11 Standby power with 35 mW load

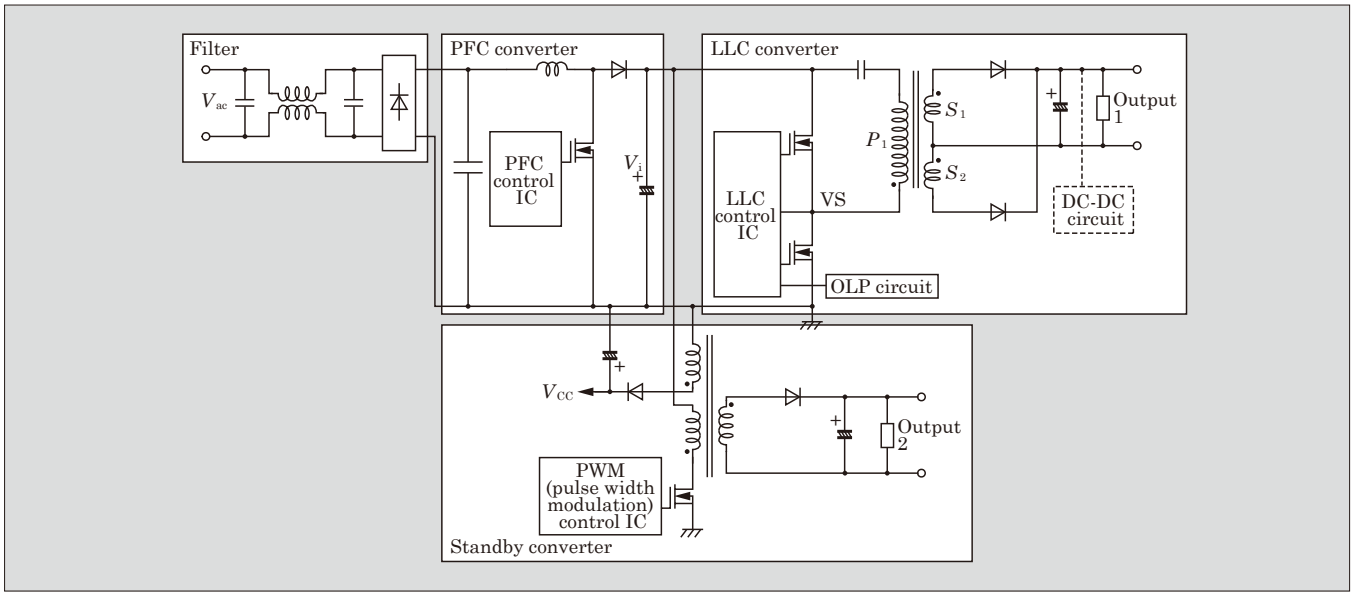

Fig.12 Configuration of general LLC current resonant power supply

Table 6 Comparison on number (approximate number) of components

		Filter	PFC converter	Standby converter	LLC converter			Total number of components
					Main	DC-DC	High-precision OLP	
FA5760N		10	30	40	60	Not required	10	150
FA6A00N Series	75 W or more	10	30	Not required	60	20	Not required	120
	less than 75 W	10	Not required	Not required	60	20	Not required	90

5. Postscript

This paper has described the 2nd-generation LLC current resonant control IC "FA6A00N Series." This IC, which inherits the characteristics of the 1st-generation product "FA5760N," has achieved further evolution of current resonant control with features including the high-precision overload protection function.

We intend to continue working on establishing new technologies that realize even higher efficiency and further noise reduction, and developing power supply control ICs that contribute to the miniaturization and profile lowering of power supply.

One-Chip Linear Control IPS, "F5106H"

NAKAGAWA Sho* OE Takatoshi* IWAMOTO Motomitsu*

ABSTRACT

In the field of vehicle electrical components, the increasing demands for miniaturization, reliability improvement and functional enhancement are required. To meet these demands, Fuji Electric has developed one-chip linear control intelligent power switch (IPS), "F5106H," which mounts a high-precision current detection amplifier on the conventional IPS. Applied with 4th generation IPS device and process technology, it can be integrated into one chip and mounted in a SOP-8 package. In addition, the maximum rating of the junction temperature has been set to 175 °C to improve the durability in a harsh temperature environment, and low power operation voltage can be allowed down to 4.5 V.

1. Introduction

In recent years, in the field of vehicle electrical component, further safety performance enhancement, exhaust gas reduction and improvement of fuel efficiency have been implemented with "safety," "environmental protection" and "energy saving" as the keywords. In order to achieve these objectives, advancement of vehicle control technology and expansion of electronic control systems of automobiles have been promoted. Among these, in order to secure a spacious indoor interior, miniaturization and functional enhancement are required in an electronic control unit (ECU). Furthermore, along with high-density mounting of the ECU, handling high temperature in addition to miniaturizing and functional enhancement in mounting parts is also in demand.

In addition, as for a solenoid valve that is controlled by the ECU, there is an increasing tendency to apply linear control that uses a linear solenoid valve. A linear solenoid valve can control oil pressure linearly according to current value; therefore, it is possible to control the vehicle by fine oil pressure commanding, and help to reduce exhaust gas and improve fuel efficiency. However, it is necessary for this linear control to detect the current that flows in the linear solenoid with high accuracy.

Fuji Electric has been developing intelligent power switch (IPS) products for vehicle electrical component systems for years, which are applied for a transmission, engine, brake and the like. The IPS is a product with a vertical-type power metal-oxide-semiconductor field-effect transistor (MOSFET) that is used as an output stage, and horizontal-type MOSFET that comprises a control and protection circuit, integrated on the same chip. The IPS has been contributing to the miniaturization of ECUs by enabling reduction in the number of circuit components and mounting area of an ECU. In recent years, by virtue of the application of the fourth-generation IPS device process technology, further miniaturization of the chip became possible. This time, by applying these technologies, we have developed an IPS "F5106H" for one-touch linear control in which a high-precision current detection amplifier is integrated in the existing IPS.

2. Features

The external view, outline drawing and terminal board schedule of F5106H are shown in Fig. 1, a circuit block diagram in Fig. 2 and usage examples in Fig. 3. In addition, the maximum rating is described in Table 1. The main characteristics of F5106H are the following 6 items, and they support miniaturization, performance enhancement and reliability improvement of the vehicle electrical component system:

(a) By applying the fourth-generation IPS device process technology, an external operational amplifier and a high-side type IPS*1 are integrated into one chip, which is mounted in the SOP-8 package. This decreases the number of parts, thus contributing to miniaturization of a system and the total cost reduction.

(b) By having a built-in operational amplifier, which enables high-precision detection of a load current, high precision linear control is established.

* Electronic Devices Business Group, Fuji Electric Co., Ltd.

*1: High-side type IPS: An IPS in which a semiconductor device is mounted on the power side and a load on the ground side respectively.

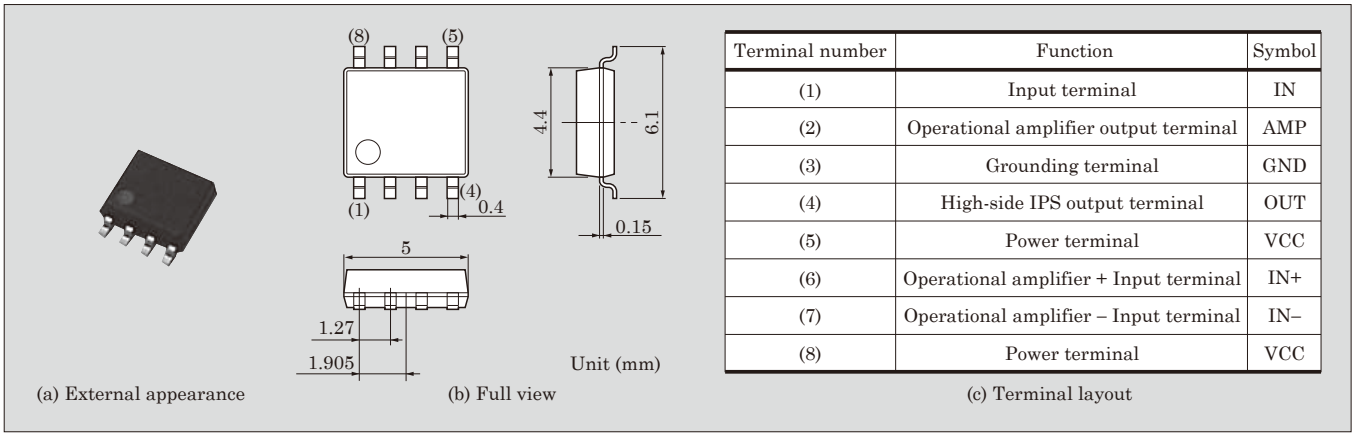

Terminal number	Function	Symbol
(1)	Input terminal	IN
(2)	Operational amplifier output terminal	AMP
(3)	Grounding terminal	GND
(4)	High-side IPS output terminal	OUT
(5)	Power terminal	VCC
(6)	Operational amplifier + Input terminal	IN+
(7)	Operational amplifier – Input terminal	IN–
(8)	Power terminal	VCC

(c) Terminal layout

Fig.1 External appearance, full view, terminal layout of "F5106H"

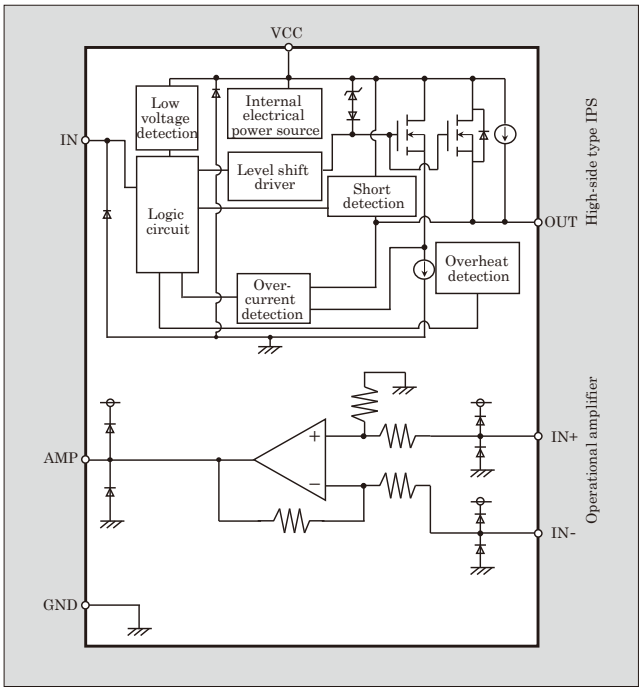

Fig.2 Circuit block diagram of "F5106H"

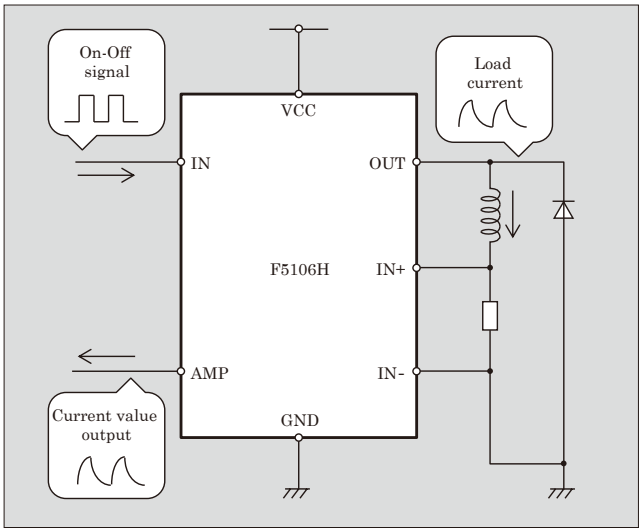

Fig.3 Usage examples of "F5106H"

Table 1 Maximum rated value of "F5106H" (T_a=25°C)

Item	Symbol	Condition	Rated value	Unit
High-side IPS: Common to operational amplifier				
Power voltage (1)	V_{CC} (1)	Pulse 0.25s	50	V
Power voltage (2)	V_{CC} (2)	DC	−0.3 to +35	V
Junction temperature	T_j	—	175	°C
Storage temperature	T_{stg}	—	−55 to +175	°C
High-side IPS				
Output current	I_D	DC	2	A
Output voltage	V_{OA}	—	V_{CC}−50	V
Consumption power	P_D	DC	2	W
Input voltage (1)	V_{IN} (1)	DC R_{IN}=0 Ω	−0.5	V
Input voltage (2)	V_{IN} (2)	DC	7	V
Input current	I_{IN}	DC	±10	mA
Operational amplifier				
IN+ Voltage	V_{IN+} (1)	DC	−0.5 to +7	V
	V_{IN+} (2)	5s	−1.1 to +18	V
IN– Voltage	V_{IN-} (1)	DC	−0.5 to +7	V
	V_{IN-} (2)	5s	−1.1 to +18	V
IN+ Current	I_{IN+}	DC	10	mA
IN– Current	I_{IN-}	DC	10	mA
AMP Voltage	V_{AMP}	DC	7	V
AMP Current	I_{AMP}	DC	10	mA

(c) The maximum rated value of junction temperature is set at 175°C, which improves durability in a severe temperature environment.
(d) Low power voltage operation up to 4.5 V is enabled.
(e) Load short-circuit protection function is built in.
(f) Zener Diode for low impedance surge absorption is built in, which secures high electrostatic discharge (ESD) tolerance dose.

2.1 Features of high-side type IPS

Table 2 shows the electrical characteristic of the

Table 2 Electrical characteristic of high-side type IPS

Item	Symbol	Condition	Standard value		Unit
			Min.	Max.	
Operation power voltage	V_{CC}	V_{IN}=5 V	4.5	16	V
Low voltage detection	$UV1$	V_{IN}=5 V	2.0	4.3	V
Low voltage return	$UV2$		2.2	4.5	V
Input threshold voltage	V_{IN}(H)	V_{CC}=4.5 to 16 V R_L=10 Ω	3	7	V
	V_{IN}(L)		0	1.5	
On-resistance	$R_{DS(on)}$	T_a=25 °C I_{OUT}=1.5 A	—	0.12	Ω
		T_a=150 °C I_{OUT}=1.5 A	—	0.24	Ω
Overcurrent detection	I_{OC}	V_{CC}=13 V V_{IN}=5 V	2	7	A
Overheat detection	T_{trip}	V_{IN}=5 V	175	207	°C

Unless otherwise noted, T_a=−40 to +175 °C, V_{CC}=8 to 16 V.

high-side type IPS.

Load short-circuit protection and reduction of operation power voltage are described as below:

(1) Load short-circuit protection

In order to prepare for the case when an overcurrent flows in the output stage power MOSFET, an overcurrent detection function is built in to protect load and elements. Figure 4 shows a waveform at overcurrent operation. The function detects overcurrent and keeps down the peak current to a certain level when output current enters an oscillating state. By doing so, it is possible to suppress noise generated by the element even at abnormal states. In addition, by optimizing the duty ratio*2 in an output oscillation state, it is possible to suppress the average output current, contributing to refinement of ECU wiring as well as thinning and weight reducing of a wire harness. Furthermore, it is equipped with an overheat detection function because there is a risk of a breakdown due to heat generated by the output stage power MOSFET when an abnormality state continues. Because responsiveness is important for the overheat detection

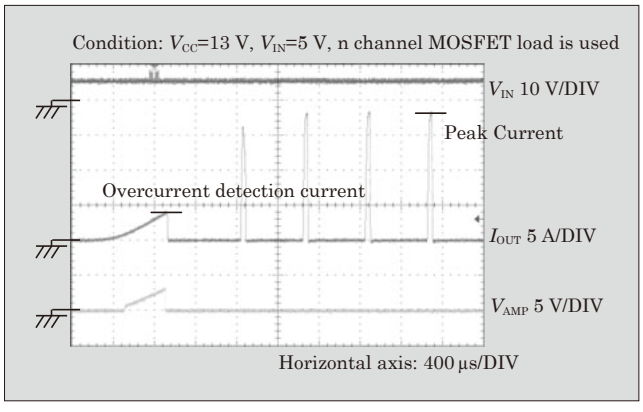

Fig.4 Waveform at overcurrent operation

Table 3 Electrical characteristic of operation amplifier section

Item	Symbol	Condition	Standard value		Unit
			Min.	Max.	
Output voltage range	V_{OH}	R_{AMP}=5 kΩ	0	5	V
Output current	I_{AMP} (SOURCE)	V_{IN+}=366 mV	—	–0.1	mA
	I_{AMP} (SINK)	V_{IN+}=384 mV	0.1	—	mA
Gain	G	—	typ.=8		times
Overcurrent detection accuracy	$I_{sns}1$	V_{IN+}=375 mV R_{AMP}=50 kΩ	–2.3	2.3	%
	$I_{sns}2$	V_{IN+}=375 mV R_{AMP}=50 kΩ V_{CC}=14 ± 1 V T_a=25 °C	–1.6	1.6	%

Unless otherwise noted, T_a=−40 to +175 °C, V_{CC}=8 to 16 V.

function, a temperature sensor is arranged within the active portion of the output stage power MOSFET to speed up the response.

(2) Low power voltage operation

Power voltage is designed to be able to maintain the on-resistance even when the voltage momentarily drops at engine start. By reducing the threshold of element devices that comprises the circuit, even if a power voltage drops to 4.5 V, it is possible to maintain almost the same level of on-resistance as a normal voltage of 13 V. In addition, a low voltage detection function is integrated so that circuit operation does not become unstable in the region where a power voltage is below 4.5 V. As a result of these improvements, performance and redundancy of the element is maintained at the same level as the normal state even when the power voltage drops.

2.2 Features of operational amplifier

Table 3 shows the electrical characteristic of the operational amplifier section. In order to achieve high current detection accuracy at −40 to +175 °C, the following three points are implemented:

(a) By adopting a p-type MOSFET for the differential amplifier, a gate size is optimized.

(b) By implementing a common centroid*3 layout for the differential amplifier, fluctuation of current detection accuracy is reduced.

(c) Trimming circuit is built in to reduce the variation of offset.

3. Applied Technology

For F5106H, the fourth-generation IPS device pro-

*2: Duty ratio: Ratio of on-status at output oscillation state.

*3: Common centroid: To separate and arrange MOSFET pairs so that each center of gravity matches to reduce fluctuation in properties.

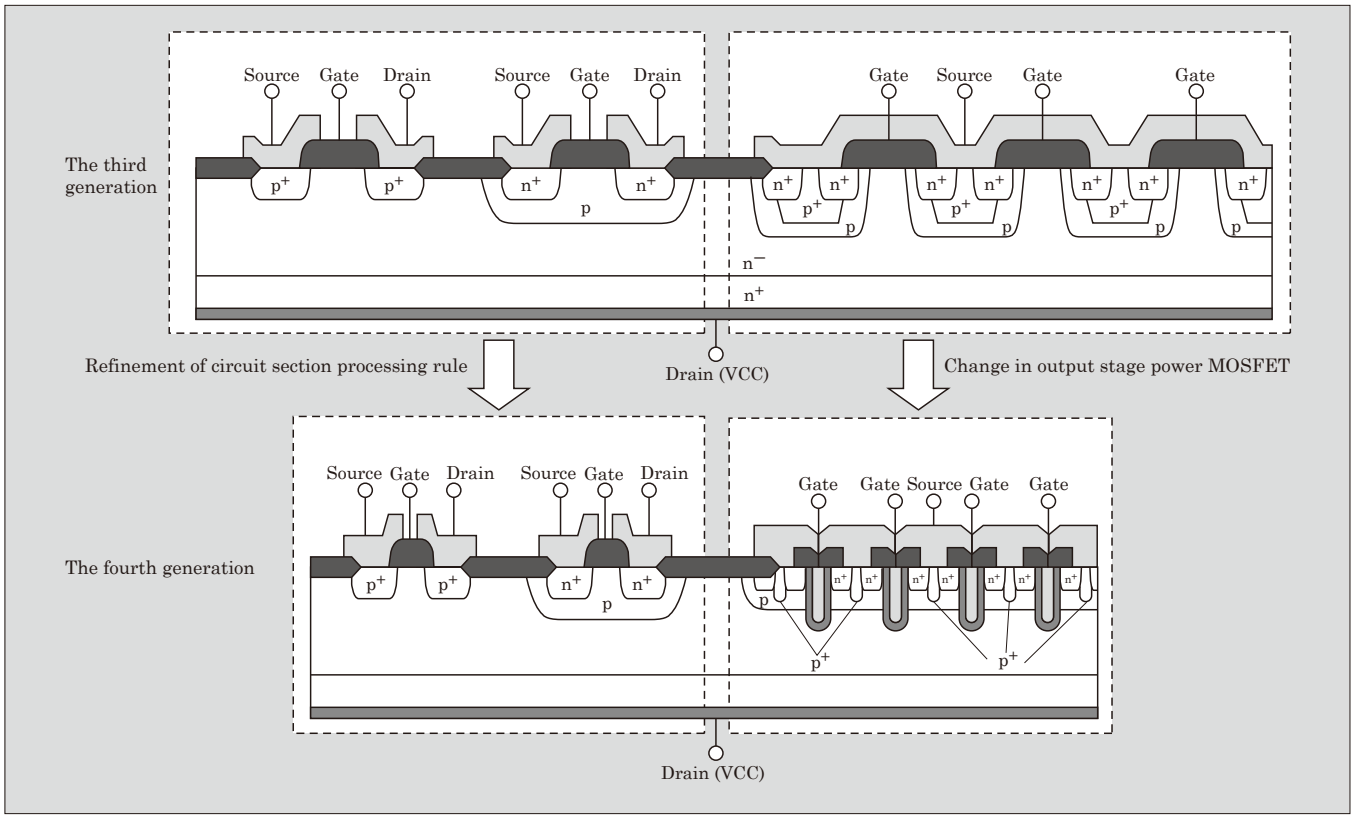

Fig.5 Characteristic of the fourth-generation IPS device processing technology

cess technology is applied[1]. Figure 5 shows the fourth generation IPS device structure.

In order to miniaturize the chip size, the output stage power MOSFET is changed from the existing planar gate type to a trench gate type and the area of the wiring that connects between device elements is reduced by applying multi metal layer technology in addition to thinning the element devices themselves.

By developing this technology, the high-side type IPS and operational amplifier are integrated into one chip, enabling to mount it into the SOP-8 package. The following two points are considered to integrate into one-chip design:

(a) Chip rear surface becomes high voltage (battery voltage) as a result of integrating into one chip. A device structure that suppresses the substrate bias effect is adopted in order to eliminate the influence of this effect.

(b) A layout that reduces variation in electrical characteristics of the operational amplifier is implemented. Specifically, a layout that minimizes the influence of the differential amplifier due to generation of heat from the output stage power MOSFET is implemented, and the differential amplifier is aligned in the center of the chip considering residual stress within the package.

In order to enable operation at a temperature of 175 °C, the following two points are implemented.

(a) In order to secure noise surge tolerance even under an environment with a temperature of 175°C, the product is designed to keep a good balance of blocking voltage between the output stage power MOSFET and device elements of circuit section.

(b) By reviewing package material, high reliability is achieved even under 175°C environment.

4. Postscript

This paper described one-chip IPS “F5106H” for linear control, which can help to achieve miniaturization and performance enhancement of ECUs. Continuously, Fuji Electric will be developing various IPS products by using the fourth-generation device processing technology and contributing to functional enhancement, miniaturization and reliability improvement of vehicle electrical component systems.

Reference

(1) Toyoda, Y. “60 V- Class Power IC Technology for an Intelligent Power Switch with an Integrated Trench MOSFET.” ISPSD. p.147-150, 2013.

Supplemental Explanation

Supplemental explanation 1 3-level power conversion

p.230

3-level power conversion method is explained using inverters as an example in follows.

The 3-level power conversion system (3-level inverter) has a lot of advantages compared to 2-level power conversion system (2-level inverter).

As shown in the Figure below, the voltage waveform at the conversion output of the 2-level inverter is $\pm E_d$ pulse width modulated (PWM) pulses centered about the zero point. However, the 3-level inverter is PWM pulses of $\pm E_d/2$ and $\pm E_d$ centered about the zero point. Because the output waveform of the 3-level inverter more closely resembles a sine wave, the size of the LC filter used to convert the output waveform into a sine wave can be reduced. The width of voltage fluctuation per one-time switch operation is half that of the 2-level inverter. Therefore, the switching loss occurring in a switch device is roughly halved that of the 2-level inverter and the noise generated by the equipment can also be reduced. The 3-level inverter having these characteristics can be effective for realizing smaller size and higher efficiency of a system.

Among the 3-level inverters, the method shown in the Figure in which an inverter is wired to the intermediate potential (N) of the DC power source, is known as the neutral-point-clamped (NPC) system. The naming of this method originates from the fact that the voltage applied to the switching device is always clamped to half the DC voltage E_d.

Compared to the NPC system, the advanced T-type-NPC (AT-NPC) system enables a simpler circuit configuration because of the following reasons; the series-connected insulated gate bipolar transistors (IGBTs) have twice the rated voltage as the IGBTs which are used with the NPC system, an reverse blocking IGBT (RB-IGBT) is used between the intermediate potential point (N) of the DC power source and an intermediate point (U) of the series-connected IGBTs. Because of having fewer devices on the current routes, the AT-NPC system has the advantages of realizing lower power dissipation, and the fewer number of power supplies for the gate driving circuit.

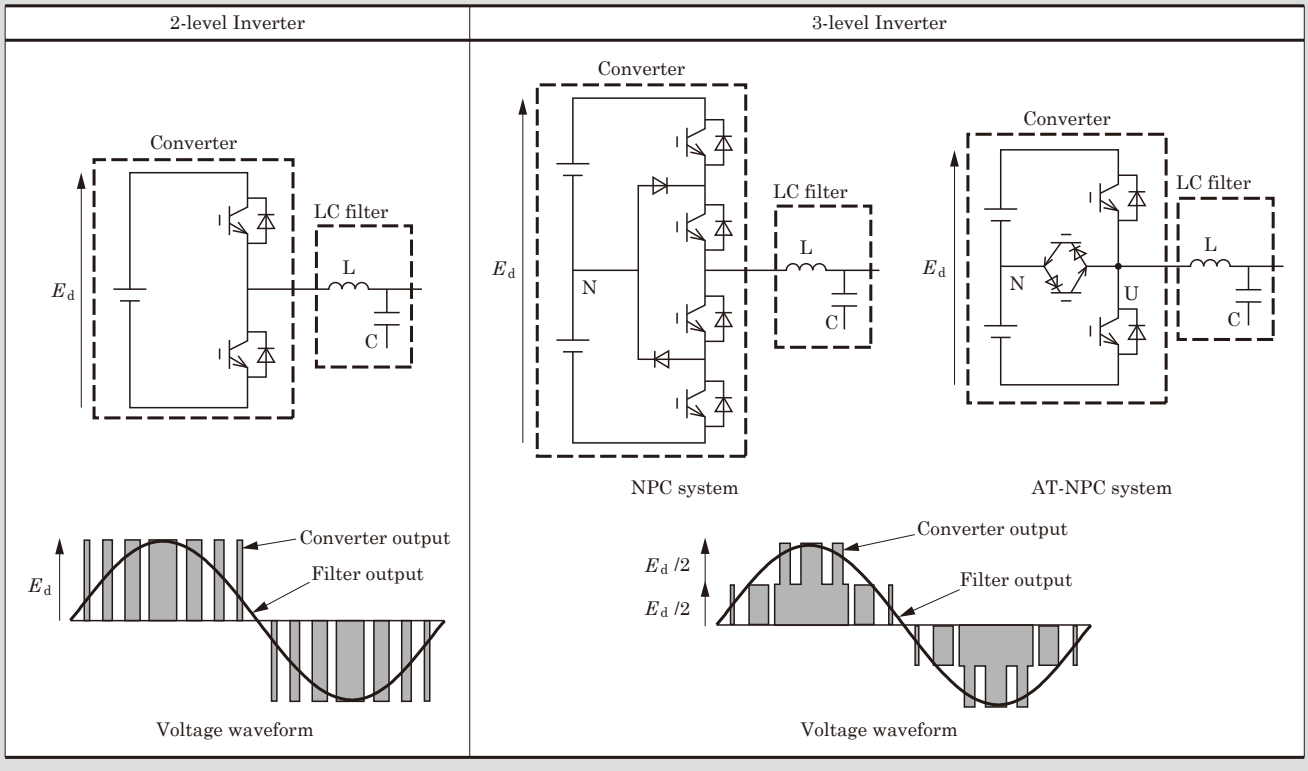

Figure Comparison of 2-level inverter and 3-level inverter circuits and voltage waveforms

Top Runner Motor of Fuji Electric– Premium Efficiency Motor "MLU and MLK Series"

TACHI Norihiro*

In recent years, the movement to reduce energy usage to prevent global warming has spread throughout the world. Japan, in accordance with its "Act on the Rational Use of Energy" (i.e., Energy Saving Act), employs a top runner approach and has increased the types of devices subject to this approach. Three-phase induction motors will also be subject to this approach as of 2015.

Fuji Electric launched the "MLU and MLK Series" of motors that optimize slot shape and core material etc. to satisfy efficiency standards (top runner standards) through the top runner approach. These products achieve low noise operation, and are environmentally friendly as well as energy conserving.

1. Features

The main specifications of the "MLU and MLK Series" of premium efficiency motors in accordance with the top runner approach are listed in Table 1.

(1) High efficiency

To satisfy the top runner standards, copper loss, iron loss and mechanical loss were reduced to improve efficiency by 3 to 10%.

The efficiency classes (IE codes) of single-speed, three-phase, cage-induction motors specified in "Rotating electrical machines – Part 30" of IEC 60034-30, a standard of the IEC (International Electrotechnical Commission), are examples of international standards for motor efficiency. The present efficiency of standard motors is in the level shown in Fig. 1 as the standard efficiency (IE1). In contrast, these "MLU and MLK Series" products satisfy the premium efficiency (IE3) level.

Table 1 Main specifications of the "MLU and MLK Series"

Item	Specification
Housing structure	Totally-enclosed fan-cooled type Indoor or outdoor
Type	MLU (cast iron frame) MLK (steel frame)
Output	0.75 to 375 (kW)
Number of poles	2, 4, 6
Frame number	80M to 355M
Rating	S1 (continuous)
Thermal class	155 (F)
Direction of rotation	CCW (counterclockwise when viewed from the load end)
Color of coating	Munsell N1.2 (no black gloss)

* Corporate R&D Headquarters, Fuji Electric Co., Ltd.

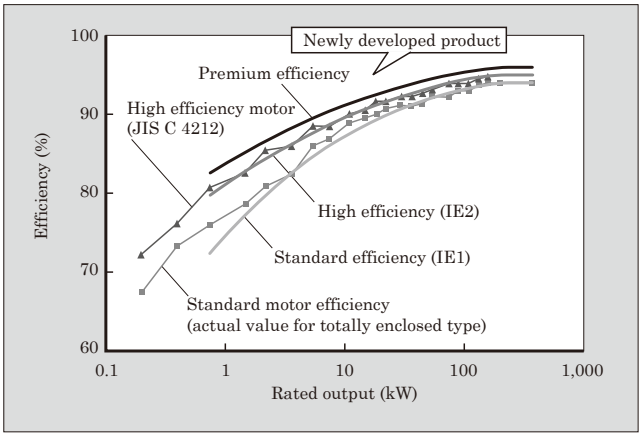

Fig.1 Motor efficiency values for each efficiency class

(2) Compatibility with prior products

Because of the high demand for motors to replace existing products, it is important that the motors be compatible with the dimensions and electrical characteristics of prior products.

Dimensions in international standards are provided as a frame number (dimension of axle or leg width etc. with respect to the distance from the base bottom to the axle center) and are not provided for various output capacities or number of poles. On the other hand, JIS C 4213, which is to be enacted during 2013, is expected to prescribe frame numbers as well as the dimensions of each part corresponding to respective output capacity and number of poles.

In compliance with JIS C 4213 and for the ease of replacing existing parts with these products, these products are designed so as not to exceed the maximum cut-off current of existing electromagnetic switches.

(3) Low noise

In order to improve the work environment, there is great demand for lower noise devices, and low noise motors, which provide the driving source for those devices, are strongly demanded. The MLU series, which uses a cast iron frame to improve rigidity and also employs an optimized cooling fan, achieves a 5 to 8 dB reduction in noise compared to conventional products (IE1). The MLK series, which uses a steel frame, also realizes up to a 5 dB reduction in noise.

(4) Long life

The adoption of thermal class F type insulation as

a standard enables these motors to realize an insulation lifetime that is about 4 times longer than that of conventional products (IE1, IE2). Moreover, the motors can also be used at ambient temperatures of up to 50°C.

(5) Improved surge resistance

For realizing energy-efficient fans and pumps, inverter-based rotational speed adjustment is more efficient than flow control using a damper and the like. Accordingly, surge resistance has been improved by about 10% in these products so that there will be no problems even if driven by an inverter that generates a sharp pulse-like waveform voltage.

(6) Improved corrosion resistance

Many manufacturers employ aluminum alloy die-cast frames for lighter weight, but the MLU series employs a cast iron frame in order to improve the corrosion resistance.

2. Background of High Efficiency Motors and Standards

As shown in Fig. 2, motors are widely used as drive sources for various industrial devices such as fans and pumps. Such applications account for 40% of the power consumption worldwide (see Fig. 3). If the efficiency of all motors could be increased by 1%, the worldwide power consumption would be reduced by 80 million MWh and CO_2 emissions reduced by 32 million tons per year.

In Japan, energy savings has been advanced with systems that incorporate inverter technology, and therefore efforts to increase the efficiency of motors themselves have been stalled. For this reason, annual shipments of high-efficiency motors (JIS C 4212) comprised about merely 1 to 3% of total motor shipments.

Meanwhile, for nations that are large consumers of energy, including the U.S. and Europe, increasing the efficiency of motors is regarded as an extremely efficient way to reduce both power consumption and CO_2 emissions, and efforts to improve the efficiency of motors have intensified.

In the U.S., the high efficiency (IE2) and premium efficiency (IE3) levels account for 90% of all motors. In Europe, more than half of all motors are thought to be at the IE2 level, and the enforcement of IE3 regulations is expected to begin in 2015. Meanwhile in Japan, efficiency regulations based on the top runner standard are finally being enforced.

The top runner standards in Japan, while being based on the IE3 efficiency level, take into account the three types of rated power supply that are unique to Japan. Namely, the prescribed efficiency values for 200 V/50 Hz and 220 V/60 Hz conform to IE3, but the value for 200 V/60 Hz is an IE3 level multiplied by a factor to arrive at an IE2 equivalent value. The target standard values are not set a finely as in Europe but instead are set by dividing approximately into 36 categories, 1/3 of Europe.

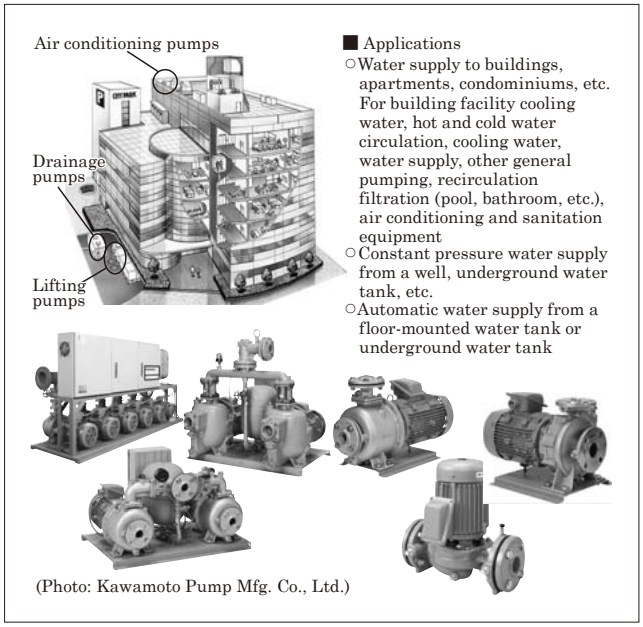

Fig.2 Motor usage examples

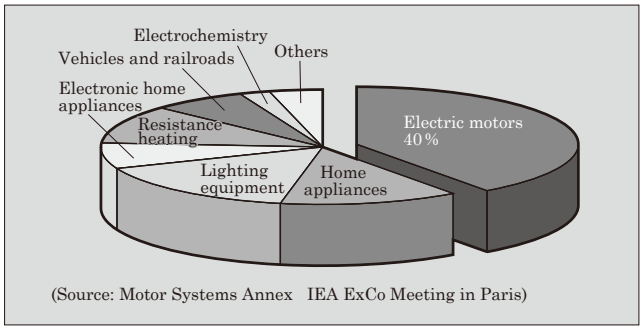

Fig.3 Breakdown of worldwide power consumption

3. Background Technology

Figure 4 shows a cross-section of motor structure and loss reducing features. Loss occurs in various parts of the motor, and in order to satisfy the prescribed ef-

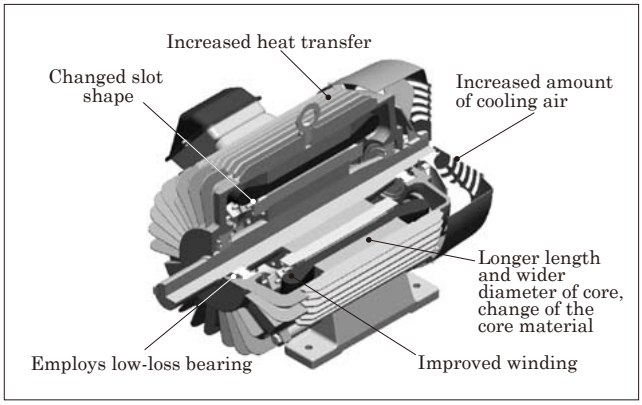

Fig.4 Cross-section of motor structure and loss reducing measures

ficiency values, loss must be reduced everywhere it occurs. In particular, the reduction of copper loss (primary and secondary), which accounts for approximately 50%, and iron loss, which accounts for approximately 30% of the total loss, is important.

(1) Reduction of copper loss

The primary loss is joule loss due to the electrical resistance and current in the motor windings. By optimizing the stator slot shape, improving the packing density of the windings and increasing the cross-sectional area of the conductors, and also by shortening the coil end and reducing the length of the conductor, electrical resistance was lowered and copper loss was reduced.

Additionally, the shape of the rotor slot was revised so as to achieve lower secondary copper loss and to optimize torque characteristics and current characteristics as well.

(2) Reduced iron loss

Iron loss is the sum of the eddy current loss and hysteresis loss generated by the change in magnetic flux inside the iron core. In order to reduce the iron loss of the material itself, a high-grade low-loss electromagnetic steel sheet is used, and in order to reduce the change in magnetic flux inside the iron core, the magnetic flux balance suitable for the material was optimized.

Additionally, because the application of stress to various parts of the iron core causes an increase in loss, relaxing that stress is also an important topic. For example, the amount of interference after press-fitting the core into the frame was reevaluated in order to reduce core deformation and to prevent an increase in loss.

To reduce the iron loss, various parameters such as the number of slots (slot combinations) in the rotor and stator, the slot dimensions and so on must be considered. Moreover, because it is important for iron loss to be reduced significantly while considering the balance with copper loss and the overall electrical characteristics, individual existing calculation programs and magnetic field analysis tools were used accordingly to achieve optimization.

(3) Reduction of mechanical loss due to cooling fans

The motor is equipped with a fan for cooling the housing, and the windage loss caused by the fan rotation is included in the loss of the motor. In order to minimize the required fan cooling to the minimum amount necessary, the motor temperature must be computed with high accuracy during the design stage. Therefore, a thermal fluid network method was employed to implement a thermal design that reduces the loss caused by the cooling fan. The thermal fluid network method is a technique in which wind speed is computed using thermal fluid network calculations, and then the temperatures at various parts are computed using thermal fluid network calculations.

(4) Reduction of loss variation among products

For the top runner standards, since it is necessary to satisfy prescribed efficiency values with weighted averages, it is important that individual loss variation among products be minimized. Rigorous processing accuracy and management are being carried out during production to minimize any such variation.

Launch time

June 1, 2013

Product Inquiries

Drive Division, Power Electronics Business Group,
Fuji Electric Co., Ltd.
Phone: +81-3-5435-7059

High-Voltage Air Load Break Switch (LBS)

KIKUCHI Masanori*

A high-voltage load break switch is a switching device used for making or breaking the load current in a high-voltage power receiving and distributing circuit. In particular, a high-voltage load break switch (LBS) with striker-tripped*1 current-limiting fuse provides switching-protection functions over a wide current range, from switching the load current to breaking short-circuit current. As a result, LBSs are used in various applications such as the main breaking device in cubicle-type high-voltage power receiving equipment, or in a protection device on the primary side of a transformer. Notably, LBSs are employed in most main breaking devices used in PF-S type high-voltage power receiving unit of 300 kVA or less.

In recent years, LBSs have also been used in circuits on the high-voltage side of solar power equipment, and their applications are expanding further. Moreover, with the miniaturization of switchgear, smaller size is also being required of the LBS and other devices that are contained within the switchgear.

In response to these demands, Fuji Electric has developed a small-size, easy-to-use LBS.

1. Features

Figure 1 shows the appearance of Fuji Electric's newly developed LBS, and Table 1 lists its specifications. The main features are described below. The characteristics are as follows:

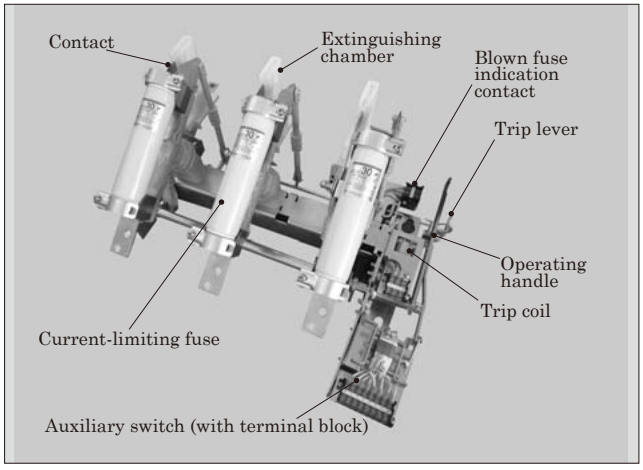

Fig.1 LBS

Table 1 LBS specifications

Item	Specification	
Model	LBS-6 A/200 (F)	LBS-6 A/210 (F)
Rated voltage	3.6/7.2 kA (50/60 Hz)	
Rated insulation level	60 kV	
Rated current	200 A	
Rated making/breaking current	12.5 kA (1 switching iteration)	
Rated switching capacity	Load current 200 A (200 switching iterations) Excitation current 10 A (10 switching iterations) Charging current 10 A (10 switching iterations) Capacitor current 50 A (200 switching iterations, with 6% reactance reactor)	
Overload breaking current	1,100 A (1 switching iteration)	
Method of operation	Manual hook operation	
Contact structure	Integrated conduction contacts and arc contacts	
Arc-extinguishing method	Slit, gas-cooled arc extinguishing	
Type of fuse used	JC-6/5 to 75	JC-6/100
Fuse current rating	G5 to G75 A	G100 A
Compliance	JIS C 4611	

(1) Smaller size

Compared to conventional devices, the depth dimension has been reduced by approximately 40 mm and the total volume is 10% smaller.

(2) Improved workability and safety when replacing current-limiting fuse

Conventional LBS devices had an integrated structure of contact and current-limiting fuse parts, and because the current-limiting fuse moved in conjunction with the operation of the contact during switching operation, the area on which the current-limiting fuse was mounted moved easily while the switch was in an open state, and therefore the task of replacing the current-limiting fuse was performed in an unstable state. In contrast, Fuji Electric's newly developed LBS is constructed so that the contacts and the current-limiting fuse are separated and the current-limiting fuse does

* Technology & Manufacturing Group, Fuji Electric FA Components & Systems Co., Ltd.

*1 Striker tripping method: A current-limiting fuse is structured so that a blowout indication pin protrudes outward at the time when the fuse is blown. In this method, the protruding force of this pin is utilized to operate the link mechanism of the load switch, thereby opening the load switch.

not move. Accordingly, workability and safety when replacing the current-limiting fuse are improved.

(3) Improved ease of handling

(a) In a conventional LBS, the contact output that operates at the time when the current-limiting fuse is blown only provides an output momentarily. The newly developed LBS, however, is devised so that after operation, the output will continue until the current-limiting fuse is replaced. As a result, it is possible to eliminate the self-holding circuit that uses this output, which has been provided in the control circuit of the switchgear.

(b) The method of attaching the interphase barrier was changed from screw fastening to a one-touch structure to improve the ease of mounting.

(c) Furthermore, the auxiliary circuit wiring was concentrated on the right-hand side of the LBS unit and a terminal block for auxiliary switches was provided to improve workability when wiring in the switchgear.

(4) Environmental friendliness

In compliance with the RoHS directive*2, Fuji Electric's new LBS does not contain any environmentally hazardous substances.

2. Background Technology

2.1 Reconsideration of structure of movable part of main circuit

In order to achieve a small and simple structure, Fuji Electric conducted a fundamental review of the structure of the movable part of the main circuit. Figure 2 shows the structure of the contact and the movable part.

In conventional products, the switching operation caused the arcing contacts, main contacts and current-limiting fuse to all move together, and this was an impediment to reducing the depth dimension. Therefore, the newly developed product employs a structure in which the movable contacts and the arcing contacts are integrally formed and the current-limiting fuse is immobile, thereby reducing operation range of the movable part and achieving a smaller depth direction.

2.2 Integration of the contacts

Conventional products have a structure in which main contacts, through which load current flows, are connected in parallel with arcing contacts, which are used for extinguishing arcs in the arc-extinguishing chamber at the time of current breaking. Consequently, the roles of arc extinguishing and of conducting the load current are shared respectively.

Fuji Electric's newly developed product employs a structure of integrated arcing contacts and main contacts in order to reduce the product size. In order to achieve this structure, the realization of required performance for both arcing and load conducting became a challenge. Accordingly, the shape of the arc-extinguishing chamber, conduction temperature, contact erosion, and switching durability performance etc. were exam-

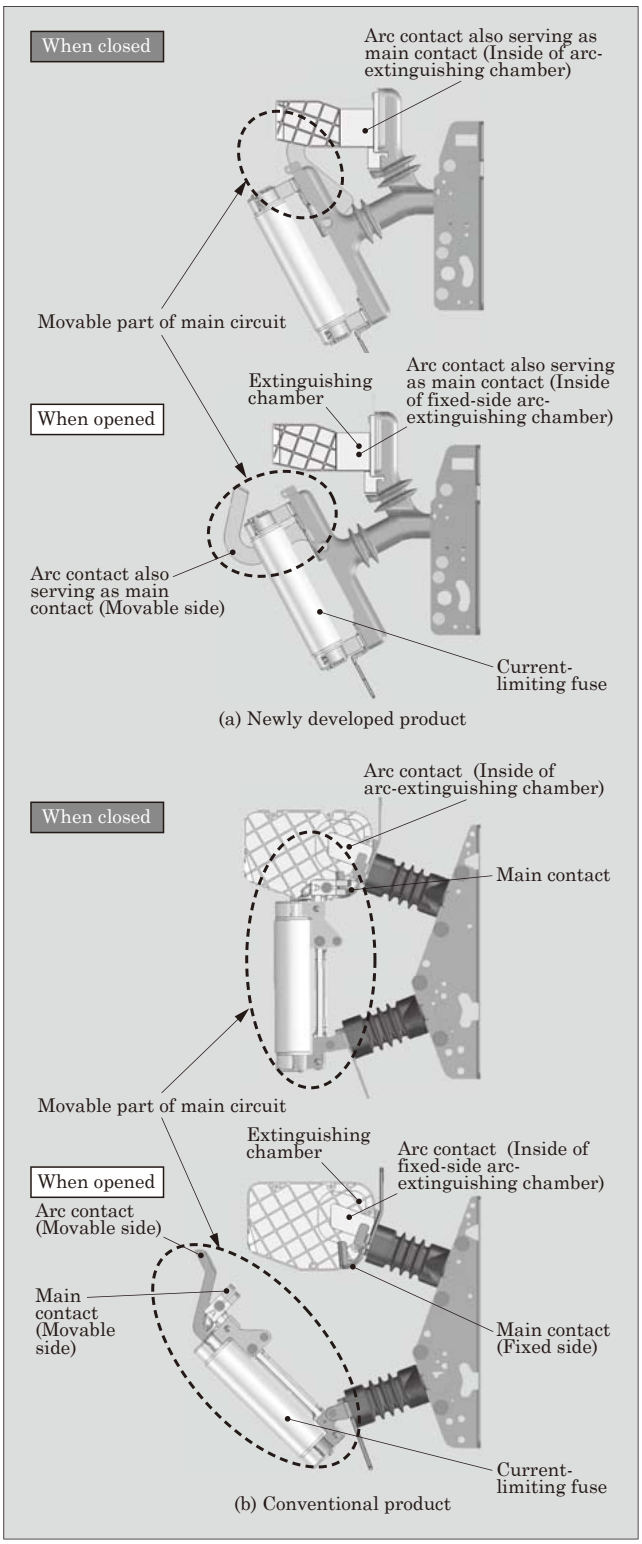

Fig.2 Structure of contact and movable parts

*2 RoHS Directive: EU (European Union) directive on the restriction of use of certain hazardous substances in electrical and electronic equipment

ined individually; and optimal materials, shapes, surface treatments, contact pressure, and other elemental technologies for integration were established and their associated issues were resolved to solve the above challenge.

2.3 Structure of the arc-extinguishing part

As in conventional products, there employed the structure in which the generated arc is extinguished at the slit portion of the arc-extinguishing chamber.

In order to reduce the size of the product, it is essential that individual functional components be miniaturized. In air breaking, arc must be extinguished in the arc-extinguishing chamber, but if the volume of the arc-extinguishing chamber is reduced, the arc will be incompletely extinguished, resulting in breaking operation failure. Accordingly, optimizing the relationship between the length of the arc-extinguishing chamber and the dissociation rate of the contacts, and securing the insulation distance between poles after dissociation, and the like, are challenges.

Figure 3 shows the structure of the arc-extinguishing part. The interior of the arc-extinguishing chamber is provided with a fixed-side contact and an arc guide; the movable-side contact is provided with a curved shape so that the arc is always generated between the arc guide and the tip of the movable-side contact. The interaction between various structural elements, such as the required distance for extinguishing the arc and the rotational speed of the movable contact, were considered to optimize the size of the arc-extinguishing chamber. As a result, the newly developed product maintains stable switching and breaking performance with an approximate fifty-percent reduction in size of the projected area of the arc-extinguishing chamber compared to conventional products.

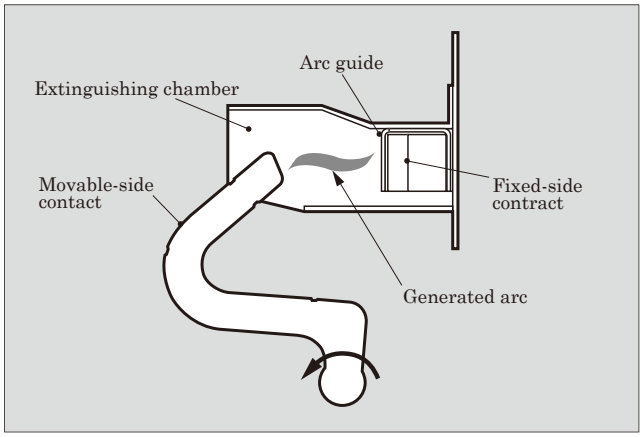

Fig.3 Structure of arc-extinguishing part

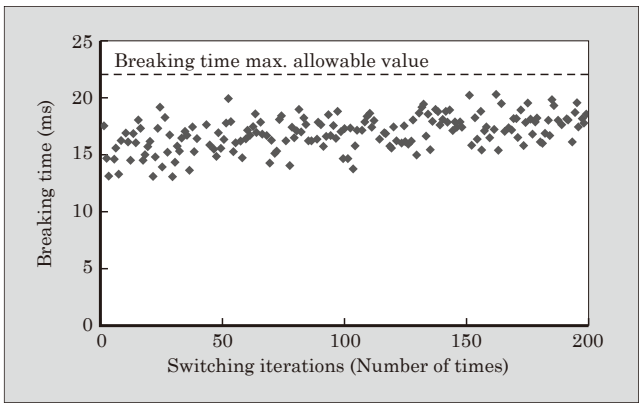

Fig.4 Relationship between load current switching iterations and breaking time

Figure 4 shows the relationship between the breaking time and the load current switching iterations during a 200 A load current switching test with the aforementioned structure of the arc-extinguishing chamber. In the figure, the maximum allowable value of the breaking time is the time by which breaking must be accomplished inside the arc-extinguishing chamber. The breaking time, until reaching 200 times of load current switching iterations, is less than or equal to the maximum allowable value, and it can be seen that the breaking operation has been accomplished stably.

Launch time

October 2013

Discrete RB-IGBT “FGW85N60RB”

HARA Yukihito*

Fuji Electric’s reverse-blocking insulated gate bipolar transistor (RB-IGBT), which is mass-produced with Fuji’s proprietary technology, was equipped in a discrete package and released as “FGW85N60RB” (see Fig. 1).

How to improve the power conversion efficiency of an uninterruptible power supply (UPS), a photovoltaic power conditioning system (PCS), or the like, has presented challenges. Power conversion circuits that use advanced T-type neutral-point-clamped (AT-NPC) technology (see Fig. 2) are one means to meet this challenge. The use of an RB-IGBT for the neutral point clamp in an AT-NPC circuit enables power conversion efficiency to be increased further.

Fuji Electric has commercialized AT-NPC modules equipped with RB-IGBTs. The FGW85N60RB is a product that includes RB-IGBTs, having been optimized for discrete products, equipped in a TO-247 package, and is able to realize high-efficiency AT-NPC even with a discrete configuration.

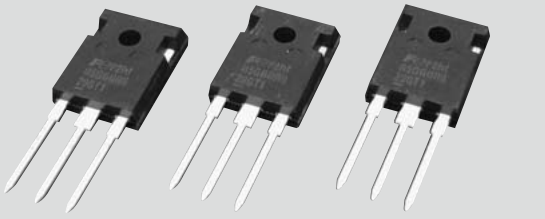

Appearance

Model	Package	Rating	$V_{CE(sat)}$
FGW85N60RB	TO-247	600 V/85 A	2.45V(typ.)

Specification outline

Fig.1 Appearance and specification outline of “FGW85N60RB”

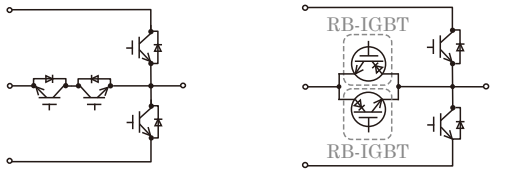

(a) Anti-series IGBT-diode connection (conventional product)

(b) Anti-parallel RB-IGBT connection

Fig.2 Power conversion circuits using AT-NPC technology

1. Features

(1) Industry’s first 600 V discrete RB-IGBT
(2) Industry standard TO-247 package
(3) Low inductance package

With a discrete product, the internal package inductance is lower than in the case of a module product and the turn-off surge can be minimized and turn-off loss reduced even without increasing the external gate resistance.

(4) A bidirectional switch can be formed with an anti-parallel connection

Since a reverse switch can be formed with two RB-IGBTs, significantly lower conduction loss (see Fig. 3) and approximately 3% lower generated loss (see Fig. 4) can be achieved comparing with a conventional product

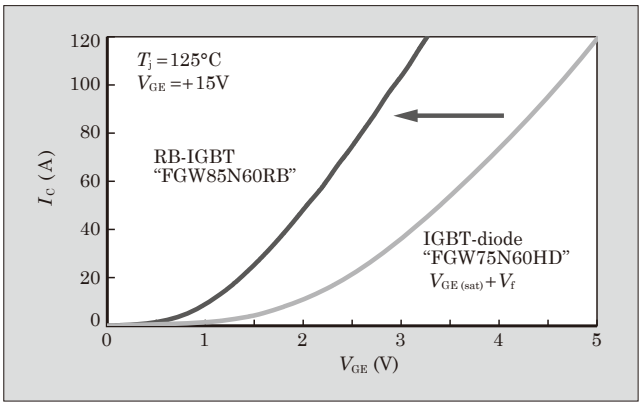

Fig.3 V_{CE}-I_C characteristics

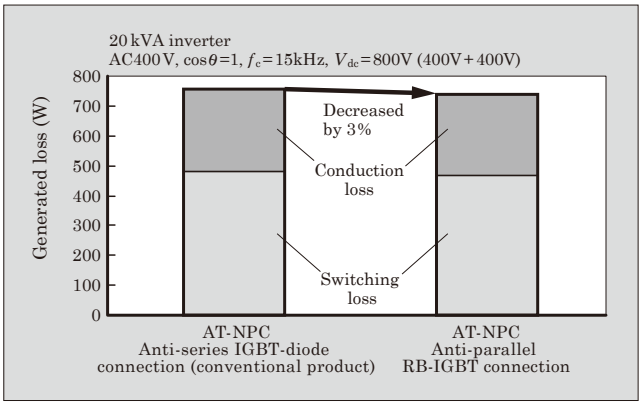

Fig.4 Comparison of inverter circuit loss

* Electronic Devices Business Group, Fuji Electric Co., Ltd.

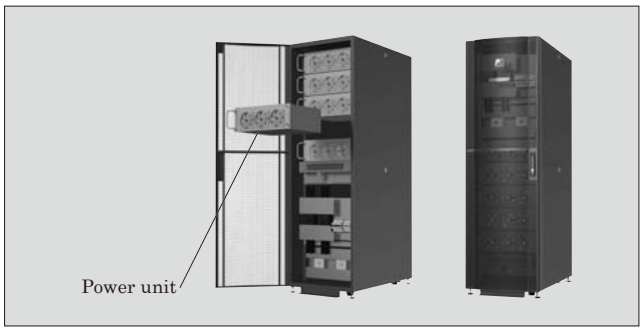

Fig.5 UPS example

configured with two IGBTs and two diodes.

2. Application Examples

An example application to a UPS is described below. The UPS shown in Fig. 5 allows power units (20 kVA/unit) to be added in a stacked configuration, and its capacity can be expanded up to 200 kVA. Employing the FGW85N60RB as the neutral point clamp in a converter and inverter configured with AT-NPC circuitry enables conduction loss to be reduced and UPS efficiency to be improved.

3. Background Technology

3.1 Chip technology

With an ordinary IGBT, because the pn junction makes contact with the dicing surface, the application of a reverse bias between the collector and emitter causes many carriers to be generated, and due to the high density of crystalline defects resulting from the dicing, the voltage cannot be maintained. Accordingly, in order to apply a reverse voltage to an ordinary IGBT, the use of a blocking diode for maintaining the reverse voltage has been necessary. In the case of a RB-IGBT, since a deep p^+ separation layer is formed by a high-temperature long-duration diffusion process in the scribe region, even if a reverse bias is applied, the depletion layer will not extend into the dicing surface and the reverse breakdown voltage will be maintained (see Fig. 6). In the process that forms the deep p^+ isolation layer, diffusion is carried out at high-temperature for a long duration, and thereby, a large number of crystalline defects are generated in the n^- drift layer. Because the leakage current increases when crystalline defects increase, a review of the process was conducted in order to establish a process for forming a p^+ separation layer whereby crystalline defects are less likely to occur. As a result, stable manufacturing productivity can be ensured.

On the other hand, the leakage current when a reverse voltage is applied between the collector and emitter of a RB-IGBT is greater than the leakage current when a forward voltage is applied. The mechanism that generates the reverse leakage current is as follows.

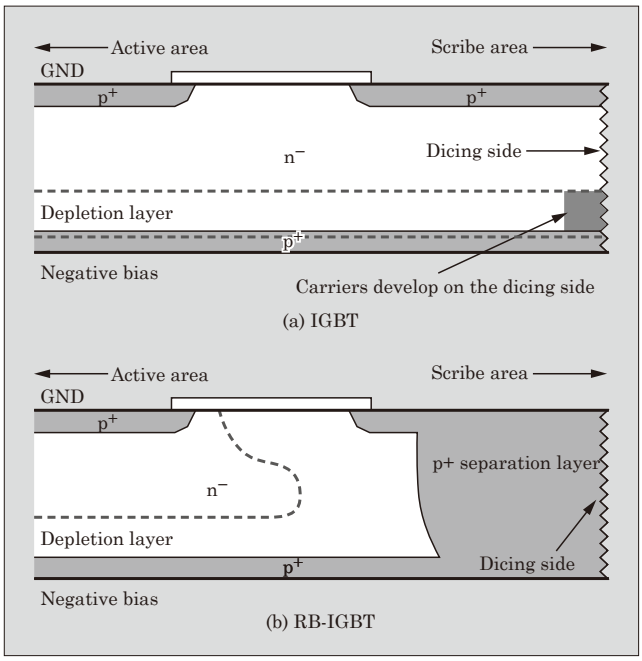

Fig.6 RB-IGBT chip cross-sectional structure

(a) A reverse voltage is applied between the collector and emitter.
(b) Holes are generated in the p layer on the back surface and electrons flow to the emitter region.
(c) The electrons form the base current of a pnp transistor.
(d) Holes are additionally generated in the p layer on the back surface, and a large reverse leakage current is formed.

The reverse leakage current can be reduced by applying a forward voltage to the gate (see Fig. 7). By applying a forward voltage to the gate, electrons flow to the channel instead of flowing to the emitter region to

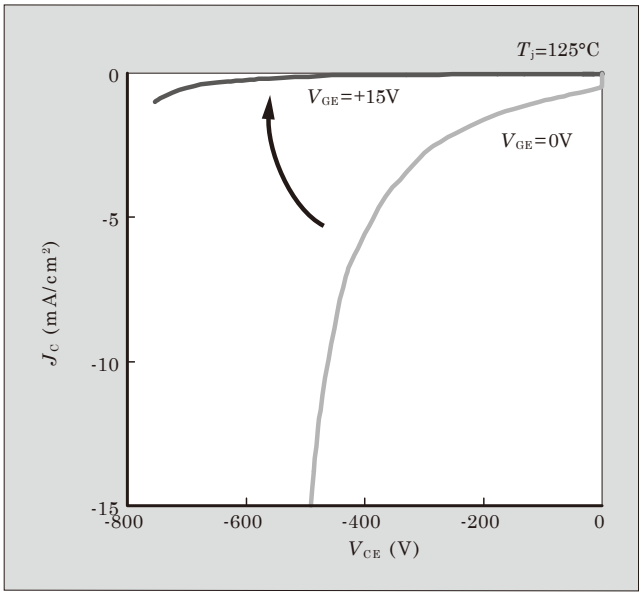

Fig.7 RB-IGBT reverse leakage current

form the base current of a pnp transistor, and as a result, holes are not generated in the p layer on the back surface.

Moreover, by applying to the gate a forward voltage that is larger than the threshold voltage, reverse recovery operation similar to that of a conventional diode becomes possible.

3.2 Package technology

The package of FGW85N60RB uses the same industry-standard TO-247 package that is also used with Fuji Electric's "High-Speed V series" of discrete IGBTs. This allows conventional IGBTs to be replaced easily.

As with the discrete IGBT High-Speed V series, the FGW85N60RB uses lead-free solder as the die solder underneath the chip, and is fully compliant with the RoHS directive* and the EU 2002/95/EC directive. Moreover, in a reliability test that applies thermal stresses from a power cycle or heat cycle simultaneously, a high degree of durability has been confirmed.

Launch time

October 1, 2013

Product Inquiries

Discrete & IC Technology Dept., Business Planning Division, Electronic Devices Business Group, Fuji Electric Co., Ltd.
Phone: +81-263-28-8734

* RoHS Directive: EU (European Union) directive on the restriction of use of certain hazardous substances in electrical and electronic equipment

Fuji Electric
Innovating Energy Technology

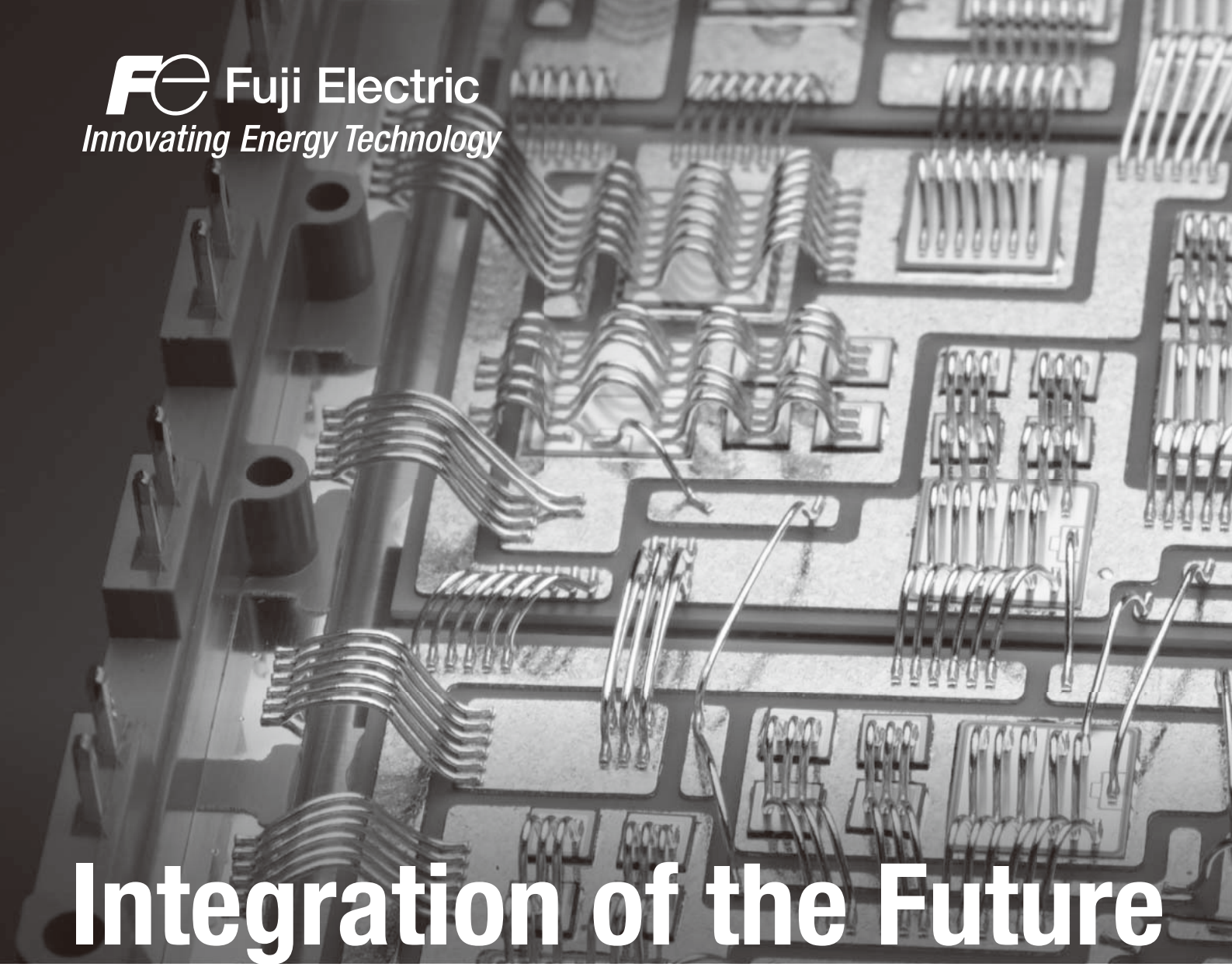

Integration of the Future

Fuji Electric's power semiconductors concentrate the company's proprietary power electronics technology and application potential. The key devices, which are being advanced in terms of high blocking voltage/increased capacity, decreased power loss and small and lightweight packaging, are utilized in various scenes ranging from the field of regenerative energy including photovoltaic power generation and wind power generation, field of energy conservation called for by industries and households and field of traffic such as hybrid/electric vehicles. In addition, we have developed next-generation power semiconductors with increased performance that use SiC, a new material.
Fuji Electric is committed to continued innovation of energy technology and intends to make contributions to the realization of a sustainable society with safety and security ensured.

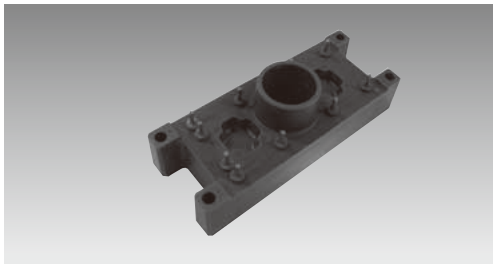

All-SiC power semiconductor module

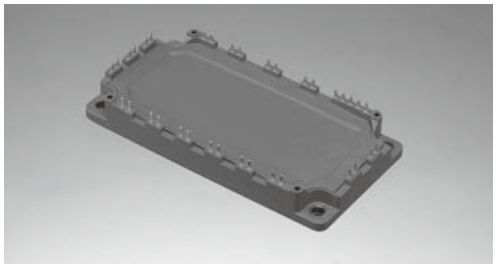

Hybrid module integrating SBD with SiC applied

Fuji Electric's power semiconductors

Innovating Energy Technology

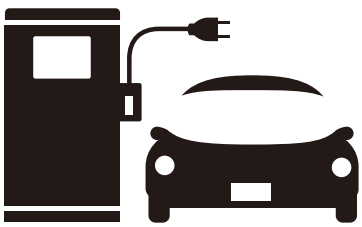
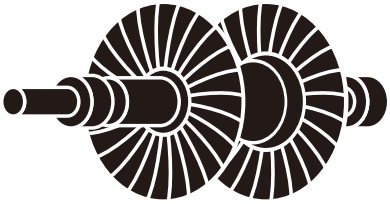

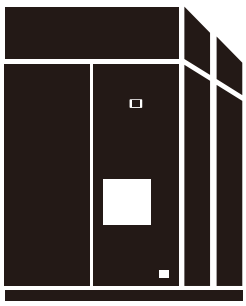
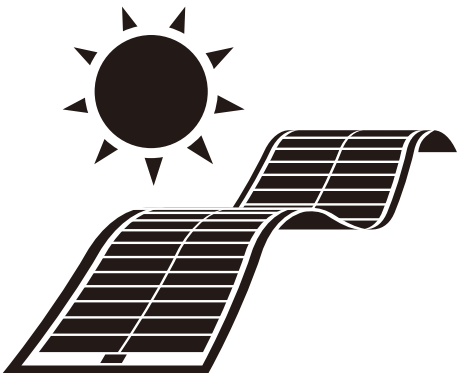
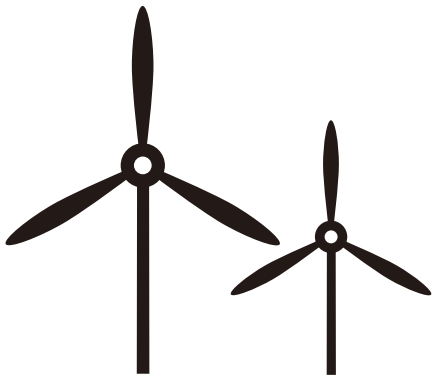

Fuji Electric will meet the demands
of a new age with our energy technologies.

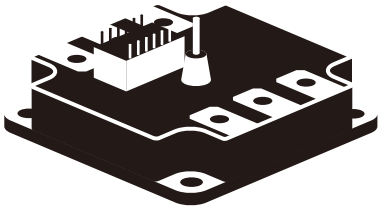



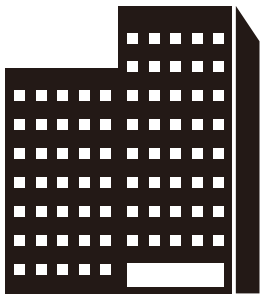

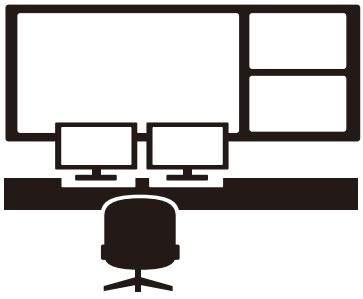

"Energy creation" to produce clean energy,
"energy conservation" to reduce wasteful energy consumption and
"energy management" to make the most of both the above approaches.
Fuji Electric will contribute to the creation of sustainable societies
through our unique technologies that freely control electricity.

Fuji Electric

Overseas Subsidiaries

* Non-consolidated subsidiaries

America

Fuji Electric Corp. of America
Sales of electrical machinery and equipment, semiconductor devices, drive control equipment, and devices
Tel +1-732-560-9410
URL http://www.americas.fujielectric.com/

Fuji Electric Brazil-Equipamentos de Energia Ltda *
Sales of inverters, semiconductors, and power distribution
Tel +55-11-2283-5991
URL http://www.americas.fujielectric.com/portugues

Asia

Fuji Electric Asia Pacific Pte. Ltd.
Sales of electrical distribution and control equipment, drive control equipment, and semiconductor devices
Tel +65-6533-0014
URL http://www.fujielectric.com/asia/company/offices/fap.html

Fuji Electric (Thailand) Co., Ltd. *
Sales and engineering of electric substation equipment, control panels, and other electric equipment
Tel +66-2-210-0615

Fuji Electric Power Supply (Thailand) Co., Ltd.
Manufacture and sales of small- to medium-size UPS and internal power supplies
Tel +66-2-5292178

Fuji Electric Vietnam Co.,Ltd.
Sales of electrical distribution and control equipment and drive control equipment
Tel +84-4-3935-1593

Fuji Furukawa E&C (Vietnam) Co., Ltd. *
Engineering and construction of mechanics and electrical works
Tel +84-4-3755-5067

PT Fuji Electric Indonesia *
Sales of inverters, servos, UPS, tools, and other component products
Tel +62 21 398-43211

Fuji Electric India Pvt. Ltd. *
Sales of drive control equipment and semiconductor devices
Tel +91-22-4010 4870
URL http://www.fujielectric.co.in

Fuji Electric Philippines, Inc.
Manufacture of semiconductor devices
Tel +63-2-844-6183

Fuji Electric Semiconductor (Malaysia) Sdn. Bhd.
Manufacture of semiconductor devices
Tel +60-4-494-5800
URL http://www.fujielectric.com.my/

Fuji Electric (Malaysia) Sdn. Bhd.
Manufacture of magnetic disk and aluminum substrate for magnetic disk
Tel +60-4-403-1111
URL http://www.fujielectric.com.my/

Fuji Furukawa E&C (Malaysia) Sdn. Bhd. *
Engineering and construction of mechanics and electrical works
Tel +60-3-4297-5322

Fuji Electric Taiwan Co., Ltd.
Sales of semiconductor devices, electrical distribution and control equipment, and drive control equipment
Tel +886-2-2511-1820

Fuji Electric Korea Co., Ltd.
Sales of power distribution and control equipment, drive control equipment, rotators, high-voltage inverters, electronic control panels, medium- and large-sized UPS, and measurement equipment
Tel +82-2-780-5011
URL http://www.fujielectric.co.kr/

Fuji Electric Middle East Branch Office
Promotion of electrical products for the electrical utilities and the industrial plants
Tel +973-17 564 569

Europe

Fuji Electric Europe GmbH
Sales of electrical/electronic machinery and components
Tel +49-69-6690290
URL http://www.fujielectric.com/europe/company/offices/fee.html

Fuji Electric France S.A.S
Manufacture and sales of measurement and control devices
Tel +33-4-73-98-26-98
URL http://www.fujielectric.fr/

China

Fuji Electric (China) Co., Ltd.
Sales of locally manufactured or imported products in China, and export of locally manufactured products
Tel +86-21-5496-1177
URL http://www.fujielectric.com.cn/

Shanghai Fuji Electric Switchgear Co., Ltd.
Manufacture and sales of switching equipment, monitoring control appliances, and related facilities and products
Tel +86-21-5718-1234
URL http://www.fujielectric.com.cn/sfswgr/

Shanghai Fuji Electric Transformer Co., Ltd.
Manufacture and sales of molded case transformers
Tel +86-21-5718-7705
URL http://www.fujielectric.com.cn/sfswgr/

Wuxi Fuji Electric FA Co., Ltd.
Manufacture and sales of low/high-voltage inverters, temperature controllers, gas analyzers, and UPS
Tel +86-510-8815-2088

Fuji Electric (Changshu) Co., Ltd.
Manufacture and sales of electromagnetic contactors and thermal relays
Tel +86-512-5284-5642
URL http://www.csfe.com.cn/

Fuji Electric (Zhuhai) Co., Ltd.
Manufacture and sales of industrial electric heating devices
Tel +86-756-7267-861

Fuji Electric (Shenzhen) Co., Ltd.
Manufacture and sales of photoconductors and semiconductor devices
Tel +86-755-2734-2910
URL http://www.szfujielectric.com.cn/FUJIWebSite/index.html

Fuji Electric Dalian Co., Ltd.
Manufacture of low-voltage circuit breakers
Tel +86-411-8762-2000

Fuji Electric Motor (Dalian) Co., Ltd.
Manufacture of industrial motors
Tel +86-411-8763-6555

Dailan Fuji Bingshan Vending Machine Co.,Ltd.
Development, manufacture, sales, servicing, overhauling, and installation of vending machines, and related consulting
Tel +86-411-8754-5798
http://www.fushibingshan.com/index.html

Fuji Electric (Hangzhou) Software Co., Ltd.
Development of vending machine-related control software and development of management software
Tel +86-571-8821-1661
URL http://www.fujielectric.com.cn/fhs/cn/

Zhejiang Innovation Fuji Technology Co., Ltd. *
Design, development, and services pertaining to software
Tel +86-571-8827-0011
URL http://www.fujielectric.com.cn/sif/

Fuji Electric FA (Asia) Co., Ltd.
Sales of electrical distribution and control equipments
Tel +852-2311-8282
URL http://www.fea.hk/

Fuji Electric Hong Kong Co., Ltd.
Sales of semiconductor devices and photoconductors
Tel +852-2664-8699
URL http://www.szfujielectric.com.cn/hkeng/company/index.htm

Hoei Hong Kong Co., Ltd.
Sales of electrical/electronic components
Tel +852-2369-8186
URL http://www.hoei.com.hk/

Innovating Energy Technology

Through our pursuit of innovation
in electric and thermal energy technology,
we develop products that maximize energy efficiency
and lead to a responsible and sustainable society.

Fuji Electric